CHAPTER II

LOW-DIMENSIONAL SEMICONDUCTOR NANOSTRUCTURES: QUANTUM CONFINEMENT AND ITS EFFECT ON OPTICAL PROPERTIES

The content of this chapter mentions about a low-dimensional semiconductor nanostructures based on dimensional confinement and comparison of important intrinsic properties of nanostructures. These are reviewed to be useful for the interpretation of nanostructure characteristics. Effect of quantum confinement on optical properties nanostructures is also presented. In another part of this chapter, self-assembled growth of the nanostructures is briefly introduced to provide basic of quantum dot formation from strain-releasing in lattice mismatch system included with shortly review about the fabrication of self-assembled aligned quantum dots. The next section, the fundamental concept of electric field on nanostructures and discussion about this phenomena is presented. Finally, the theoretical studies of polarization on the quantum dots and information from several groups related with this work is provided.

2.1 BASIC CONCEPTS OF LOW-DIMENSIONAL NANOSTRUCTURES

One of the most noticeable characteristics of these semiconductor structures is delocalization of electrons that can spread their wave functions over a larger distance **[1]**. Over the past two decades, rapid progress in semiconductor fabrication technology, especially in the fabrication of nanostructures, has developed semiconductor materials to be constructed with a confined electron structure. Reducing the size or dimension of a material into a micrometer and then to a nanometer scale in order about the de Broglie wavelength of an electron, various changes in electronic and optical properties were observed in these structures **[38]**. We can

roughly classify the kind of semiconductor structure by investigating the dimension. First, if one dimension of 3-D structure is reduced into a nano-scale while the other dimensions remain large, then this structure is called a **quantum well [39]**. Afterwards, if two dimensions are reduced while the other remains large, this structure is called a **quantum wire [40]**. The final case of this process is in which the size is reduced in all three dimensions into a nano-range, as a result, this structure is called a **quantum dot (QDs) [41]**. All of these structures have an enormous changes in electrical and optical properties of these after reducing their sizes arise from the quantum mechanical nature of physics as a result of the ultra small size.

Consideration the electronic structures, there are apparently different between bulk materials and atom-like nanostructures about the energy level **[42-43]**, namely, the electronic structures in the case of atom-like nanostructures are characterized by discrete energy levels while those of bulk crystal structures are characterized by relation of bands. The density of states of bulk semiconductors and low-dimensional nanostructures may be calculated by using quantum mechanics to describe the number of states at each energy level that are available to be occupied. In that case the band offset between the low-dimensional nanostructures and the surrounding materials provide the energy potential to confine carriers **[44-46]**. For calculating the electronic states of bulk materials and nanostructures, the effective-mass approximation **[47]** can efficiently be used, based on the assumption that the envelope wave function does not significantly change in the unit cell with a length scale of the nanostructure and this assumption can be applied to all low-dimensional nanostructures. By assuming the parabolic band dispersion, band-edge electron states of a semiconductor can then be demonstrated by the Schrödinger equation.

2.1.1 Carrier Confinement and Energy Level Quantization

The band theory of crystals has been strictly developed from the quantum theory for atoms since the last century **[48-49]**. From the quantum theory, when we place atoms, which have discrete energy levels, together, this result in the interaction between each atom. The closer distance, the more interaction, then they become solid. The energy levels of solid crystal become energy bands which have continuity and more than one energy band. From the engineering point of view the most relevant bands are the conduction band and the valence band which are separated in energy by the band gap. At temperature is 0 K, the conduction band is absence of electrons, while the valence band is rich of electron. At $T > 0$ K, these two bands are intermixing with electrons and holes, which act as charge carriers in devices operations. Controlling the carrier transition between these two bands is the main of band gap engineering. Therefore, consider only these two bands. In this section, the important properties of nanostructures are reviewed. Since nano-structures with low-dimensional shapes provide the potential well resulted from difference of energy band gap (E_g) of two materials, the carriers (electrons and holes) can be confined and results in a quantization of carrier energy. Therefore, the certain-energy photon would be emitted when nanostructures are stimulated.

In low-dimensional nanostructures large carriers are confined in one or more directions and the length scale of confining direction is in the order of the de Broglie wavelength (carrier wavelength). The de Broglie wavelength, $\lambda_{deBroglie}$, depends on the carrier effective mass, m^*, and temperature, T **[50]**:

$$\lambda_{deBroglie} = \frac{h}{p} = \frac{h}{\sqrt{3m^* k_B T}} \qquad \textbf{(2.1)}$$

where h is Planck's constant, p is carrier momentum, and k_B is Boltzmann's constant. The de Broglie wavelength for electrons in III-V semiconductor materials is in the order of 20 nm at 300 K. Several aspects of carrier confinement effects are useful for semiconductor device applications such as intersubband transition in crystals which is the important mechanism for photodetector in the range of far-infrared with wavelength over 9 micrometers.

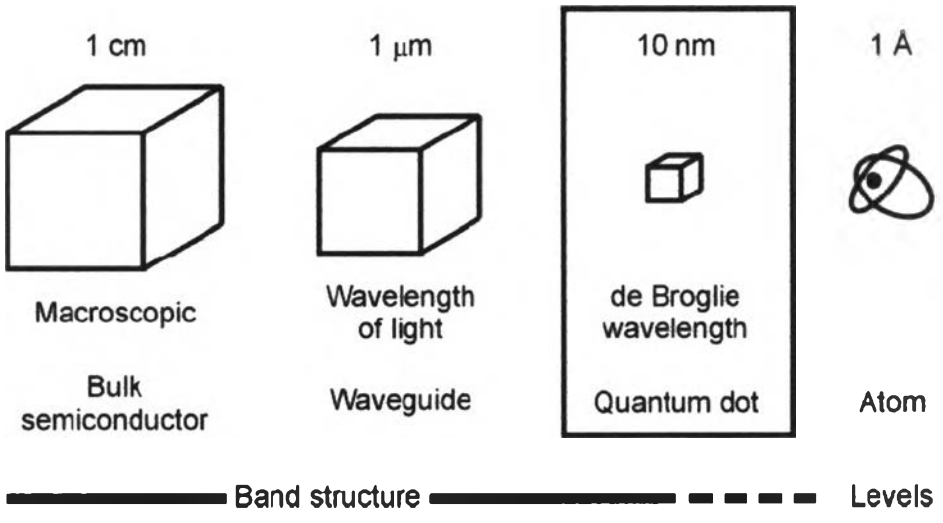

Figure 2.1 Schematic comparison of bulk semiconductor, waveguide for visible light, QD, and atom **[51]**.

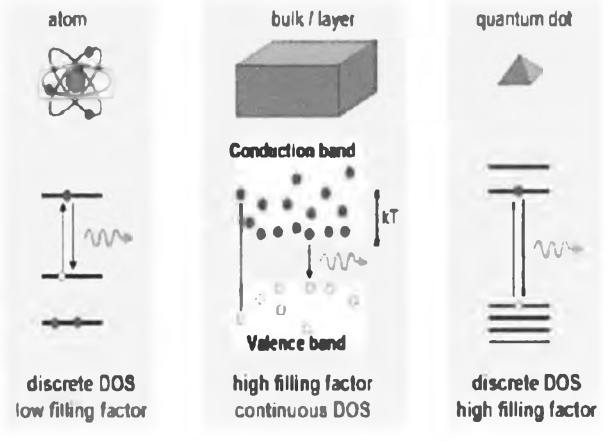

Figure 2.2 Comparison of electronic levels and spectral properties in atoms, bulk semiconductors and QDs **[52]**.

Figure 2.1 shows a schematic comparison between a bulk semiconductor, a waveguide for visible light, a QD, and an atom. The electronic structure of the bulk material and the atom are different. The electronic structure in the case of the atom is described by discrete energy levels, while in the case of the bulk-crystal structure, the band theory is used. Because the structural size is varied continuously, there exists a description between the two cases (discrete levels and continuum band structure). The densities of states of bulk semiconductor and low-dimensional nanostructures are illustrated in **Figure 2.3**. In confining direction, the band offsets between the low-dimensional nanostructures and the surrounding material provide the energy potential or potential well in energy band to confine the carriers. Therefore, the carrier motion is limited in this direction and can move freely only in other dimensions, which exist no potential well. In case of quantum well, electrons and holes can freely move in the x-y plane; those in a quantum wire can only move in x direction. In a QD, zero-dimensional-nanostructure, the charge carriers are completely localized which results in a quantization of the carrier energy and in a variation of the carrier density of states.

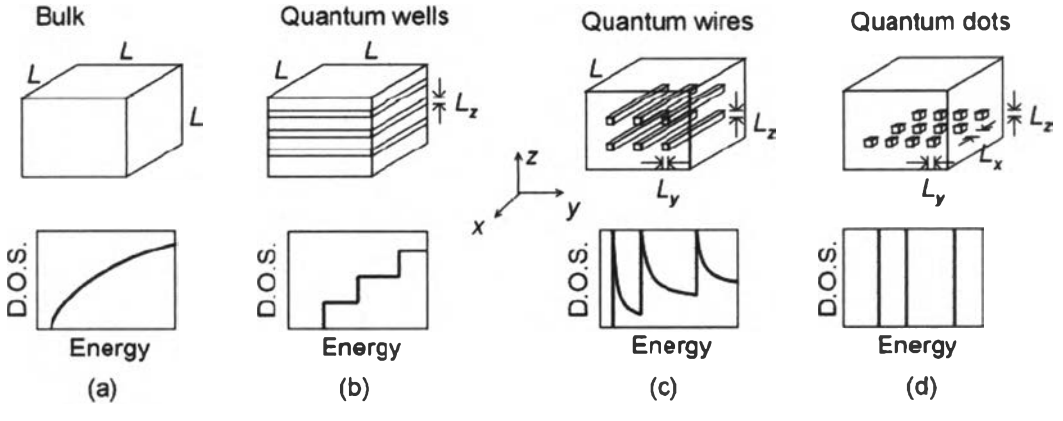

Figure 2.3 Schematic views and graphs of (a) bulk, (b) quantum wells, (c) quantum wires, and (d) QD and their density of states (D.O.S.) **[53]**. L is in macroscopic scale (~cm), while L_x, L_y, L_z are in nanoscale.

The quantization phenomenon can be demonstrated by wave-like properties of electrons, since any substance would exhibit its wave properties of which de Broglie wave length can be calculated from **Eq. (2.1)**. In potential well, confined carriers are limited its motion, so they are looked-like stationary. The wave-like properties of the *stationary* electron can be only de Broglie wavelengths which create standing wave within the width of the potential well, that is, the width of the nanostructures. The discrete-values of electron de Broglie wavelengths would be exhibited, and cause discrete energy levels in such 3-D confinement structures. **Figure 2.4** represents the lowest three level of carrier's energy quantization appeared in potential well.

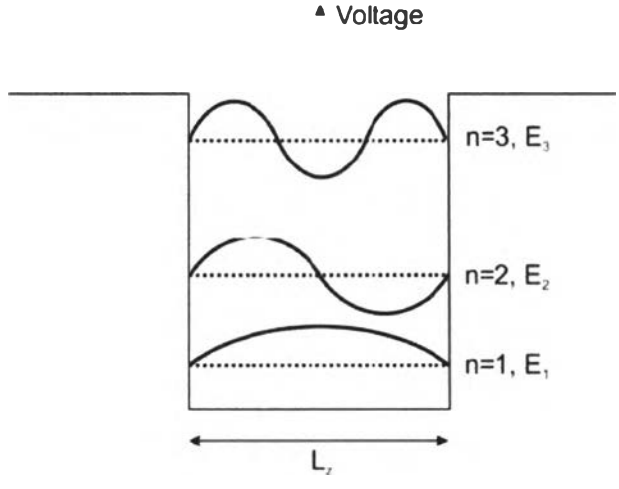

Figure 2.4 Schematic representation of the lowest three level of carrier's energy quantization in potential well with the width of L_z (comparable to de Broglie wavelength) **[53]**. The picture shows examples of the three lowest-energy standing waves which can be happened in potential well (solid line) and the corresponding carrier's energy level of the de Broglie wavelength from the standing wave (dotted line), i.e. E_1, E_2 and E_3. The energy of each level is given by $E_{n_z} = \hbar^2 (n\pi)^2 / 2m^* L_z^2$, where n is a integer number of the level.

In quantum wells structures, an effective-mass approximation is widely used for calculating the quantized energy levels as a function of the well width **[51]**. The main assumption of the effective-mass approximation is that the envelope wave function does not significantly vary in the unit cell with a length scale of sub-nanometers, therefore this assumption is valid in all low-dimensional nano-structures. Assuming parabolic band dispersion, band-edge electron states of semiconductors can be described by Schrödinger-like equation as

$$\left[-\frac{\hbar^2}{2m^*}\nabla^2 + V(r)\right]F(r) = EF(r) \qquad \textbf{(2.2)}$$

Where, m^* is the effective mass; $\hbar$ is the reduced Planck's constant; $r = (x, y, z)$ is the carrier position vector; $V(r)$ is the confinement potential due to band offset. $F(r)$ is the envelope wave function; and E is the carrier energy. From **Eq. (2.2)**, by assuming the barrier potentials with *infinite height*, the carrier energy E and density of states per unit volume (D.O.S.) (the number of states between the energy E and $E + dE$, of each quantum nanostructure) in case of bulk, quantum well (QW), quantum wire (QWR) and QD can be written as follows **[59]**.

2.1.2 Bulk Material

In bulk materials, the conduction electrons are delocalized in a volume and their wavefunctions spread in all dimensions. Considering the electrons in bulk as free electron gas, the electrons are free to wander around the crystal with unaffected by the core potential of the atomic nuclei. If a free electron has a velocity v and a momentum $p = mv$. Its energy consists entirely of kinetic energy, and the potential energy tends to be zero ($V = 0$). Therefore, the total energy (E) of the bulk material can be considered as

$$E_{bulk} = E(k) = \frac{\hbar^2 k^2}{2m^*} \tag{2.3}$$

$$D_{bulk} = \frac{1}{2\pi^2}(\frac{2m^*}{\hbar^2})^{\frac{3}{2}} E^{\frac{1}{2}} \tag{2.4}$$

where D is the density of states and k is electron wave number, $k = (k_x, k_y, k_z)$ defined by $k^2 = k_x^2 + k_y^2 + k_z^2$

2.1.3 Quantum Wells

Quantum wells are a type of structure in which a thin layer of smaller-bandgap semiconductor is sandwiched between two layers of wider-bandgap semiconductors. The hetero-junction between the smaller- and the wider-bandgap semiconductors constructs a potential well confining the electrons and holes within the smaller-bandgap material region results in quantization of electrons in the direction of confinement, namely, the z direction, and this becomes the model of particles in a one-dimensional box which energy levels in the other two dimensions are not discrete. Assuming that the confinement potential barrier for the square QW has infinite height, obtaining the energy levels in other two dimensions given by the effective-mass approximation as

$$E_{n,k_x,k_y} = E(c) + \frac{n^2\hbar^2}{8m_e^* l_z^2} + \frac{\hbar^2(k_x^2 + k_y^2)}{2m_e^*} \tag{2.5}$$

Where $n = 1,2,3,...$ are the quantum numbers, the first term $E(c)$ in the right-hand side is the energy corresponding to the bottom of the conduction band, the second

term is quantized energy, and the third term gives the kinetic energy of the electron in the x-y plane in which electrons are free to move. The density of states for a quantum-well structure is given by

$$D_{Qwells}(E) = \frac{m}{\pi\hbar^2}\sum_i H(E - E_i) \qquad \textbf{(2.6)}$$

where $i = 1, 2, 3, \ldots$ and $H(E - E_i)$ is the Heaviside's unit step function. It takes the value of zero when E is less than E_i, and value of 1 when E is equal to or greater than E_i. E_i is the i^{th} eigen-energy level within the quantum well.

2.1.4 Quantum Wires

Quantum wires represent two-dimensional confinements of carriers. Such confinement allows free-electron behavior in only one direction, along the length of the wire, says, the z direction then, the system of quantum wires may be described as one-dimensional electron gas, where electrons are present in the conduction band. A quantum wire can be cylindrical with a circular cross section as well as rectangular or square in the lateral x-y plane. A representative model of quantum wire in this thesis is a rectangular one with lateral dimensions l_x and l_y. Assuming that the confinement potential barrier for the square quantum wires has infinite height, the electronic energy levels of a quantum wire are given by

$$E_{n,k_x,k_y} = E(c) + \frac{n^2\hbar^2}{8m_e^* l_x^2} + \frac{n^2\hbar^2}{8m_e^* l_y^2} + \frac{\hbar^2 k_z^2}{2m_e^*} \qquad \textbf{(2.7)}$$

The energy of the one-dimensional quantum wire consists of a sum of four parts. The first term is due to the continuous band value given by the effective-mass approximation. The second and the third terms mention the quantization of electrons in the confinement directions, and the last term gives the kinetic energy of the electron in the z direction where electron is freely move. For this case, the density of states is given by

$$D_{Qwires}(E) = \frac{1}{\pi}\left(\frac{2m}{\hbar^2}\right)^{\frac{1}{2}} \sum_i H \frac{n_i(E-E_i)}{(E-E_i)^{\frac{1}{2}}} \qquad \textbf{(2.8)}$$

where $H(E-E_i)$ is the Heaviside's unit step function, and n_i is the degeneracy factor. For quantum structures with dimensions lower than 2, it is possible to find the same energy levels rather than one arrangement of confined states, therefore, a second factor $n_i(E)$ has been introduced for described about this.

2.1.5 Quantum Dots

When carriers are bounded in the three-dimensional confinement, which typical dimensions range between nanometers and tens of nanometers, a quantum - dot structures are represented . The electronic energy levels of the quantum dot are considered as

$$E_n = \frac{\hbar^2}{8m_e^*}\left(\frac{n_x^2}{l_x^2} + \frac{n_y^2}{l_y^2} + \frac{n_z^2}{l_z^2}\right) \qquad \textbf{(2.9)}$$

The density of states for the zero-dimensional quantum dot is

$$D_{Qdots}(E) = \sum_{E_n} \delta(E - E_n) \qquad \textbf{(2.10)}$$

where $\delta(E - E_i)$ is the delta function (sharp peak) which is similar to discrete energy level of atoms and $D(E)$ always has discrete values. A discrete value of $D(E)$ produces a sharp peak in the absorption and the emission spectrum of quantum dots even at room temperature which leads to the changes of structure and electrical properties. This kind of behavior is for the ideal case, however, due to other side effects, broadening of spectrum is generally observed in reality.

The change of density of states for the low-dimensional nanostructures (**Figure 2.1**) considerably affects the fundamental properties of the devices, which use these nanostructures as an active layer **[54]**. The electronic properties for QD structure differ drastically from the bulk system due to the discrete energy levels and delta peak density of states, which are in different from the continuous spectrum of the bulk. Hence QD structure sometimes was name as **artificial atom**. In case of QD structures, there are several theoretical and experimental proving that semi-conductor lasers consisting of QD structures have the lowest threshold current density because of the delta-function-like density of states **[55]**. **Figure 2.5** shows the historical evolution of the threshold current of semiconductor lasers **[56]**.

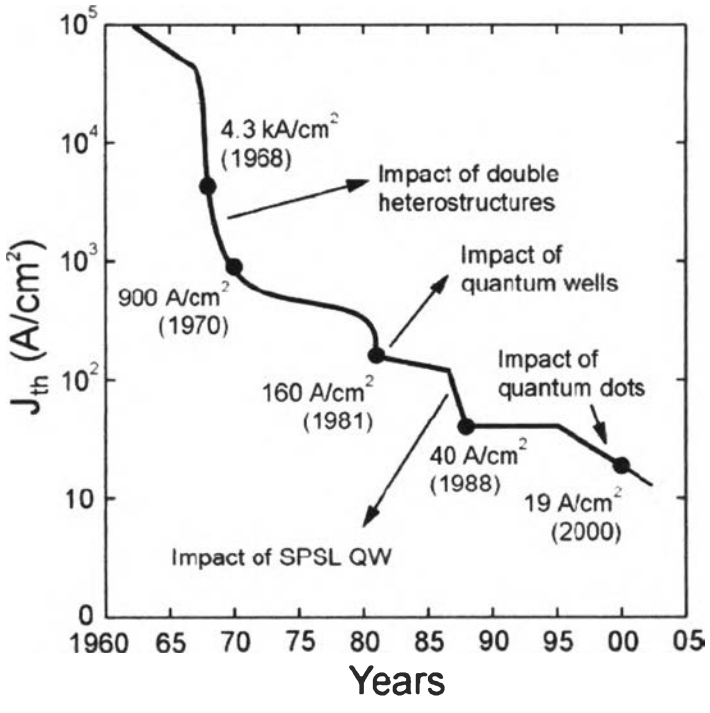

Figure 2.5 Evolution of the threshold current of semiconductor lasers **[56]**.

Utilizing QDs as an active layer for semiconductor lasers, there are two especially important considerations. First, the density of QDs must be high enough to achieve the lasing condition (gain overcomes the loss). Second, the QD size distribution should be narrow because the optical gain spectra depend on the size distribution. In other words, QDs should have the same size in order to reduce the charge carriers needed for the population inversion condition. It is possible to increase the maximum optical gain by increasing the QD density and/or reducing the size distribution of the QD ensemble.

In summary, the concept of low-dimensional nanostructures, i.e. QWs, QWRs, and QDs compared with bulk semiconductors was introduced. The general theoretical view of the size and the electronic properties, i.e., density of states was presented.

2.2 Quantum Confinement effects on Optical Properties of Semiconductor Nanostructures

In quantum dots structures, electrons are confined in all directions or being zero dimensional so important effects related with the electronic, physical, and optical properties of semiconductor nanostructures are interesting because these useful concepts lead to photonic device applications based on optical characterizations of low-dimensional nanostructures. In particular, quantum confinement effects are focused in this section since these are closely related with the optical properties **[57-59]** to describe some behaviors of them. The optical processes of nanostructures are summarized in the tree diagram as below.

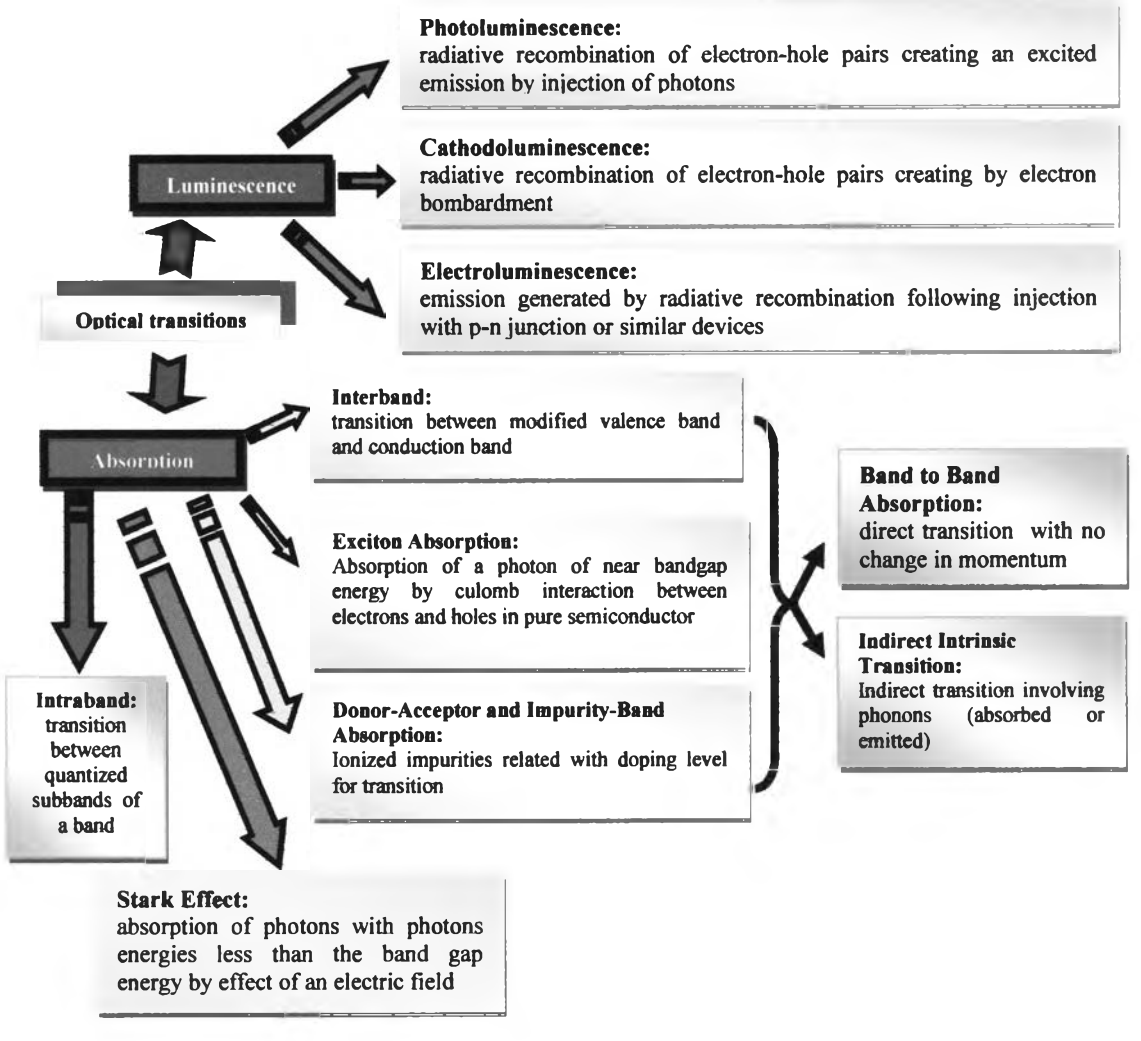

Figure 2.6 Tree diagram of optical transition of quantum-confined semiconductors.

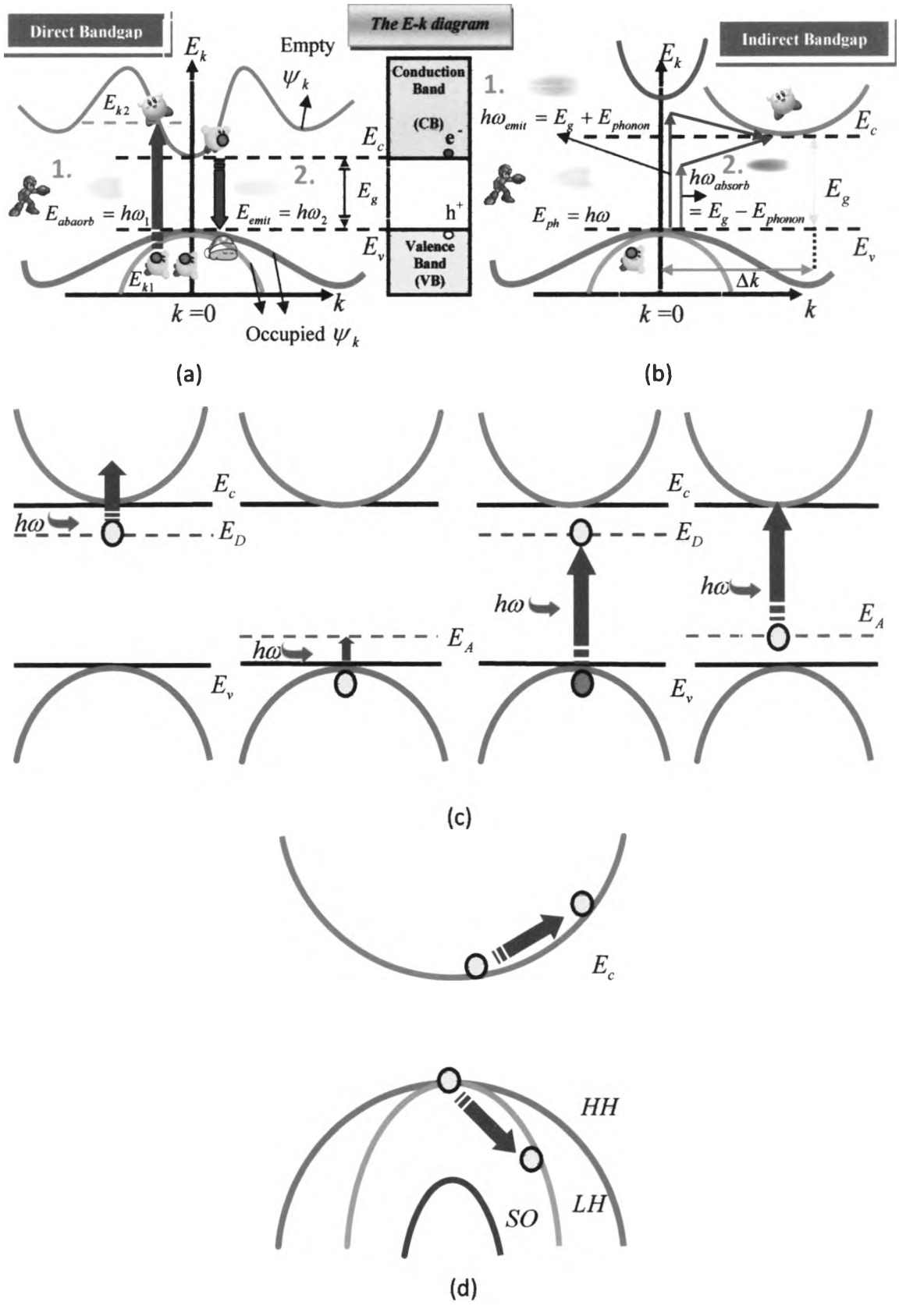

Figure 2.7 Process of the optical transition: (a) direct bandgap transition (b) indirect bandgap transition (c) impurity-band transition and (d) Intraband transition.

2.2.1 Optical Properties With Size Dependence

Quantum confinement is closely related to the bandgap of the nanostructure which optical characteristics depend on the size and shape of the individual crystal. By increasing the dimension of confinement bandgap is also increased (resulting in a blue shift) as well as appearance of discrete subbands corresponding to quantization along the direction of confinement. Therefore, quantum dots which smaller size have a larger bandgap with the greater the difference in energy between the highest valence band and the lowest conduction band becomes, more energy is needed to excite the dot, thus the interband transition shifts to the shorter wavelength or higher frequency (the structure of a certain size shows optical transition (absorption and emission) at a given frequency) and consequently, more energy is released when the carriers returns to its resting state. On the other hand, energy gap converges to the bulk value for a large size. These property is useful because of high level of control possible over the size of the crystals produced and allow for controlling the conductive properties of semiconductor materials.

2.2.2 Increase of Oscillator Strength

Optical transition is an important process to describe optical properties of semiconductor. An atom or a molecule can absorb light and move from one quantum state to another. The oscillator strength is a dimensionless quantity to express the strength of the transition which indicates the probability of an electron being excited from ground state to an excited state. For quantum confinement, it produces a major modification in the density of states, both for the valence band and the conduction bands. Instead of continuous, smooth distribution of the density of states, the energy is squeezed in a narrow energy range. This packing of energy states near the bandgap becomes more explicitly as the dimensions of confinement increase from bulk to quantum dot. For the quantum dots, the density of states has non-zero values only at discrete energies. The **oscillator strength** of an optical transition for an interband transition depends on the joint density of states of energy

levels in the conduction band and the valence band, between which the optical transition occurs. In addition, it also depends on the overlap of the envelope wavefunctions of electrons and holes. Both these factors produce a large enhancement of oscillator strength with a quantum confinement. This effect is more pronounced in quantum wires and quantum dots which are more confined structures. The presence of external factor such as magnetic field is also affected on oscillator strength via the increase of the exciton binding energy and oscillator strength due to the shrinkage of the exciton wave-function when increase a magnetic field and then exhibits a populated oscillator strength.

2.2.3 New Intraband Transition

The intraband transition involves the promotion of electrons from one state to another in the conduction band or hole from one state to another in the valence band as known in the name "free carrier absorption" in bulk semiconductor. These mechanism corresponding to absorption of a photon by the interaction with a free carrier within a band, which is consequently raised to a higher energy. In real bulk semiconductor, the valence band consists of three subbands; the light-hole band (LH), the heavy-hole band (HH) and the split-off band (SO) which are separated by the spin-orbit interaction and each band is different by curvature (effective masses of the corresponding holes). The absorption of photons with the right energy can result in transition from LH-to-HH, SO-to-HH, or SO-to-LH band, depending on the impurity doping (excess electron or hole) and temperature of the sample or charge injection by a bias field (photoinjection). In bulk semiconductor, transition from one level to another level within the same valley must conserve momentum. This momentum change is provided by optical or acoustic phonons, or by impurity scattering. The probability for an intraband transition in bulk semiconductor to occur is low compared with an interband transition because it is no requirement to change k value. Free carrier absorption usually manifests in the long wavelength region of the spectrum as a monotonic increase in absorption which depends on the

nature of the momentum-conserving scattering (ex. the involvement of acoustic phonons, optical phonons, or ionized impurities).

In quantum-confined nanostructures, there are subbands characterized by the different quantum numbers (n = 1, 2, 3, ...) corresponding to quantization along the direction of confinement (growth). Therefore, in the conduction band, the electron can move from one sublevel to another without changing its momentum. These new transitions are in IR and have been utilized to produce some devices such as inter-subband detectors and lasers, and still require the presence of a carrier in the conduction band (electron) or in the valence band (hole). The absorption coefficient of intraband transition increases rapidly with decreasing the size of the nanostructure. However, as size becomes small, the electronic states are no longer confined within the well, which produces a leveling off of the absorption coefficient.

2.2.4 Increased Exciton Binding Energy

Quantum confinement of electrons and holes also leads to enhanced binding energy between them and produces increased exciton binding energy compared with the exciton binding energy for bulk materials. However, actual binding energy is smaller than in the bulk because the wavefunction of the carriers penetrates into the barrier nearby. This binding produces the excitonic state just below the bandgap, giving rise to the sharp excitonic peaks at temperatures where the exciton binding energy is higher than the thermal energy. Thus, excitonic resonances are very pronounced in quantum confined structures and, in the strong confinement condition, can be seen even at room temperature.

2.2.5 Dielectric Confinement Effect

Quantum-confined structures also exhibit the dielectric confinement effect produced by the difference in the dielectric constant of the confined semiconductor region and the confining potential around it. However, each confined structure (quantum wells, quantum wires and quantum dots), depending on the method of fabricating and processing, may be embedded in the different semiconductor or a dielectric such as glass or polymer. If the dielectric constant of the surrounding medium is significantly lower than that of the confined semiconductor region, there will be important manifestations derived from different dielectric confinements as follows:

- Enhancement of Coulomb interaction between quantum confined states by virtue of the polarization charges which form at the dielectrically mismatched interfaces.

- Enhancement of the local field inside the quantum structure when illuminated by light.

2.2.6 Increase of Transition Probability in Indirect-Bandgap Semiconductors

In direct bandgap semiconductor, optical transition conveniently occurs because the valence band maximum lies at the zone center of $E-k$ diagram (k =0) and directly above the conduction band minimum so an upward or downward transitions of electrons are able to make transitions without a change in momentum, consistent with the selection rules. Examples of these substances are GaAs, InSb and other III-V and II-VI compounds which are widely used in semiconductor industry for optical devices. Unlike an indirect bandgap semiconductor such as silicon germanium, the process are quite different because the bottom of the conduction band and the top of the valence band do not lie at the origin of $E-k$ diagram (not

the same wave vector k) and transition of carriers require a change in momentum, or the involvement of a phonon to satisfy conservation of energy and momentum. Therefore, transition of electrons from the conduction band to the valence band is extremely weak, consequently, emission is not probable in the bulk form, for example, in bulk silicon. However, in a quantum-confined structure, confinement of the electrons produces a reduced uncertainty Δx and increased uncertainty Δk in its quasi-momentum. Confinement will relaxes the quasi-momentum Δk selection rule, and thus allowing the enhanced emission to be observed in porous silicon and silicon nano-particles. Making use some semiconductor materials, particularly silicon materials, having a benefit in case of available substance and low cost material so improvement them to the low-dimensional structure of these may allow for increasing an efficiency and be one of the interested choices for photonic devices.

2.2.7 Nonlinear Optical Properties Caused by the Quantum Confinement Effect

In materials which have quantum-confined structures also exhibit enhanced nonlinear optical effects, compared to the corresponding bulk materials. The two types of these, corresponding as follows:

- Electro-optic Effect. This effect is described as a change in optical properties by application of electric field which is derived from the Stark effect, that is, change of energy states by electric field as it is introduced in chapter 1.

- Optically Induced Refractive Index change. This is an effective third-order nonlinear optical effect, namely, Kerr effect.

Both of these effects in quantum confined structure can be described as dynamic nonlinearities that are derived from a change in the optical absorption ($\Delta\alpha$) and this change is related to Kramers-Kronig equation, the change, $\Delta\alpha$, in the

absorption to the corresponding change, Δn , in the real part of refractive index by following equation mentioned in **[59]**. The change of these two variables can be used for all optical switching, gathering and signal processing. Some of the main mechanisms producing Δn are briefly discussed below:

- Phase-space filling. This effect arises from the intensity-dependent changes in optical absorption, derived from a number of processes such as phase-space filling and bandgap renormalization. These processes are manifested at high excitation intensities.

- Bandgap Renormalization. There is an effective bandgap shrinkage that results from the many body interactions. The main effect is due to a combination of screened electron-hole interaction and exchange. As a result, the combination of these energy gives an effective energy gap that decreases with the carrier density (excitation density).

- Formation of Biexcitons **[59]**. A new optical transition is manifested on binding of excitons to produce bi-excitons. Pronounced changes in optical spectra are observed by applying an electric field along the confinement direction. This is called the "quantum-confined Stark effect" and can be utilized in electro-optic modulator.

The interesting effect of optical properties on quantum confinement regime is "**Quantum-Confined Stark effect**" considered deeply as a main topic in this thesis, particularly, in the quantum dot structure and extend to linearly aligned structure. The basic concepts will be discussed in **section 2.5**.

2.3 Quantum dots : Fundamentals, Physics, and Quantum Theoretical Concepts

2.3.1 Energy Levels

This section is introduced basic concepts of theoretical calculations because the thesis is focused on computational mathematics by using quantum mechanics theory, so the concepts related with this topic is moderately proposed to understand about the basic model used in this thesis work and prepare for deeply analysis on next chapter.

In theoretical studies about quantum dots many calculations both analytical or numerical approach are highlighted on the energy levels because it is important like a doorway to describe the information such as its electronic structures, carriers behavior, density of states, wavefunctions etc. Though perception about theoretical calculations an atomic structure of quantum dots remain inexplicit and need more development, many researchers attempt to modify the mathematical models to become more accuracy so that these models expect for represent as realistic models as possible. The complicated model related with numerical models are applied that include various parameters such as realistic shapes, effects of strain **[60-62]**, temperature dependent, effective mass, internal and external electric field, quantum spin.... etc. These parameters are strongly affect the result of the energy levels of the quantum dots, but to understand qualitative analysis, energy levels are often calculated by using the effective-mass approximation **[63]** by assuming a single electron in the conduction band of a periodic semiconductor and ignoring its spin for simplicity. For a plane wave with momentum k , its wavefunction can be written as

$$\psi_e(r) = e^{ik.r} u_{e,k}(r) \tag{2.11}$$

where $u_{e,k}(r)$ is periodic: $u_{e,k}(r+R) = u_{e,k}(r)$, where *R* is any lattice vector.

For a periodic potential, the electronic band structure and wavefunction can be derived from the Hamiltonian, which satisfies the symmetry of the semiconductor crystal following the Bloch theorem **[63]**. The framework of study focuses about near the band edges of direct-bandgap semiconductors, where the wave vector k (momentum of the particles) deviates by a small amount from a vector k_0 where a local minimum or maximum occurs. In the effective-mass approximation, the wavefunction of an electron that experiences a slowly varying potential in a direct-bandgap semiconductor is approximated as

$$\psi_e(r) = f(r) u_{e,0}(r) \tag{2.12}$$

where $f(r)$ is the envelope function, which satisfies the Schrödinger equation:

$$\left[-\frac{\hbar^2}{2m^*} \nabla^2 + V(r) \right] f(r) = E f(r) \tag{2.13}$$

where *m** is the effective mass, related to the curvature of the conduction band at $k = 0$, $V(r)$ is effective potential coming from different band offsets of different materials, and E is the energy of the state. Since $V(r)$ is periodic, all observable

quantities associated with the particle also be periodic and electron probability $|\psi_e(r)|^2$ must also be periodic following the condition on $f(r)$

$$|f(r+R)|^2 = |f(r)|^2 \tag{2.14}$$

In buried QDs (quantum-confined tiny region which is surrounded by another semiconductor material), the confining barrier V is of finite height as defined by the band offset of two different materials. Let assume that self assembled quantum dots are highly flattened in the growth direction (in z direction) comparing with lateral dimensions (x and y direction). It has been reported that the energy level spacing in the z direction can be fairly constant **[64]**. The lateral confinement of carriers by chosen potential for this kind of structure can be described in two dimensional potential

$$V(r) = \begin{cases} \frac{1}{2} m^* \omega_0^2 (x^2 + y^2) \text{ for } |z| < \frac{L}{2} \end{cases} \tag{2.15}$$

$$V(r) = +\infty \text{ for } |z| > \frac{L}{2} \tag{2.16}$$

where L defines the height of the quantum dots. The energy levels resulting from this Hamiltonian are **[65]**

$$E = (n_x + n_y + 1)\hbar\omega_0 + (\frac{\pi^2 \hbar^2}{2m^* L^2}) n_z^2 \tag{2.17}$$

where $n_x = n_y = 0, 1, 2, \ldots$, and n_z is an integer ≥ 1. Usually, L is assumed to be small, so that only the $n_z = 1$ states are considered. For InAs quantum dots, the spacing $\hbar\omega_0$ between the lowest two electron energy levels is typically in the range of 30-80 meV. The relevant wavefunctions that satisfy **Eq. (2.13)** are:

$$f(R) = H_{n_x}(x)H_{n_y}(y)e^{-\frac{1}{2}\frac{m^* \omega_0}{\hbar}(x^2+y^2)} \cos(\frac{\pi z}{l}) \quad \textbf{(2.18)}$$

where H_n are the Hermite polynomials **[66]**.

Generally, transition of electrons in the conduction band, the atomic orbital functions contained in $u_{e,0}(r)$ have *s*-like symmetry, and there is a spin degeneracy in the conduction band because the corresponding atomic orbital functions have *p*-like symmetry in the valence band. There are three subbands (heavy-hole, light-hole, split-off) having interaction with the conduction band **[63]**. The interesting will focus near the valence band edge and the conduction band edge mentioned above for simplicity ,so only the heavy holes in the valence band have been taken into account in calculation. It is assumed that the highest valence-band state (the hole "ground state") has a heavy-hole nature when the quantization axis is taken to be z, the axis of symmetry. It is often further assumed that the splitting between the first heavy-hole state and the first light-hole state is large, so that the light-hole states can be neglected in the perturbation-theory calculations.

2.3.2 Size Quantization in Quantum Dots

In calculation of electronic states in quantum dots, they are strongly depend on the dot shape and size which are determined by the growth conditions **[67]**. Theoretically, the shape of a dot was modelled in various types: lenses **[68]**, cones **[69]**, pyramidals **[70]**, disks or cylinders **[71]**, rectangular and spheres **[71]**. Moreover, types of fabrication process are also produce the different types of quantum dots. Recently, a rapid progress in nanofabrication techniques allowed researchers to use lateral structures fabricated using different growth techniques in order to create artificial quantum dots. Example of such technology is x-ray

nanolithography, e-beam lithography, nanoprinting, particularly, metalorganic vapour phase epitaxy (MOCVD) and molecular beam epitaxy (MBE) **[72]** which widely used over the past two decades. MOCVD grown quantum dots usually have pyramidal shape **[73]**. MBE grown quantum dots produce more shapes as mentioned above which is more precisely in case of controlling the substrate thickness and purely crystal.

The simplest models are rectangular and spherical quantum dots with infinite barriers treated in the isotropic-effective mass approximation. For such geometry, the Schrödinger equation in the effective mass approximation has to be solved numerically. This is another important difference between the reality and a simple model of a quantum dot. The model used in this thesis work is rectangular quantum dots which extend to finite barrier. However, this simple approach does not fully account for the physics of quantum dots, but sometimes it is an interesting choice in case of saving time for calculation and prediction the behaviors approximately to find the direct way before investigate intensively. The details of quantum dots model will be represented again in chapter 3 so this topic give a fundamental concept **only rectangular and spherical quantum dots**, corresponding all of the reasons mentioned above.

In heterostructures the space dependence of the effective mass lead to a strong interdependence of the longitudinal and transverse motion in systems with heterointerfaces **[74-75]**. Such interdependence results in additional non-parabolicity of the longitudinal, at large energies, the effective mass changes sign and the longitudinal two-dimensional spectrum terminates at a certain critical value of the longitudinal momentum. The space dependence of the effective mass also strongly increases the transmission through a potential barrier for electrons with large incidence angles. These effects have important consequences for impact ionization and tunneling phenomena in heterostructures.

The simple rectangular quantum dots model was described in Ivchenko *et al* **[76]**. The envelope function of electron confined in a $a_x \times a_y \times a_z$ rectangular quantum dots, or a quantum box is a product of this three envelopes below

$$\psi\ (r) = \varphi_{\nu_x}(x, a_x)\varphi_{\nu_y}(y, a_y)\varphi_{\nu_z}(z, a_z) \tag{2.19}$$

where

$$\varphi_\nu(x;a) = \sqrt{\frac{2}{a}}\begin{cases}\cos(\nu\pi x/a) & \text{for odd } \nu \\ \sin(\nu\pi x/a) & \text{for even } \nu\end{cases} \tag{2.20}$$

which describes the size-quantization in one particular direction, respectively x or y or z . The electron energy levels are

$$E_{e\nu_x\nu_y\nu_z} = \frac{\pi^2\hbar^2}{2m_A}\left[\left(\frac{\nu_x}{a_x}\right)^2 + \left(\frac{\nu_y}{a_y}\right)^2 + \left(\frac{\nu_z}{a_z}\right)^2\right] \tag{2.21}$$

where m_A is the electron's effective mass in the material A.

The electron states in a spherical quantum dots radius R are characterized by the electron orbital angular momentum l by the value of $l = 0$ when reaches the lowest energy electron state. For an infinitely high barrier, the ground state electron wave function has the form

$$\psi_s(r) = f(r)\,|\,s\rangle, f(r) = \frac{1}{\sqrt{2\pi R}}\frac{\sin(\pi r/R)}{r} \tag{2.22}$$

where spin index s assumes the values $\pm 1/2$ and the Bloch function $|s\rangle = c_s S$ by c_s $(s = \pm 1/2)$ are spin-up and spin-down states. The confinement energy is

$$E = \frac{\pi^2 \hbar^2}{2 m_A R^2} \tag{2.23}$$

Refining the procedure by finite barriers, then for the ground state

$$f(r) = \frac{C}{r} \begin{cases} \sin(kr) & \text{for } r \leq R \\ e^{-\aleph(r-R)} \sin(kR) & \text{for } r \geq R \end{cases} \tag{2.24}$$

where $\aleph = \sqrt{(\frac{2m_A(V-E)}{\hbar^2}) + k_z^2}$ and k_z is plane wave vector in z direction. C is a normalizing factor. By taking k_z = 0 the eigen-energies satisfy the equation

$$1 - kR \cot kR = (m_A / m_B)(1 + \aleph R) \tag{2.25}$$

One can present the spin or wave function $u(r)$ in general form as

$$u_s(r) = \left[f(r) + i\sigma_\alpha h_\alpha(r) \right] c_s \tag{2.26}$$

where i is imaginary term, for k_z = 0, $f(r), h_\alpha(r)$ are real functions. Symmetry of nanostructures impose restrictions on coordinate dependence of these functions. In particular, in rectangular structure, $f(r) = \sqrt{x^2 + y^2 + z^2}$ while the three functions $h_\alpha(r)$ or $(h_x(r), h_y(r), h_z(r))$ are identically equal to zero.

For the ground state of electron in rectangular box, all functions in **Eq. (2.26)** are nonzero and allow presentation

$$f(r) = f(x^2, y^2, z^2) \qquad h_x(r) = yzM_x(x^2, y^2, z^2)$$
$$h_y(r) = xzM_y(x^2, y^2, z^2) \qquad h_z(r) = xyM_z(x^2, y^2, z^2) \tag{2.27}$$

where f and M_α are arbitrary functions of x^2, y^2 and z^2.

A confined-hole state formed the four-fold spin degenerate band cannot be characterized by any definite value of the hole orbital angular momentum L. In the spherical approximation for the Luttinger Hamiltonian **[77]**, this is the total hole angular momentum $F = J + L$ by J is original angular-momentum which serves as a good quantum number. Therefore the hole state is $(2F+1)$ - fold degenerate due to the projection F_z of the angular momentum F along the z axis.

For the ground state $F = 3/2$, $F_z = \pm 1/2, \pm 3/2$. Orbital states with $L = 0, 2$ are involved in the formation of this four-degenerate state and the hole wave functions at the ground level are

$$\psi^{(h)}{}_{F_z}(r) = \sum_m \Re_{m,F_z}(r) \,|\, 3/2, m\rangle \tag{2.28}$$

As a function of r and J_i, the matrix $\hat{\Re}(r)$ must be a spherical invariant. There are only two linearly independent invariants, $r_\Delta{}^2 I$ and $(J_\Delta . r_\Delta)^2$, which can be obtained from products of the bilinear function r_i, r_j and the 4x4 matrices presented in **[77]**. Thus, matrix $\hat{\Re}(r)$ inside the dot is

$$\hat{\Re}(r)=\frac{1}{\sqrt{4\pi}R^{3/2}}\left\{f_0(\frac{r}{R})-f_2(\frac{r}{R})\left[\left(J_{\Delta}.\frac{r_{\Delta}}{r}\right)^2-\frac{5}{4}\right]\right\} \quad \textbf{(2.29)}$$

The radial functions $f_l(x)$ are defined as

$$f_l(x)=C\left[j_l(\phi x)-(-1)^{l/2}\frac{j_0(\phi)}{j_0(\sqrt{\beta}\phi)}j_l(\sqrt{\beta}\phi x)\right] \quad \textbf{(2.30)}$$

where $j_l(x)$ are the spherical Bessel functions, C is determined by the normalization condition

$$\int_0^1\left[f_0^2(x)+f_2^2(x)\right]x^2dx=1 \quad \textbf{(2.31)}$$

β is the light-to-heavy hole mass ratio, ϕ is the dimensionless parameter according to the hole-quantum-confinement energy at the ground state with energy

$$E^h=\frac{\hbar^2\phi^2}{2m_{hh}R^2} \quad \textbf{(2.32)}$$

For the infinite barrier potential the envelope function vanishes at $r=R$ and leads to simple equation

$$j_0(\phi)j_2(\sqrt{\beta}\phi)+j_2(\phi)j_0(\sqrt{\beta}\phi)=0 \quad \textbf{(2.33)}$$

which the spherical Bessel functions

$$j_l(x)=\sqrt{\frac{\pi}{2x}}J_{l+1/2}(x) \quad \textbf{(2.34)}$$

and the first three terms are

$$j_0 = \frac{\sin x}{x},\ j_1 = \frac{\sin x}{x^2} - \frac{\cos x}{x},\ j_2 = \left(\frac{3}{x^3} - \frac{1}{x}\right)\sin x - \frac{3\cos x}{x^2} \qquad \textbf{(2.35)}$$

For $\beta \to 1$, the light and heavy-hole subbands in a bulk semiconductor merge to form one four-fold degenerate band. In this hypothetic limit the envelope function is spin-independent and, for the ground state, coincides with the electron envelope.

Additionally, it has been reported in other research as rectangular quantum dots **[78-80]** included this thesis work. The details about modification of rectangular quantum dots will be discussed in chapter 3.

2.3.3 Spontaneous Emission of Quantum Dots

The topic described in this section is related to the effect of spontaneous emission of quantum dots by electron-hole pairs interaction. Scull *et al* **[81]** used the Hamiltonian corresponding equation with dipole approximation to explain the optical properties of the quantum dot under the electromagnetic field. The spontaneous emission mentioned in this topic is focused on the lowest-energy electron-hole state. There are two cases for describing about luminescence from the quantum dots. Firstly, in the low excitation state, carriers (electron-hole pairs) are slowly injected into a quantum dot. Both electrons and holes relax their energy from the higher excited state to the lowest state quickly in the same band (intraband transition) via releasing phonon, after that, electrons from the lowest state in conduction band is moving to the valence band to manifest the radiative recombination with small transition lifetime (about 1 ns). The second is in circumstance with high excitation (rapidly carriers injected), emission from higher

excited states becomes prominent so the ground-state recombination is faster than the carrier injection, therefore, the quantum dots begin to be filled with carriers.

To extend the effect mentioned above more obviously, electronic density of states the optical properties of quantum dots are related to, in particular, optical transitions are allowed only at discrete energies due to the zero-dimensional density of states. Photoluminescence from a single QD is shown in **Figure 2.8**. The δ-like sharp transition is strictly true only in the limit of small carrier numbers (1 exciton per dot on average) since many-body effects **[82]** come into play that can include the recombination from charged excitons or multiexcitons. At very low excitation density the recombination spectrum consists only of the one-exciton (X) line. With increasing excitation density small satellites on either side of the X-line develop that are attributed to charged excitons (trions) **[83]** X^+ and X^-. On the low-energy side, the biexciton (XX) appears. Moreover, the excited states are populated and a multitude of states contribute with rich fine structure. The charging state of the exciton can be controlled in a field-effect structure. The recombination energy is modified due to Coulomb and exchange effects with the additional carriers.

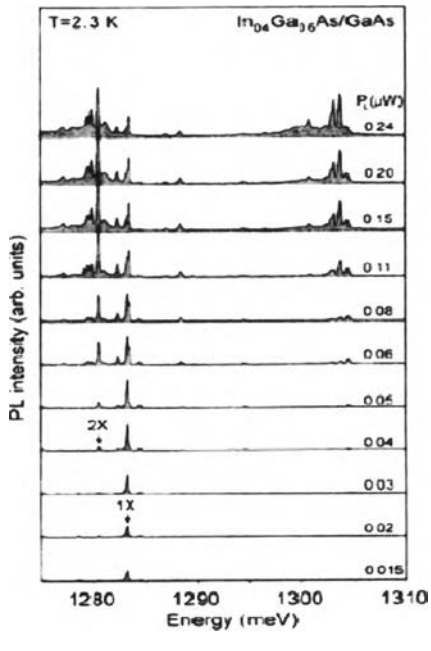

Figure 2.8 Optical emission spectra of a single InGaAs/GaAs QD at different laser excitation levels **[35]**.

The size of quantum dots is also affected to the emission of light because of some important factor such as degree of confinement, size-dependent with bandgap, carriers interaction etc. Scull *et al* represented this phenomena by assuming the transition occurs between conduction electrons and heavy holes. The effective-mass approximation were used with conserve in a dipole transition and consider of total angular momentum with spin values corresponding to the exciton state of electron and hole wavefunction. Manipulating these condition so the result indicates that the spontaneous emission rate by emitted photon depends on the dipole moment which depends on the material parameter and especially on the overlap between the electron and hole envelope functions or transition strength. For the large quantum dot, the spontaneous emission rate is higher than the miniature quantum dot which non-interacting-particle approximation is often used in this case. To explain the effect of emission from the large quantum dot, the electron and the hole become correlated, due to the electrostatic interaction between them and the natural exciton Bohr radius a_B^* is smaller than the quantum dot radius a, the overlap integral of two particle envelope function is strengthen so this electron-hole overlap term can increase by (a/a_B^*) 3/2 larger than the smaller quantum dot. In a quantum dot ensemble, optical transitions are inhomogeneously broadened because of fluctuations in the quantum dot size and the size dependence of the confinement energies. Interband transitions involving electrons and holes suffer from the variation of the electron and hole energies. The confinement effect leads to an increase of the recombination energy with decreasing quantum dot size. In addition, when the dot size is closed to the wavelength of light in the crystal, the lifetime does not decrease further, but rather the emission becomes directional. The center-of-mass angular momentum of the exciton is transferred into the momentum of the emitted photon, as in quantum-well structures.

The information about spontaneous emission of quantum dots have been extended by many research groups in case of the theoretical calculations go along with the experimental to investigate the absolutely effects under this crucial

phenomena. Many theoretical calculations have been attempted to explain the optical properties which expect for good agreement with the experimental results for describing these results in form of the definitive concepts and physical meanings. Some interesting theoretical calculations were appeared in Zora *et al* **[84]** which is related to the effect of spontaneous emission of quantum dots by electron-hole pairs in linear regime. Zora *et al* developed a quantum mechanical theory interaction of light and electron–hole excitations in semiconductor quantum dots for estimating even in the realistic structures. Zora *et al* demonstrated a theory for the spontaneous emission of individual quantum dots or quantum dot molecules, taking into account the interaction of the electron–hole excitations with light. To overview the method, first, assuming that the total Hamiltonian of the system consists of the single-particle Hamiltonian, the free-photon Hamiltonian, the electron–hole interaction Hamiltonian, and the Hamiltonian that expresses the interaction of carriers with the light. Then, utilizing the Heisenberg equation of motion to the photon number expectation values, to the carrier distribution functions $f^{\mu e}$, $f^{\nu h}$ and to the correlation term between the photon generation or destruction and electron–hole pair destruction or generation to obtain a set of luminescence equations. Finally, solving these equations under incoherent **[85]** and quasi-equilibrium conditions in the linear regime $(1-f^{\mu e}-f^{\nu h}\approx 1)$ for solution of the photoluminescence intensity.

2.3.3.1 The physical system

To begin with, the physical system can be described by the following Hamiltonian:

$$H = H_{sp} + H_{\gamma} + H_{cc} + H_{c\gamma} \qquad \textbf{(2.36)}$$

H_{sp} describes the single-particle system in the presence of an external electric or magnetic static field. The second term, H_{γ} refers to the free-photon system. H_{cc} is the carrier–carrier interaction and $H_{c\gamma}$ stands for the interaction of the carrier under the photon field. Next, the usual second-quantization field operators were introduced for explicit form in quantum dots as follows:

$$\begin{aligned}\Psi^{\dagger}(r,t) &= \sum_{\mu} c^{\dagger}{}_{\mu}(t)\Phi^{\mu e^{*}}(r) + \sum_{\nu} d_{\nu}(t)\Phi^{\nu h}(r) \\ \Psi(r,t) &= \sum_{\mu} c_{\mu}(t)\Phi^{\mu e}(r) + \sum_{\nu} d^{\dagger}{}_{\nu}(t)\Phi^{\nu h^{*}}(r)\end{aligned} \qquad \textbf{(2.37)}$$

$\Phi^{\mu e}$ and $\Phi^{\nu h}$ are are the single-particle envelope functions **[86]**. $\mu e(\nu h)$ denotes the different electron (hole) states. $c^{\dagger}{}_{\mu}$ and $d^{\dagger}{}_{\nu}$ are the electron and hole operators respectively. The Hamiltonian of the non-interacting carriers confined in the quantum dot and subjected to an external magnetic field is given by **[87]**

$$H_{sp} = \int dr \hat{\Psi}^{\dagger}(r,t)\left[\frac{(-i\hbar\nabla_{r} - \frac{e}{c}\mathrm{A}(r,t))^{2}}{2m^{*}} + e\phi(r,t) + V(r)\right]\hat{\Psi}(r,t) \qquad \textbf{(2.38)}$$

where $V(r)$ is the three-dimensional quantum dot confining potential. $\mathrm{A}(r,t)$ and $\phi(r,t)$ are the vector and scalar potentials of the external magnetic field respectively. Inserting the second-quantization field operators to the single-particle Hamiltonian, then,

$$H_{sp} = \sum_{\mu\mu'} E^{e}{}_{\mu\mu'} c^{\dagger}{}_{\mu}(t) c_{\mu'}(t) + \sum_{\nu\nu'} E^{h}{}_{\nu\nu'} d^{\dagger}{}_{\nu}(t) d_{\nu'}(t) \qquad \textbf{(2.39)}$$

where the matrix elements $E^{e}{}_{\mu\mu'}$ and $E^{h}{}_{\nu\nu'}$ are

$$E^{e}_{\mu\mu'} = \int dr \Phi^{\mu e*}(r) \left[\frac{(-i\hbar\nabla_r - \frac{e}{c}\mathrm{A}(r,t))^2}{2m^*} + e\phi(r,t) + V(r) \right] \Phi^{\mu' e}(r)$$

$$E^{h}_{\nu\nu'} = \int dr \Phi^{\nu h*}(r) \left[\frac{(-i\hbar\nabla_r - \frac{e}{c}\mathrm{A}(r,t))^2}{2m^*} + e\phi(r,t) + V(r) \right] \Phi^{\nu' h}(r) \quad \textbf{(2.40)}$$

Since single-particle eigenfunctions are assumed to be orthonormal, the single-particle Hamiltonian is finally written as

$$H_{sp} = \sum_{\mu} E^{\mu e} c^{\dagger}_{\mu}(t) c_{\mu'}(t) + \sum_{\nu} E^{\nu h} d^{\dagger}_{\nu}(t) d_{\nu}(t) = H_{se} + H_{sh} \quad \textbf{(2.41)}$$

$E^{\mu e}$, $E^{\nu h}$ are electron and hole eigenenergies. The free-photon Hamiltonian is given by

$$H_{\gamma} = \sum_{q} \hbar\omega_q \alpha^{\dagger}_{q}(t) \alpha_q(t) \quad \textbf{(2.42)}$$

where $\alpha^{\dagger}_{q}(t)$ and $\alpha_q(t)$ are the creation and destruction nonlocal photon operator respectively, and $\hbar\omega_q$ is the photon energy.

The carrier–carrier interaction is described by the two-body Hamiltonian **[87]** by

$$H_{cc} = \frac{1}{2} \int dr \int dr' \hat{\Psi}^{\dagger}(r,t) \hat{\Psi}^{\dagger}(r',t) V^{cc}(r-r') \hat{\Psi}(r',t) \hat{\Psi}(r,t) \quad \textbf{(2.43)}$$

Inserting the second-quantization field operators and neglecting terms that do not conserve the number of electron–hole pairs (such as Auger recombination and impact ionization or terms that refer to interband exchange interaction **[88]**, the result is

$$H_{cc}=\frac{1}{2}\sum_{\mu_1\mu_2\mu_3\mu_4}V^{ee}_{\mu_1\mu_2\mu_3\mu_4}c_{\mu_1}{}^{\dagger}c_{\mu_2}{}^{\dagger}c_{\mu_3}c_{\mu_4}+\frac{1}{2}\sum_{\nu_1\nu_2\nu_3\nu_4}V^{hh}_{\nu_1\nu_2\nu_3\nu_4}d_{\nu_1}{}^{\dagger}d_{\nu_2}{}^{\dagger}d_{\nu_3}d_{\nu_4}$$
$$-\sum_{\mu_1\mu_2\nu_1\nu_2}V^{eg}_{\mu_1\nu_1\nu_2\mu_2}c_{\mu_1}{}^{\dagger}d_{\nu_1}{}^{\dagger}d_{\nu_2}c_{\mu_2}=H_{ee}+H_{hh}+H_{eh} \qquad \textbf{(2.44)}$$

The Coulomb matrix elements have been determined in **[86]** by

$$V^{cc}_{k_1k_2k_3k_4}=\int dr\int dr'\Phi^{k_1*}(r)\Phi^{k_2*}(r')V^{cc}(r-r')\Phi^{k_3*}(r')\Phi^{k_4*}(r) \qquad \textbf{(2.45)}$$

The Hamiltonian $H_{c\gamma}$ is obtained when the light field is treated quantum mechanically **[89-90]** expressed by

$$H_{c\gamma}=\mathrm{A}_0^{1/2}i\sum\omega_q^{1/2}\left[\mathrm{M}^{*}_{\mu\nu}\alpha_q^{\dagger}(t)d_{\nu}(t)c_{\mu}(t)-\mathrm{M}_{\mu\nu}\alpha_q(t)c_{\mu}^{\dagger}(t)d_{\nu}^{\dagger}(t)\right.$$
$$\left.-\mathrm{M}_{\mu\nu}\alpha_q^{\dagger}(t)c_{\mu}^{\dagger}(t)d_{\nu}^{\dagger}(t)+\mathrm{M}^{*}_{\mu\nu}\alpha_q(t)d_{\nu}(t)c_{\mu}(t)\right] \qquad \textbf{(2.46)}$$

where $\mathrm{M}_{\mu\nu}=e\int\Phi^{\mu e*}(r)r\Phi^{\nu h*}(r)$ are the total dipole matrix elements **[91]** and A_0 is the amplitude of the vector potential of the photon field. The kinetic description is based on the density matrix formalism by considering the operator $\wp_{\mu\nu}(t)=d_{\nu}(t)c_{\mu}(t)$. The expectation value which gives the microscopic (optical) polarization of the system. The intraband electron and hole single-particle density matrices are also considered below

$$\hat{n}_{\mu\mu'}=c_{\mu}^{\dagger}c_{\mu'}$$
$$\hat{n}_{\nu\nu'}=d_{\nu}^{\dagger}d_{\nu'} \qquad \textbf{(2.47)}$$

where the expectation values of the diagonal elements correspond to electron and hole distribution functions $f^{\mu e}$ and $f^{\nu h}$.

2.3.3.2 The luminescence equations

In this case the Heisenberg equation of motion is applied to the photon number expectation values $\langle a_q^\dagger a_{q'} \rangle$, and to the field–matter correlations of the type $\langle a_q^\dagger \wp_{\mu\nu} \rangle \equiv \langle a_q^\dagger d_\nu c_\mu \rangle$, so the set of luminescence equations are obtained. The dynamics for the expectation values of $\wp_{\mu\nu}, \hat{n}_{\mu\mu'} (or\ \hat{n}_{\nu\nu'})$ is partly determined by combinations of four-carrier operators due to the Coulomb interaction as well as by a mixture of one-photon and two-carrier operators as a result of the quantized light–matter interaction. For the decoupling of the above combinations we use the semiclassical Hartree–Fock scheme **[85]** which does not anticipate the influence of dephasing and this effect will included through a small damping constant γ, which in the relaxation time approximation is related to the dephasing time $\tau = \hbar / \gamma$. The main point is focused on the theoretical analysis of incoherent luminescence, where shortly after an optical excitation of the carriers high above the dot discrete states non-resonant with the bound excitonic states, all coherent polarizations dephase. In the specific case of very small electron and hole distribution functions $\overline{f^{\mu e}}^{\nu h}$ (in the linear regime where $1 - f^{\mu e} - f^{\nu h} \approx 1$), the renormalization term of the single-particle energies can be neglected **[89]**, and the three luminescence equations become

$$i\hbar \frac{\partial \langle a_q^\dagger a_{q'} \rangle}{\partial t} = \hbar(\omega_{q'} - \omega_q) \langle a_q^\dagger a_{q'} \rangle + iA_0^{1/2} \sum_{\mu\nu} \left[M_{\mu\nu}^* \omega_{q'}^{1/2} \langle a_q^\dagger \wp_{\mu\nu} \rangle + M_{\mu\nu} \omega_{q'}^{1/2} \langle a_{q'} \wp_{\mu\nu}^\dagger \rangle \right] \tag{2.47}$$

$$i\hbar \frac{\partial \langle a_q^\dagger \wp_{\mu\nu} \rangle}{\partial t} = (E^{\mu e} + E^{\nu h} - \hbar\omega_q) \langle a_q^\dagger \wp_{\mu\nu} \rangle - M_{\mu\nu} \sum_{q'} iA_0^{1/2} \omega_{q'}^{1/2} \langle a_q^\dagger a_{q'} \rangle - \sum_{\mu'\nu'} V_{\mu\mu',\nu\nu'}^{eh} \langle a_q^\dagger \wp_{\mu'\nu'} \rangle + if^{\nu h} M_{\mu\nu} A_0^{1/2} \omega_q^{1/2} \tag{2.48}$$

and

$$i\hbar\frac{\partial f^{\mu e}}{\partial t} = 2i\mathrm{A}_0^{1/2}\sum_{q\nu}\omega_q^{1/2}\,\mathrm{Im}\left[-i\mathrm{M}_{\mu\nu}^{*}\langle\alpha_q^{\dagger}\wp_{\mu\nu}\rangle\right] \qquad \textbf{(2.49)}$$

For given carrier densities, i.e., under quasi-equilibrium conditions, the above set of equations is restricted to the closed set of equations **Eq. (2.47)** and **Eq. (2.48)**.

2.3.3.3 The QD photoluminescence intensity

To reduce some complicated calculation, making the assumption that the pure stimulated term analogous to $\langle a_q^{\dagger}a_{q'}\rangle$ is artificially switched off. Using the notation $l \equiv \mu\nu$ equation **Eq. (2.48)** becomes

$$i\hbar\frac{\partial}{\partial t}\langle a_q^{\dagger}\wp_l(t)\rangle = \sum_{l'}(S_{ll'} - \hbar\omega_q\delta_{ll'})\langle a_q^{\dagger}\wp_{l'}\rangle + if^{\mu e}f^{\nu h}\mathrm{A}_0^{1/2}\omega_q^{1/2}\mathrm{M}_l \qquad \textbf{(2.50)}$$

where $S_{ll'} \equiv T_{ll'}\delta_{ll'} - V_{ll'}^{eh}$ is the excitonic matrix **[86]**, and $T_l \equiv E^{\mu e} + E^{\nu h}$ is the summation of the single-particle energies. Finally, solving analytically the closed set of equations **Eq. (2.47)** and **Eq. (2.50)** and find an approximate solution of the photoluminescence intensity $(I_{em}(\omega_q) \equiv \frac{\partial}{\partial t}\langle a_q^{\dagger}a_q\rangle)$

$$I_{em} \propto \mathrm{Im}\sum_{\lambda}\left[\frac{1}{(E^{\lambda} - \hbar\omega_q - i\gamma)}\int dr\Psi^{\lambda}(r,r)\int dr\sum C_l^{\lambda^*}\Phi^{\mu e^*}(r)\Phi^{\nu h^*}(r)f^{\mu e}f^{\nu h}\right] \qquad \textbf{(2.51)}$$

where $\Psi^{\lambda}(r,r)$ is the excitonic eigenfunction which is expanded in terms of the single-particle states **[86]**. In the high-temperature regime the carrier occupation probabilities are given by the Fermi–Dirac distribution functions **[51]**. The above

formula for the PL intensity can be applied to single or double quantum dots of any given geometry and under a magnetic field of any magnitude and orientation.

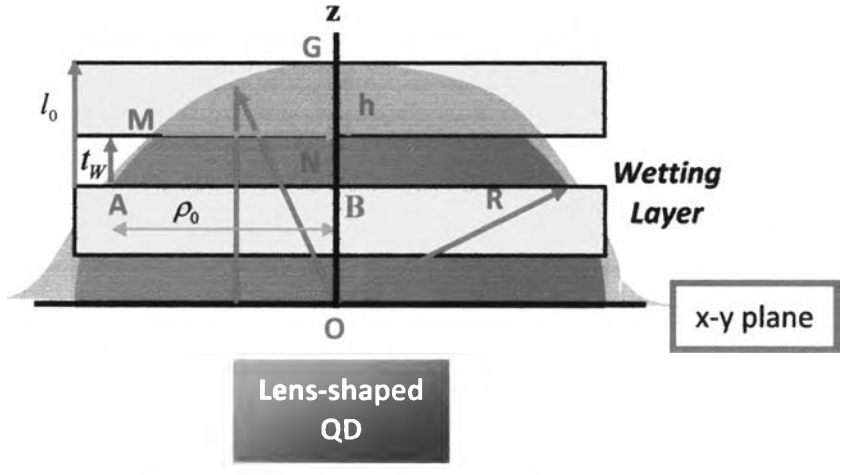

Figure 2.9 Cross-sectional view of an ideal lens-shaped QD. (AB) = ρ_0, (MN) = s the radius at the base, and (GN) = h the height of the dot.

The theoretical results were used to interpret the experimental findings reported by Matsuda *et al* **[93]**. However, Zora *et al* approximate the specific $In_{0.5}Ga_{0.5}As$ self-assembled quantum dot with a lens-shaped potential (**Figure 2.9**). *s* is the radius at the base and *h* = *(*GN*)* the height of the quantum dot. The thickness of the wetting layer (WL) is t_W = 4 ML **[93]**, which equals to 1.1 nm according to the values reported in **[94]**. As shown in **Figure 2.9**, a quantum well of thickness $l_0 = h + t_W$ can become a lens-shaped quantum dot of similar total thickness at the center and radius $\rho_0 = l_0 \sqrt{1 + \frac{s^2 - h^2 - 2t_W h}{h l_0}}$.

In the III–V semiconductor material system, the SK process allows for the dislocation free and strained coherently with the formation of InAs islands on GaAs, so the bulk GaAs effective mass value can be used approximate the strained $In_{0.5}Ga_{0.5}As$ material in the dot **[94]**. Furthermore, for strained $In_xGa_{1-x}As$ one

expects the mixing between light and heavy holes to be small, therefore, approximate the hole energy levels in the same way as for an electron **[68]** (i.e., one band approximation **[95]**) but with a different effective mass and depth of confining potential. The electron (hole) effective mass is $0.063\,m_e$ ($0.11\,m_e$) **[96]**, where m_e is the electron mass. For the conduction-band and valence-band offsets the potential energy takes a value of $\Delta V_{CB} = 224$ meV and $\Delta V_{VB} = 180$, respectively. Zora *et al* also calculate the single-particle eigenstates of electrons and holes within the effective mass and envelope function approximations **[86]** by using an expansion within a periodicity box of the electron (or hole) envelope functions into the orthonormal plane-wave basis **[86]**, then, the eigenenergies is obtained by full three-dimensional (3D) numerical diagonalization following eigenvalue problem:

$$\sum_{k'}\left[\langle k|\left(\frac{p^2}{2m^*}+V(r)\right)|k'\rangle - E^{\mu}\delta_{k,k'}\right]\langle k'|\Phi^{\mu}\rangle = 0 \qquad \textbf{(2.52)}$$

The 3D confining potential is zero inside the wetting layer and the self-assembled dot, and ΔV_{CB} (or ΔV_{VB}) inside the barrier. The single-particle eigenfunctions have cylindrical symmetry and resemble the Darwin–Fock states **[97]**.

Zora *et al* also presented the theoretical results for the PL intensity which is as good agreement as reported both in experimental **[98-99]** and in theoretical studies **[100]**, where the dephasing of optical transitions in QDs has been attributed to secondorder elastic (i.e., without changing the populations of the carrier energy levels) interaction with LO phonons. Their theoretical approach for the emission spectra of quantum dots explains satisfactorily the experimental data reported for the PL spectra collected with a high spatial resolution nearfield microscope. Additionally, it allows the determination of the inter-level spacing as well as the LO phonon dephasing time.

2.4 GROWTH OF THE QUANTUM DOT

In this section, the short review of fabrication technique is nominally described for representation the roughly growth process. It consists of two main parts. The first one is molecular beam epitaxy (MBE) which is highlighted to the equipment included some measurement tools and shown the advantages for this technique. The second one is the growth of self-assembled aligned quantum dot in order to provide some basic understanding of growth method and its structure which is used as a mathematical model for theoretical calculation.

2.4.1 Molecular Beam Epitaxy (MBE)

Molecular beam epitaxy (MBE) is a process for growing thin, epitaxial films of a wide variety of materials, ranging from oxides to semiconductors to metals. It was applied to the growth of compound semiconductors **[101]**. It is an interesting process because of the high technological value of such materials to the electronics industry. MBE has widely used in the last two decades recently as a popular technique for growing III-V compound semiconductors. In this process beams of atoms or molecules in an ultra-high vacuum environment are incident upon a heated crystal that has previously been processed to produce a nearly atomically clean surface. The arriving constituent atoms form a crystalline layer with the substrate (i.e., an epitaxial film). These films are special because the composition can be rapidly changed, producing crystalline interfaces. Thus, it has been possible to produce a unique structure, including quantum dot structure and superlattices structure. In solid-source MBE, different material source cells in separate crucibles are heated with separate heaters. They are evaporated and condensed on a wafer, where they react with each other, forming a crystal. With clean and ultra high vacuum (UHV) environment, It produce high-quality layers to form a perfect crystal.

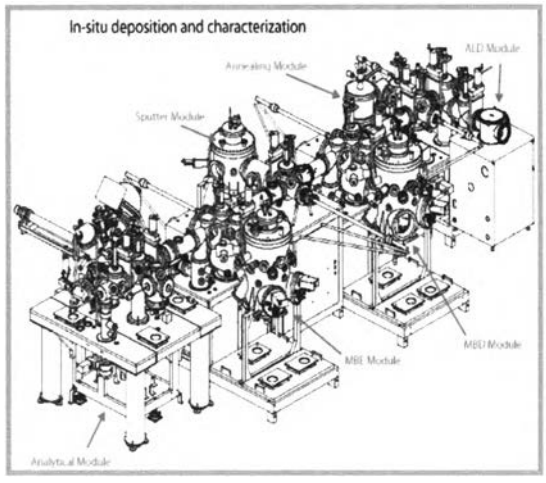

(a)

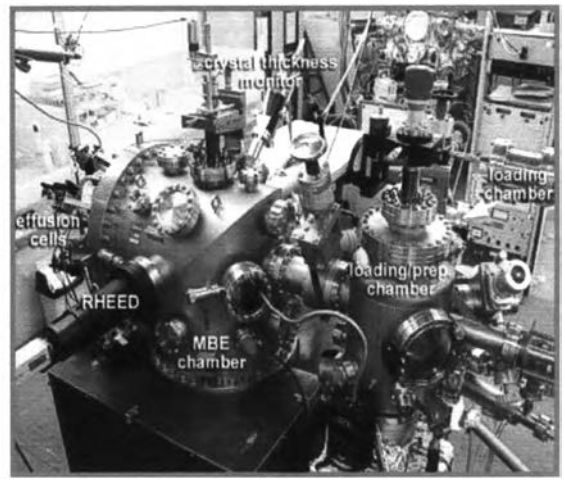

(b)

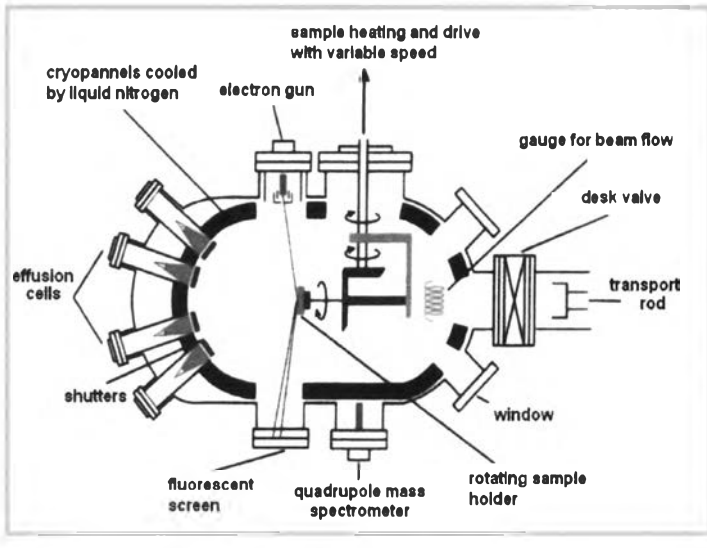

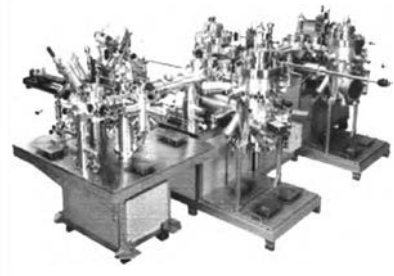

(c)

Figure 2.10 (a) and (b) Picture of MBE system. (c) Schematic diagram of the growth chamber **[102-104]**.

The remarkable advantage of MBE compared to other growth techniques is a controlled shutter in front of each cell allows precise control of layer thickness, doping, and composition via the powerful control of beam fluxes and growth conditions. The temperatures of the sources can be accurately controlled. In addition, it enables to study the surface structure all time during the growth (real-time monitoring) by reflection high energy electron diffraction (RHEED) **[105]** tool

which allows directly measurement of surface structure of the sample and the already grown epilayer. Since MBE is able to fabricate the atomic structure, quantum devices can be achieved following quantum effect with high efficiency, high speed and high performance. From the reason mentioned above, MBE structures closely approximate the idealized models used in solid state theory.

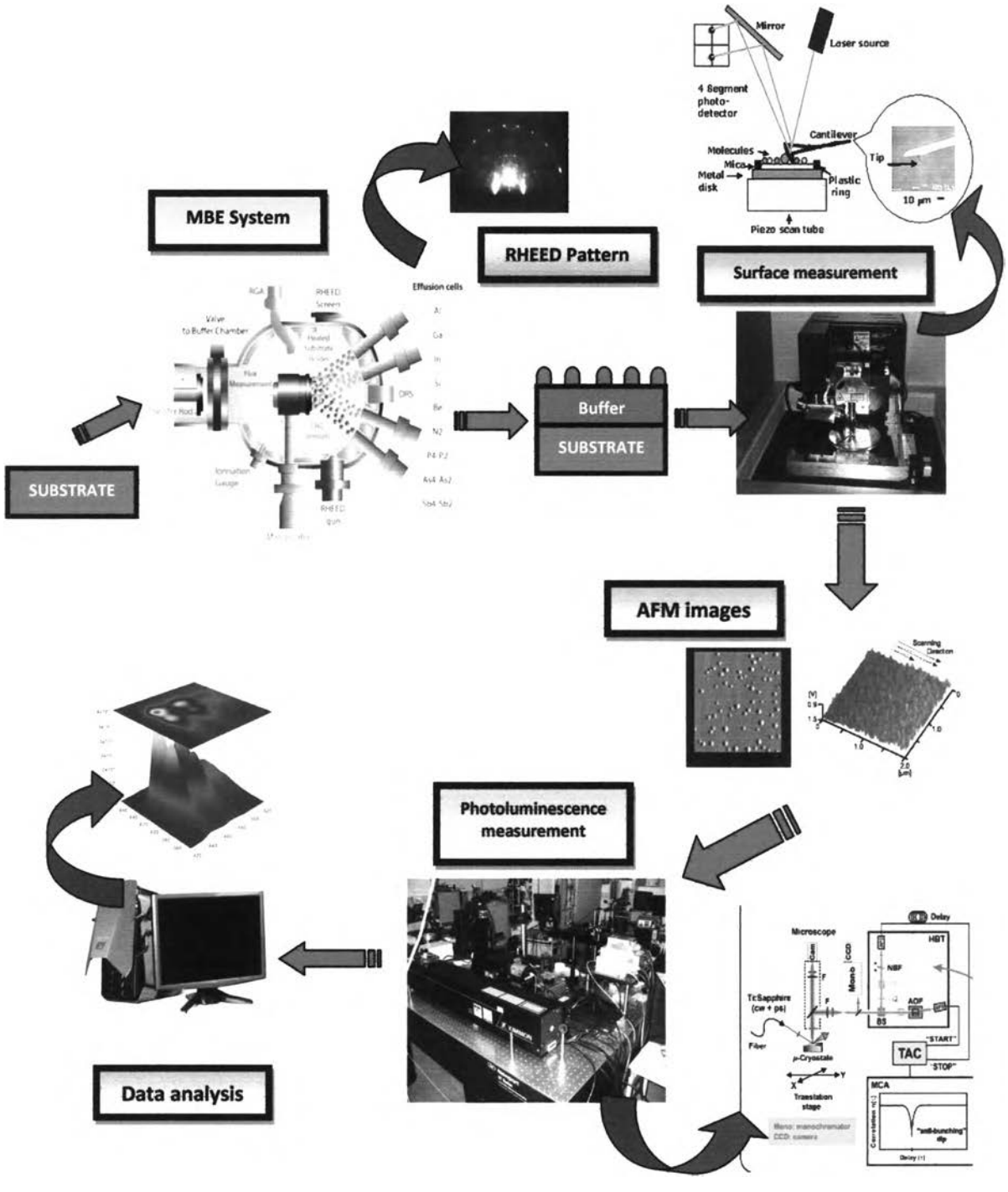

Figure 2.11 Overall process of fabrication semiconductor structure included measurement and data analysis.

The overall process of fabrication semiconductor structure is shown in **Figure 2.11**. Firstly, sample is grown on substrates in a solid-source MBE system. In sample preparation, the substrates need to be preheated by heaters in introduction chamber to eliminate contaminated substance. After that, the fabrication is started by growing buffer layer to flatten the surface. Then, opening the shutter of effusion cells (containing with different type of substances) for deposition the molecular beam of substance which desires to grow on the substrate at appropriate temperature and pressure in the growth chamber. During the growth, we can observe the surface structure by using RHEED system in terms of RHEED pattern, which gives an information of the dynamics of MBE growth. The RHEED system allows observing and measuring important parameters such as growth rates. As a result, the perfect crystal is done. For optical measurement, however, the sample needs to be capped with a thin layer (mostly by GaAs capping layer because of its bandgap properties). In case of studying the surface morphology of samples. Atomic force microscopy (AFM) is a powerful microscope for the observation of matter at nanoscale **[106]**. The AFM provides a 3D surface profile and can analyze heights at the sub-nm level. In optical measurement, Photoluminescence (PL) spectroscopy is a tool for sample luminescence characterization **[107]**. The sample was excited by laser beam by photon absorption, then, the sample releases the absorbed energy in form of emitted light which energy equals to its bandgap energy. The resolved light is finally detected by a detector for interpretation of PL data and analyzing the information to estimate the electronic structure of the sample. In addition, other measurement such as, electric field measurement (Stark effect) or magnetic field measurement are available by adding the electrode on the sample for preparation in experimental of their effects.

2.4.2 Self-Assembled Growth Modes

Following a bottom-up technology, the **self-assembled growth** has attracted increased interest as a means for fabricating epitaxial nano-scale structures, especially in QD structure, as mentioned in chapter 1. The self-assembled quantum dots growth is the the growth of epitaxial (homo or hetero) thin films with a lattice mismatched structure on a single crystal substrate, the lattice constant of the first few monolayers (MLs) **[108]** of the deposited material is forced to match that of the substrate which depends critically on the interaction strength between adatoms and the surface. The change from the desired lattice constant creates strain in the deposited layer. After a few MLs, the strain in the epilayer builds up and the strain energy is released, in some circumstances, by forming small islands. These islands are zero-dimensional, consequently, the self-assembled quantum dots (SAQDs) are formed. Mostly epitaxial growth occurs via a vapor phase technique. Molecular beam epitaxy (MBE) technique is also create an epitaxial growth with high a quality crystal.

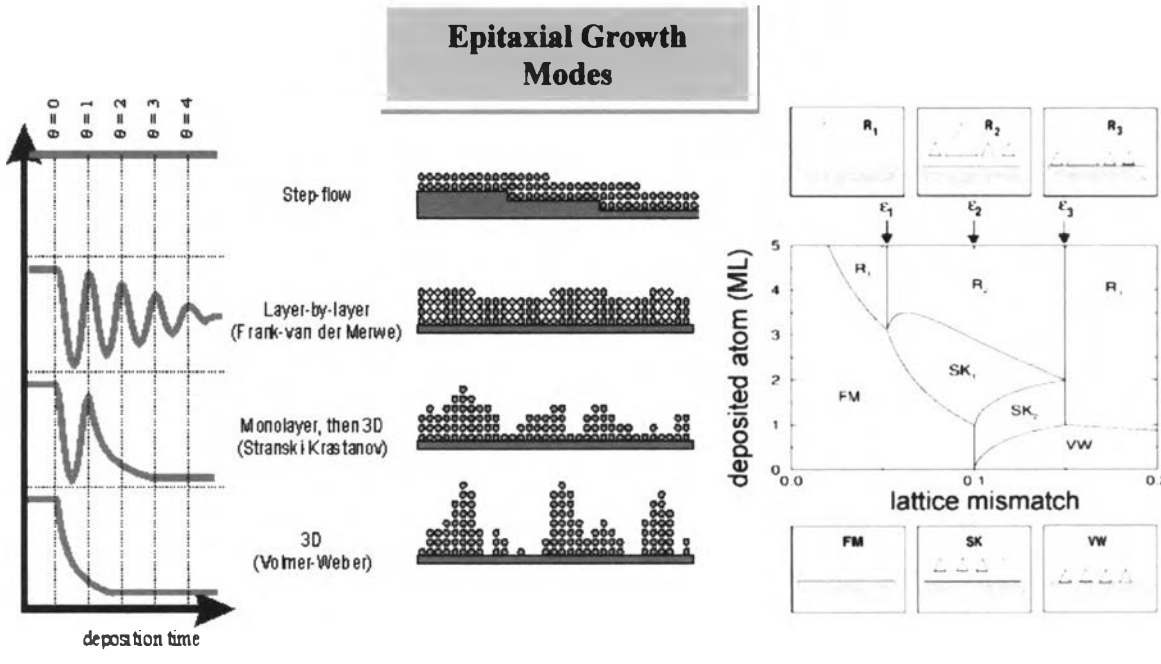

Figure 2.12 Schematic representation of the three important growth modes of a film: Frank van der Merwe (FM), Stranski Krastanow (SK), and Volmer Weber (VM) modes **[109-110]**.

There are three primary growth modes can occur when a strained epilayer is grown on a substrate under near equilibrium conditions as shown in **Figure 2.12**. **Volmer-Weber** (VW) growth mode is a growth mode which adatom-adatom interactions are stronger than those of the adatom with the surface, leading to the formation of three-dimensional adatom clusters or islands. Growth of these clusters, along with coarsening, will cause rough multi-layer films to grow on the substrate surface. Antithetically, during **Frank-van der Merwe** (FM) growth mode, adatoms attach preferentially to surface sites resulting in atomically smooth, fully formed layers. This layer-by-layer growth is two dimensional, indicating that complete films form prior to growth of subsequent layers. **Stranski-Krastanov** growth mode is an intermediary transition from the "layer-by-layer" to island-based growth occurs at a critical layer thickness which is highly dependent on the chemical and physical properties, such as surface energies and lattice parameters of the substrate and film.

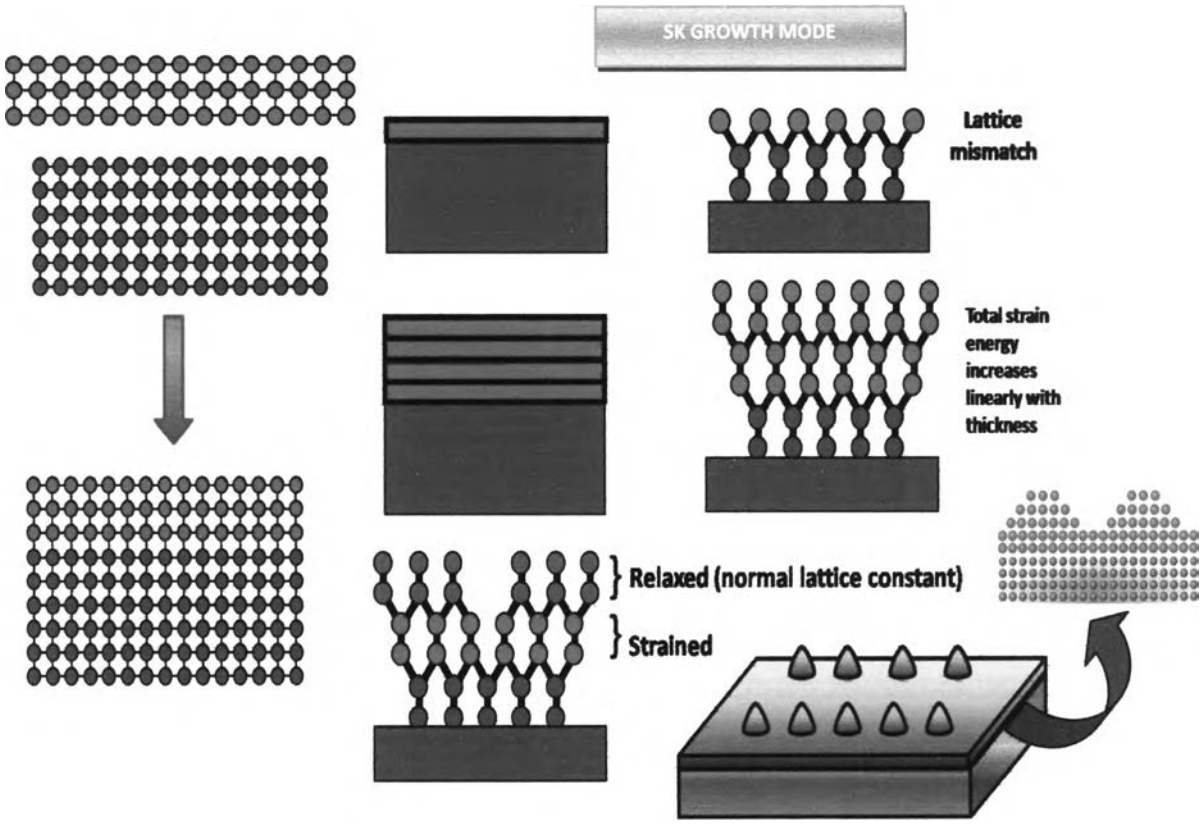

Figure 2.13 Illustration of island formation during epitaxial growth of a semiconductor material on top of another semiconductor with a smaller lattice constant in Stranski-Krastanow mode to form the QD.

Stranski-Krastanow (SK) growth mode is widely used to fabricate defect-free self-assembled QD structures in the case of lattice-mismatched system (lattice mismatch : $\varepsilon_0 < 7\%$). This mismatch complicates the free-energy and favors the growth of three-dimensional islands to compensate for the strain and thereby minimize the energy. The process is thin films grow epitaxially at a crystal surface or interface, known as "layer-plus-island growth" based on the thermodynamic instability during the deposition of an epitaxial film on a lattice mismatched substrate. The SK mode follows a two step process (sees **Figure 2.13**). In the first stage of growth, initially, complete films of adsorbates, up to several monolayers thick with a lower band gap and a larger constant is grown in a layer-by-layer fashion on top of a crystal substrate with a higher band gap and smaller lattice constant. Below a critical thickness, a pseudomorphic layer with the lateral lattice constant of the substrate is formed. During the growth, the elastic energy stored in this layer increases. With increasing thickness, the accumulated compressive strain can no longer be accommodated in a two-dimensional arrangement and the total film energy relax through the formation of coherently strain islands on top of the remaining part of the two-dimensional layer or the "wetting layer" **[111]**. Beyond a critical layer thickness, which depends on strain and the chemical potential of the deposited film, growth continues through the nucleation and coalescence of adsorbate islands. This nanoscale islands formed in this mode can be used to confine carrier in three dimensions or to form the QD structure.

Although the SK QDs grown is an excellent growth mode to fabricate the nano-structure. However, there are still some disadvantages of this technique. First, the QDs grown by SK mode exhibit wide size distribution which response to varying of energy level in the energy band, resulting in luminescence peak boarding **[112]**. Furthermore, the non-uniform strain distribution from lattice-mismatched formation would effect on the band structure of QD **[113]**. Both effects are undesirable for laser applications and essential to improve for better performance of semiconductor electronic devices.

2.4.3 Self-Assembled Aligned QDs

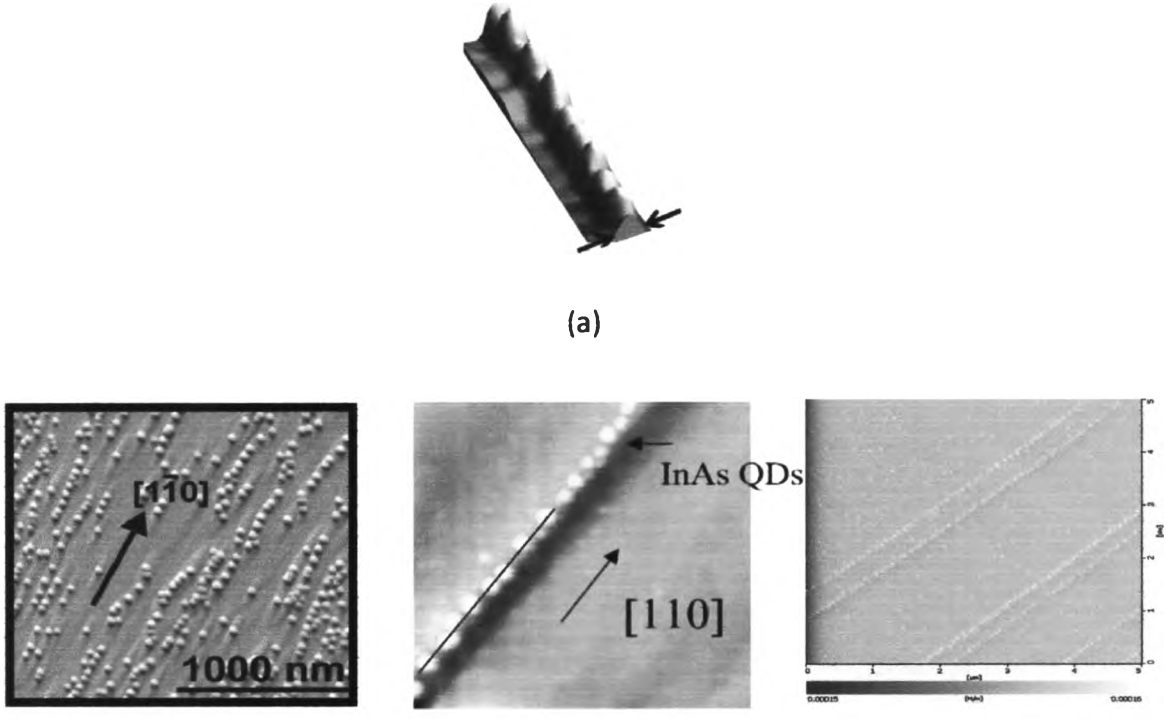

Figure 2.14 Schematic diagram of (a) 3-D self-assembled aligned QD model **[114]** and (b) the AFM images related with self-assembled aligned QD structure **[115-117]**.

As described in chapter 1, one of the QD structures which have attracted particular interest due to their many possible applications in optoelectronic devices, is **self-assembled aligned QD** structure. Because uniformity of QDs can be an important factor in order to determine all structural parameters of a QD such as size, shape, chemical composition and position which are subject to its random fluctuations, even in the presence of ordering mechanisms, so the control of self-assembled properties in QDs is of great importance for their device applications. Selective positioning of QDs can be performed through the misfit dislocation having

strain fields affects the formation of QDs since it becomes a strong source of elastic strain. The use of misfit dislocation can be a useful technique for the alignment of self-assembled QDs since any complicated pre-processes are not required as in lithographic processes. The techniques which have widely used for the growth of this structure are the superlattice template **[117]** and the InGaAs induction layer **[118]** technique. The example of timeline process about the two methods is depict in **Figure 2.15**. Both of two methods related with the building of anisotropic strain distribution area linearly aligned with parallel to each other in the certain direction as an induction layer, giving rise to the selective formation of self-assembled QD ordering on this region. Moreover, it is important to control some parameters, such as strain layer thickness, composition of the substance, temperature, and deposition time which strongly affect to the structure of QD alignment.

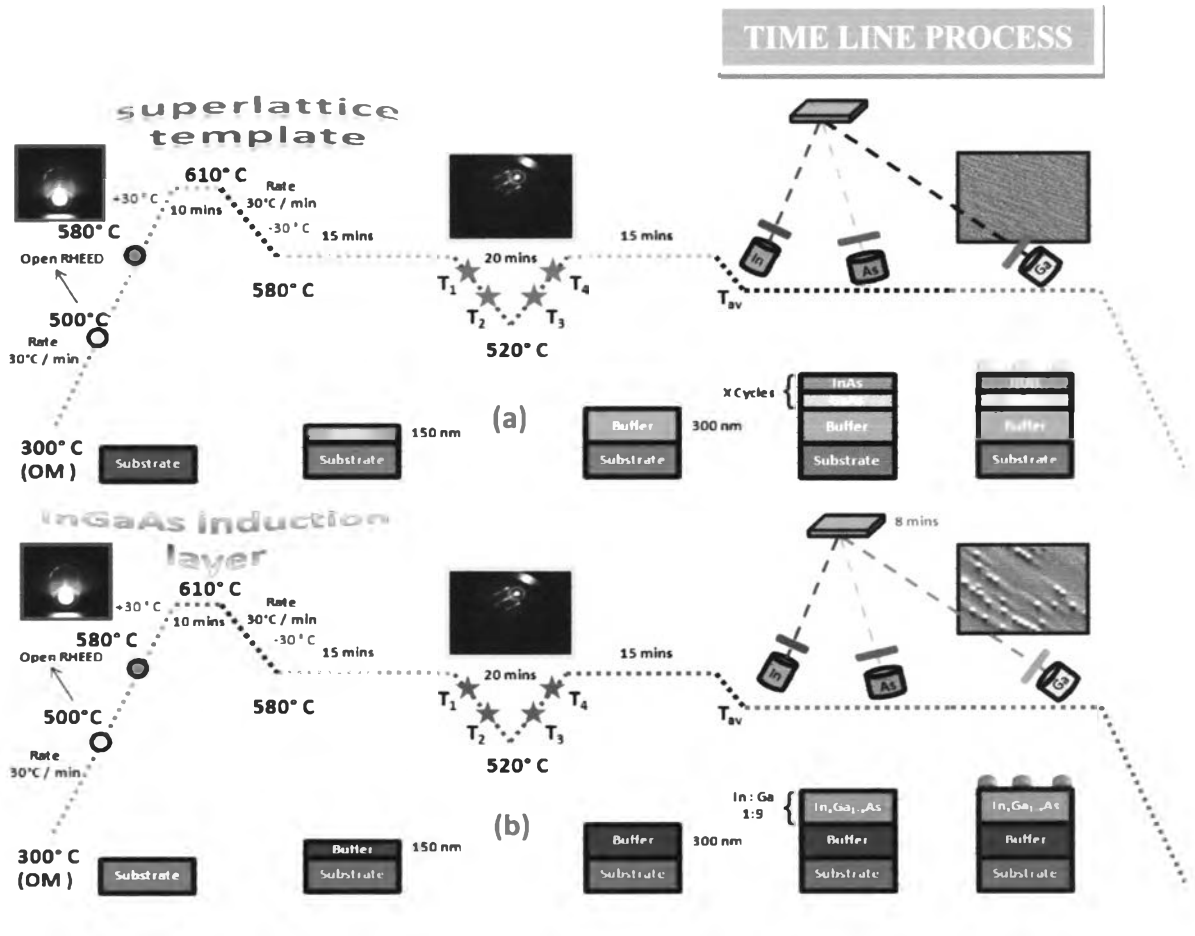

Figure 2.15 The example of timeline process of (a) the superlattice template structure and (b) the InGaAs induction layer structure.

The other interesting application of aligned for QDs in terms of low-dimensional electronic devices is single electron transistor (SET). Positioning of a single QD formed in channel between source and drain is a difficult processing technique due to the random distribution of self-assembled QDs. However, using the artificial array of QDs, narrow tip-shaped electrode is not necessary for positioning single QD in the channel. One can fabricate the SET structure with a simple process step because the electrode is not needed to be as narrow as in a conventional way, but only if the same width of electrode as the average distance of the aligned QDs. This leads to one line of aligned QDs could exist and single QD in channel can be easily obtained through the regulation of channel length for producing an efficiently electronic chip with high speed operation and low consumption an energy.

The overall review about the growth of QD is presented. Next section, the effect of the electric field on nanostructures will be discussed.

2.5 EFFECT OF THE ELECTRIC FIELD ON NANOSTRUCTURES

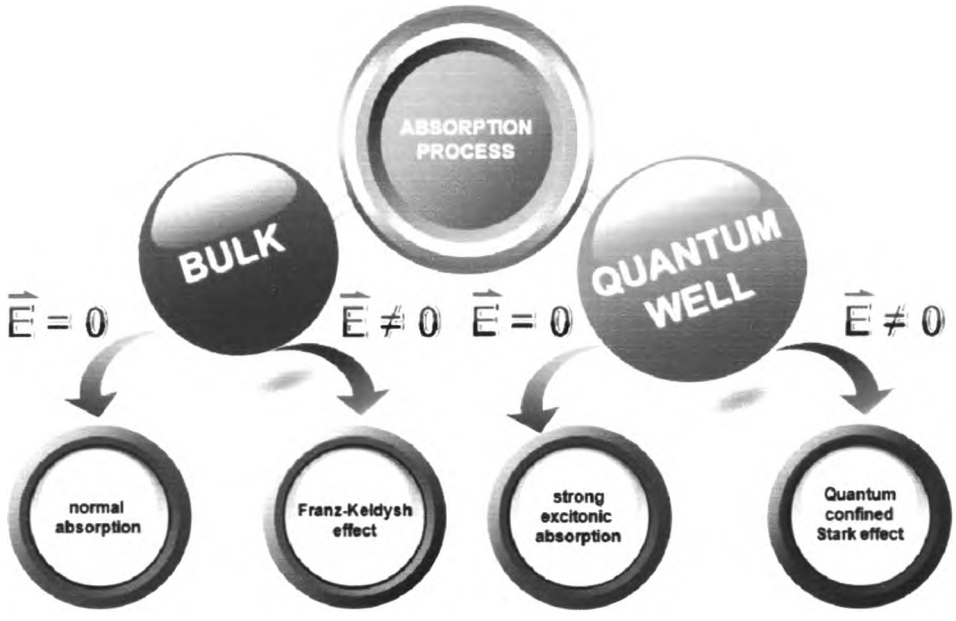

Figure 2.16 Schematic diagram of absorption process in semiconductor structure.

In the operation of some semiconductor devices such as electronic and optical devices, in particular, modulator devices which usually work under electric field by the energy levels, its optical and electronic properties depend on external electric field. These give evidence for new states of matter in many-body systems and that is why it is very important to study this effect on the materials. The effect of an applied electric field on the energy levels and, therefore, on the optical spectra is called the **"Stark effect" [119]**. The Stark effect refers an additional potential is produced when the semiconductor is under applied electric field. The shift of the atomic energy with respect to its normal state is proportional to the magnitude of the electric field, thus the results are splitting of energy levels of atoms and energy shift of the interband optical spectra is occurred related to **"electroabsorption" [120]**. The application used this concept, an electroabsorption modulator **[121]**, is a semiconductor device which can be used for controlling the intensity of a laser beam via an electric voltage. Its principle of operation is based on an applied electric field,

which changes the bandgap energy or photon energy of an absorption edge but usually does not involve the excitation of carriers by the electric field. The electroabsorption modulators are mostly made in the form of a waveguide with electrodes for applying an electric field in a direction perpendicular to the modulated light beam. Using bulk materials may restrict the performance since electro-absorption modulators of bulk materials require a large electric field. In order to increase an efficiency the concept of quantum-confined structures were used because, for modulators in telecommunications, small size and modulation voltages are desired. The quantum-confined structures such as quantum well materials can be achieved since these can operate with much lower voltages and also at very high speed (large bandwidth) **[122]**. In addition, their smaller sizes allow for integrating with other devices such as distributed feedback laser diode on form of photonic integrated circuit so a higher bandwidth and reduced chirp can be obtained. Recently, advances in crystal growth have triggered the study of **self organized quantum dots** which are possible to be used to enhance the electro-absorption coefficients and extinction ratio because of their smaller size and stronger confinement than quantum well structures which produce lower modulation voltages. Moreover, quantum dot materials with a high bandwidth (THz) can generated a coherent quantum superposition of an absorbing and a nonabsorbing exciton which may yield new applications for optical communications **[123]**. This section will be described about electric field effect on bulk materials first, then, extended to quantum well material, and finally hammer to the point on quantum - dot structures.

2.5.1 Electric Field on Bulk Structure: The Franz-Keldysh Effect

The fundamental concept of electric field on materials are started with the effect of applied field on bulk structures, so called **"The Franz-Keldysh effect"**. The Franz-Keldysh effect is a change in optical absorption by a semiconductor when an "strong" electric field is applied cause in the absorption of photons with energies less than the bandgap energy of the semiconductor.

Let consider the case of a uniform applied electric field **[124]** by disregard the Coulomb effects altogether, the stationary Schrödinger equation of the relative motion of the electron–hole pair in the presence of an electric field F (parallel to the z-axis) with the potential energy $V(r) = eFz$ can be written as

$$(-\frac{\hbar^2\Delta}{2m^*} - eFz - E_n)\psi_n(r) = 0 \qquad \textbf{(2.53)}$$

where ψ_n, E_n are eigenfunctions and energy eigenvalues of the electron–hole pair, respectively (E_n includes with the band-gap energy E_g). To solve this equation, definition an eigenfunctions by

$$\psi_n(r) = \frac{1}{L}e^{i(k_x x + k_y y)}\psi_n(z) \qquad \textbf{(2.54)}$$

where $L = V^{1/3}$ is the linear extension of the system. The energy eigenvalue are

$$E_n = \frac{\hbar^2}{2m^*}(k_{\|}^2 + \kappa_n^2) \equiv E_{n,k_{\|}} \qquad \textbf{(2.55)}$$

by $k_{\|}^2 = k_x^2 + k_y^2$. Inserting **Eq. (2.54)** and **(2.55)** into **Eq. (2.53)**, the result is

$$(\frac{d^2}{dz^2} + fz + \kappa_n^2)\psi_n(z) = 0 \qquad \textbf{(2.56)}$$

where $f = eF\frac{2m^*}{\hbar^2} = \frac{eF}{E_0 a_0^2}$. E_0 and a_0 are the usual excitonic units **[124]** shown that fa_0^3 is the ratio between the dipole energy in the field and the exciton Ryberg

energy, ea_0F/E_0. Introducing the dimensionless variable Z by $Z = f^{1/3}z$ and substituting

$$\zeta_n = Z + \kappa_n^2 f^{-2/3} = Z + (a_0\kappa_n)^2\left(\frac{E_0}{a_0eF}\right)^{2/3} \quad \textbf{(2.57)}$$

The solution of this equation is

$$\psi_n(z) = a_n Ai(-\zeta_n) \quad \textbf{(2.58)}$$

where $Ai(x)$ is the Airy function **[124]**,

$$Ai(x) = \frac{1}{\pi}\int_0^\infty du\cos((u^3/3) + ux) \quad \textbf{(2.59)}$$

and a_n is a normalization constant. $Ai(x)$ decays exponentially for positive arguments and oscillates for negative arguments **[124]**. Expressing the accelerating action of the field. The normalization constant a_n is determined by

$$a_n^{-2} = \lim_{L\to\infty}\int_{-L}^{L} dz\left|Ai(-\zeta_n)\right|^2 \quad \textbf{(2.60)}$$

Using **Eq. (2.57)** with partial equation and different equation technique, then

$$a_n^{-2} = \lim_{L\to\infty}\sqrt{\frac{L}{f^{1/3}}}\frac{1}{\pi} \quad \textbf{(2.61)}$$

where we used the fact that $Ai(x)$ and vanishs for $x \to \infty$. For $Ai(-x)$, using the asymptotic expressions **[124]** and boundary condition $\psi_n(z = L) = 0$ as

$$\frac{2}{3}\sqrt{f}\left(L+\frac{\kappa_n^2}{f}\right)^{3/2} = \left(n-\frac{1}{4}\right)\pi \qquad \textbf{(2.62)}$$

Solving **Eq. (2.62)** for κ_n and inserting the result in **Eq. (2.55)** yields

$$E_{n,k_\parallel} = \frac{\hbar^2}{2m^*}\left(k_\parallel^2 - Lf + \left[\frac{3\pi f}{2}(n-1/4)\right]^{2/3}\right) \qquad \textbf{(2.63)}$$

Using all the ingredients needed to compute the semiconductor band-edge absorption spectrum for directly allowed optical transitions $\alpha(\omega) = \alpha_b \sum_n |\psi_n(r=0)|^2 \, \delta(E_n - \hbar\omega)$, which can be written as

$$\alpha(\omega) = \int_{-\infty}^{\infty}\frac{dk_x}{2\pi}\int_{-\infty}^{\infty}\frac{dk_y}{2\pi}\sum\frac{\pi f^{1/3}}{\sqrt{L}}\delta(E_{n,k_\parallel} + E_g - \hbar\omega)$$
$$\times\left|Ai\left(f^{-2/3}\left(k_\parallel^2 - \frac{2m^* E_{n,k_\parallel}}{\hbar^2}\right)\right)\right|^2 \qquad \textbf{(2.64)}$$

Manipulating this equation intensively as described in **[124]**, the total absorption spectrum (electroabsorption for free carriers) is

$$\alpha(\omega) = \frac{\alpha_b}{2\pi}\frac{m^* f^{1/3}}{\hbar^2}\left(-\epsilon\, Ai^2(\epsilon) + \left(Ai'(\epsilon)\right)^2\right) \qquad \textbf{(2.65)}$$

where $\in = \frac{(E_g - \hbar\omega)}{E_0}\left(\frac{E_0}{ea_0F}\right)^{2/3}$.

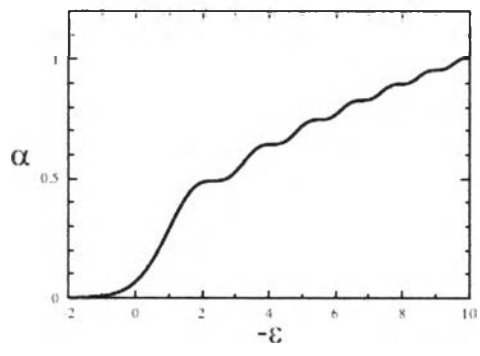

Figure 2.17 Absorption spectrum for free carriers in an electric field according to **Eq. (2.65)**.

Figure 2.17 shows the resulting absorption as function of $\in$. The oscillatory character of the Airy functions for negative arguments leads to oscillations in the absorption spectrum above the band gap. The amplitude of these oscillations decreases with increasing energy. The absorption has a tail below the gap, i.e., for $\hbar\omega < E_g$ or $\in > 0$. Using the asymptotic form **[124]**, then the below-gap absorption or **"Franz-Keldysh effect"** is

$$\alpha(\omega) \approx \frac{\alpha_b}{(32\pi)^2}\frac{f}{E_g - \hbar\omega}\exp\left\{-\frac{4}{3f}\left[\frac{2m^*(\hbar\omega - E_g)}{\hbar^2}\right]^{3/2}\right\} \qquad \textbf{(2.66)}$$

Eq. (2.66) describes the exponential low energy absorption tail which is caused by electric field f (because $f = eF\frac{2m^*}{\hbar^2} = \frac{eF}{E_0 a_0^2}$). As conceived evidently, the Franz-Keldysh effect is the result of wavefunctions leaking into the band gap. When an electric field is applied, the wavefunctions of electron and hole become

Airy functions rather than plane waves. The Airy function includes a tail which extends into the classically-forbidden band gap. The frequency range of this tail increases with *f*. The effect of overlapping between the wavefunctions of a free electron and a hole is proportional with the optical absorption, that is, the more overlapping, the stronger the optical absorption will be, corresponding to Fermi's Golden Rule. The Airy tails slightly overlap even if the electron and hole are at slightly different potentials (or slightly different physical locations along the field). The absorption spectrum now includes a tail at energies below the band gap and some oscillations above it. One may understand the appearance of the absorption tail as a photon assisted field-induced tunneling of an electron from the valence band into the conduction band, according to **Figure 2.18**. **Figure 2.18 (a)** displays the band structure of semiconductor when electric field is applied. Both the conduction band and the valence band tilt linearly to the one side, following the effect of electric field. In this case there is no photon so the valence electron has no tunnel through a triangular barrier of height E_g and thickness d, given by E_g / eF. When the photon of energy $\hbar\omega < E_g$ is coming (**Figure 2.18 (b)**), with the assistance of electric field the tunneling barrier is reduce to $d' = (E_g - \hbar\omega)/eF$, the valence electron now can easily tunnel to the conduction band, that is why the photons with energies less than the bandgap energy can be absorbed. The absorption spectrum far above the band edge, $\hbar\omega >> E_g$ or $\epsilon << 0$, can be estimated to

$$\alpha(\omega) = \frac{\alpha_b}{(2\pi)^2}\left(\frac{2m^*}{\hbar^2}\right)^{3/2}\sqrt{\hbar\omega - E_g} \qquad \textbf{(2.67)}$$

or the free-carrier absorption. The Franz-Keldysh effect occurs in uniform, bulk semiconductors which used for Electro-absorption modulators. The Franz-Keldysh effect usually requires hundreds of volts and will be small unless $E_g \geq 10^5$ V/cm, limiting its usefulness with conventional electronics.

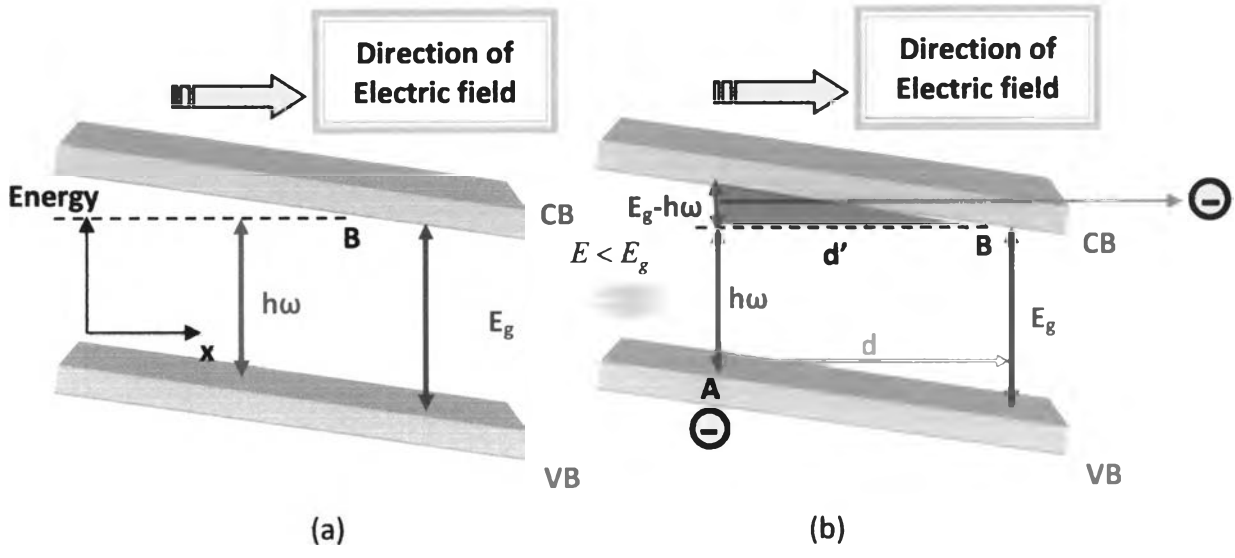

Figure 2.18 Band structure of semiconductor when electric field is applied with (a) no photon and (b) the photon of energy $\hbar\omega < E_g$.

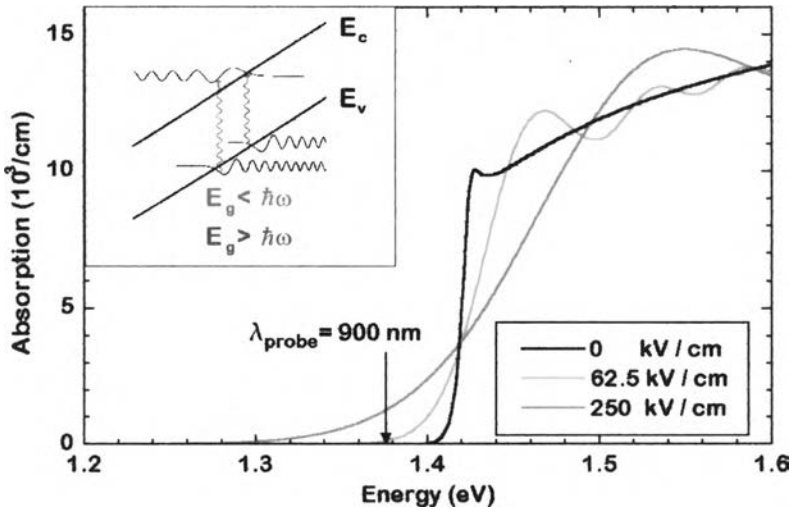

Figure 2.19 In an electric field, the band edges become tilted. The wavefunctions therefore become airy-functions and penetrate into bandgap region. This enables absorption of photons with energies below the band gap energy and to an oscillating absorption above the bandgap **[125]**.

2.5.2 Electric Field on Quantum Well Structure : The Quantum-Confined Stark Effect (QCSE)

In the bulk semiconductors, because the exciton lifetime is very short (about a few hundred of femtoseconds) after it is created and hardly detected about the absorption spectra at room temperature, except in very pure samples. (in bulk semiconductors, exciton is mostly observed at low temperature **[126]**). This effect limits for designing high performance semiconductor devices, particularly electroabsorption modulator, and interband photon-assisted tunneling or Franz-Keldysh effects which is insufficient to compensate the drawback mentioned above. This situation is drastically different in semiconductor with quantum well structure. In a single quantum well (SQW) or multiple quantum well (MQW) with thick barriers ($\geq$ 100Å), the carriers (electron and hole) are confined in two dimensional especially in the well width which restricts a tunneling of carriers and increase the overlap of their wavefunctions. These results in an increase the oscillator strength of interband transitions between discrete electron-hole energy bound states. Furthermore, strong resonances corresponding to the heavy-hole and light-hole transitions are seen near band edge of quantum well material even at room temperature **[126]**. These characteristics show the advantages over the bulk semiconductors.

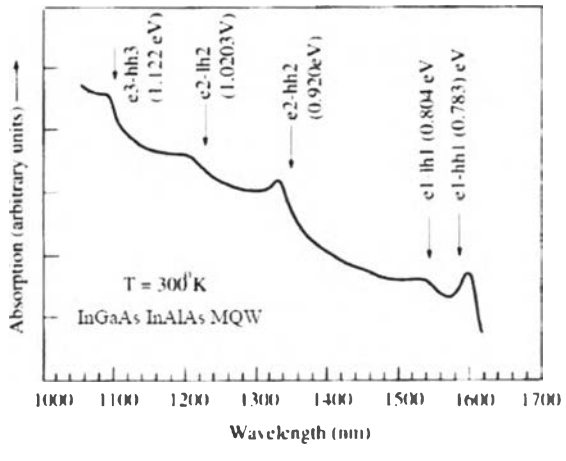

Figure 2.20 Illustration of the exciton resonances in QW structure, which are clearly seen in the absorption spectra even at room temperature **[126]**.

Since the recent development of research in semiconductor quantum-well structures, optical absorptions in quantum wells have been shown to exhibit a drastic change by an applied electric field **[127-129]**. The sharp excitonic absorption spectra in quantum wells have been observed at room temperature as mentioned above. These are so-called **"quantum-confined Stark effects (QCSE)" [127-129]**. The quantum-confined Stark effect describes the effect of an external electric field upon the light absorption spectrum of a quantum well structure. In the absence of an external electric field, electrons and holes within the quantum well may only occupy states within a discrete set of energy subbands. Consequently, only a discrete set of frequencies of light may be absorbed, but when an external electric field is applied, the electron states shift to lower energies, while the hole states shift to higher energies. This reduces the permitted light absorption frequencies. Additionally, the external electric field shifts electrons and holes to opposite sides of the well. This effect shows a significant amount of change of the absorption coefficient with an applied voltage bias due to the enhanced exciton binding energy in a quasi-two-dimensional structure. Since quantum-well barriers confine both the electrons and holes within the wells, therefore, the exciton binding energy is increased and the exciton is more difficult to ionize, results in the reduction of the absorption coefficient of the system. The separation between the electrons and holes is limited by the presence of the potential barriers around the quantum well, that is, excitons are able to exist in the system even under the influence of an electric field.

Broadening the horizon in intellectual aspect to understand obviously, quantum theory of electroabsorption can be achieved **[124]**. If the electric field is applied by perpendicular to the layer of a quantum well, the situation is quantitatively different from that in bulk material. Because the carriers are opposite charges, the field pushes electron and hole toward the opposite walls of the well. Hence, the overlap between the corresponding their wavefunctions is drastically modified. To investigate this effect, the time being the modifications caused by the electron–hole Coulomb interaction is disregard for simplicity calculation. In a

spatially inhomogeneous situation, such as in a quantum well, one has to use a two-point susceptibility function in real space representation $\chi(R,R',\omega)$ which connects non-locally the polarization and the field according to

$$P(R,\omega)=\int d^3R'\chi(R,R',\omega)E(R',\omega) \qquad \textbf{(2.68)}$$

The optical susceptibility is given by a generalization of optical transitions $\alpha(\omega)=\alpha_b\sum_n|\psi_n(r=0)|^2\,\delta(E_n-\hbar\omega)$ as

$$\chi(R,R',\omega)=\chi_0\sum_\mu\frac{\psi_\mu^*(R,r=0)\psi_\mu(R',r'=0)}{\hbar(\omega+i\delta)-E_\mu} \qquad \textbf{(2.69)}$$

$\psi_\mu(R,r)$ is the wavefunction of an electron–hole pair and R, r is the center-of-mass and relative coordinates, respectively. In spatially homogeneous situations, χ depends only on $R-R'$. The Fourier transform with respect to the difference of the center-of-mass coordinates yields the spatial dispersion (i.e., the wave-vector dependence of the susceptibility). However, due to the spatially inhomogeneous situation in a quantum well has $\chi(R,R',\omega)\neq\chi(R-R',\omega)$.

The light wave length in the visible range is of the order of 10^{-4} cm. This value is much larger than the typical quantum-well width (for GaAs is around 10^{-6} cm. Therefore, utilizing a susceptibility which is averaged over volume of the quantum well structure,

$$\bar{\chi}=\frac{1}{V}\int d^3R\int d^3R'\,\chi(R,R',\omega) \qquad \textbf{(2.70)}$$

This averaged susceptibility locally connects the optical polarization and the electromagnetic field. For simplicity in the calculation, assuming that a potential well has infinite depth extending over $-L/2 \le z \le L/2$. The pair wave function of a narrow quantum well can be taken as the product of particle-in-a-box wavefunctions for the electron and hole multiply with the function describing the relative motion in the plane of the layer

$$\psi_{\mu}(R,r) = \psi_{n_e}(z_e)\psi_{n_h}(z_h)\phi_{k_{\|}}(r_{\|}) \tag{2.71}$$

Electron and hole wavefunctions in the z direction obey the equation

$$\left(-\frac{\hbar^2}{2m_i}\frac{d^2}{dz_i^2} \pm eEz_i\right)\psi_{n_i}(z_i) = E_{n_i}\psi_{n_i}(z_i) \tag{2.72}$$

where the $+(-)$ sign is linked to $i = e(h)$. The boundary conditions are

$$\psi_{n_i}(z = \pm L/2) = 0 \tag{2.73}$$

Using the simple trigonometric functions with even and odd parity

$$\psi_n^0(z) = \begin{Bmatrix}\cos(k_n z)\\ \sin(k_n z)\end{Bmatrix} \text{ with } k_n = \frac{\pi}{L}\begin{Bmatrix}2n+1\\ 2n\end{Bmatrix} \text{ for } n = 0,1,2,\ldots \tag{2.74}$$

The absorption spectrum resulting from **Eq. (2.69) - (2.74)** or **"Quantum Confined Franz-Keldysh spectrum"** is

$$\alpha(\omega)=\frac{\alpha_b}{L}\sum_{k_{\parallel},n_e,n_k}\frac{\delta(\hbar\omega-E_g-E_{k_{\parallel}}-E_{n_e}-E_{n_h})}{A_{n_e}A_{n_h}} \times\left|\int_{-L/2}^{L/2}dz\psi_{n_e}(z)\psi_{n_h}(z)\right|^2 \quad \textbf{(2.75)}$$

with $E_{k_{\parallel}}=(\hbar k_{\parallel})^2/2m$ and the normalization $A_{n_i}=\int_{-L/2}^{L/2}dz\left|\psi_{n_i}(z)\right|^2$. Solving **Eq. (2.75)** by using linear combination of Airy functions mentioned in **[124]**. The complete absorption spectra in quantum well structure is

$$\alpha(\omega)=\frac{\alpha_b}{L}\sum_{k_{\parallel}}\int_{-eEL/2}^{\infty}dE_h\frac{d^2n_e}{dE_e^2} \times\delta(\hbar\omega-E_g-E_{k_{\parallel}}-E_e-E_h)I_{eh} \quad \textbf{(2.76)}$$

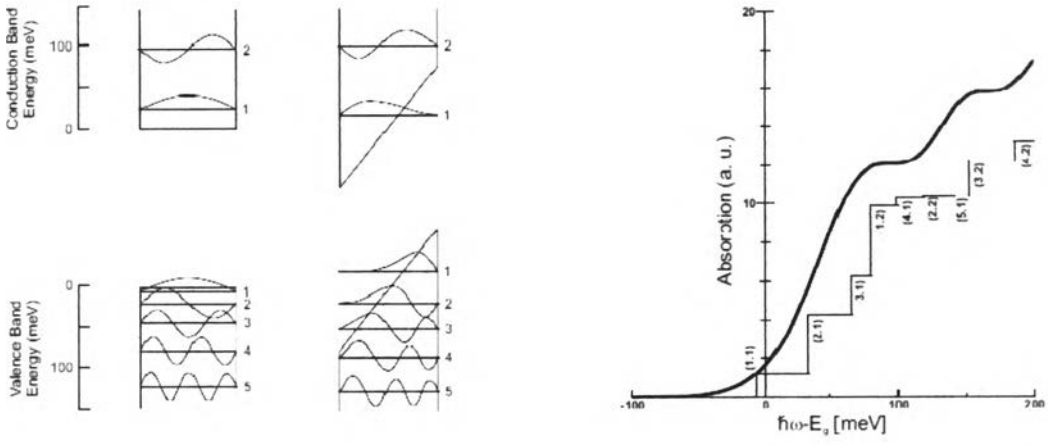

Figure 2.21 Illustration of (a) calculated wave functions and energy levels for a 150 Å thick GaAs-like quantum well structure at 0 and 10^5 V/cm and (b) calculated absorption of a 150 Å thick GaAs-like quantum well at 10^5 V/cm. The individual transitions are labeled (n_v,n_c) where $n_v(n_c)$ is the valence (conduction) subband number. The smooth line is the calculated Franz-Keldysh effect for bulk material (**Figure 2.17**) **[124]**.

where I_{eh} is the square of normalized overlap integral between electron and hole wavefunctions

$$I_{eh} = \frac{\left|\int_{-L/2}^{L/2} dz \psi_{n_e}(z)\psi_{n_h}(z)\right|^2}{A_{n_e} A_{n_h}} \qquad \textbf{(2.77)}$$

Figure 2.21 (a) shows the calculated wave functions in the potential well with and without an electric field. The picture of the wavefunctions gives the information how the overlap integral I_{eh} changes due to the field for the various inter-subband transitions. **Figure 2.21 (b)** shows plot of the calculated absorption spectrum for a GaAs quantum well with L = 100Å width in the presence of an electric field of 10^{-5} V/cm. It is observe that the transition between the second valence subband and the first conduction subband, which was forbidden without field, obtains a large oscillator strength in the field. For the limit $L \to \infty$, the inter-subband transitions approach the modulation of the bulk Franz-Keldysh spectrum.

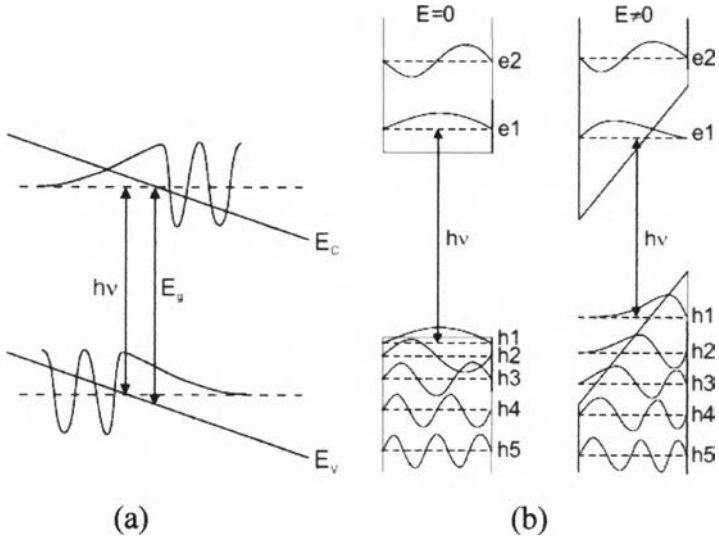

Figure 2.22 Impact of an electric field on (a) bulk material (tilt of bands) and (b) a quantum well (QCSE) **[35]**.

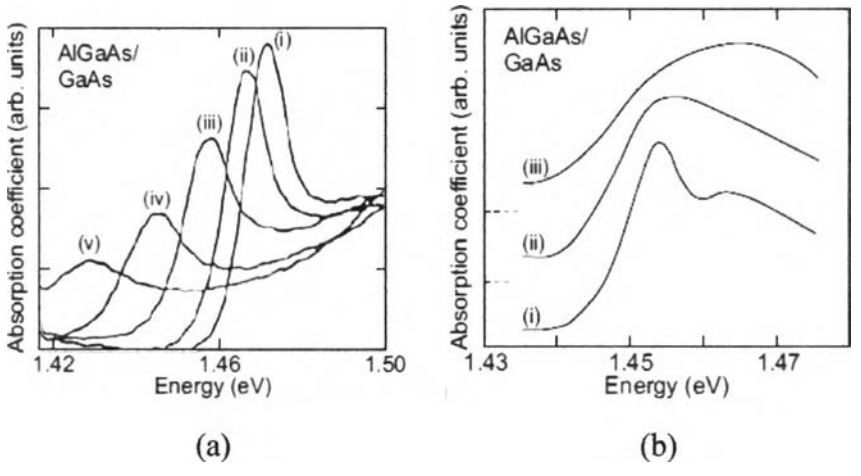

Figure 2.23 Impact of electric fields on the absorption spectrum of a AlGaAs/GaAs quantum well. (a): Electric field along the [001] growth direction, (i) – (v): E = 0, 0.6, 1.1, 1.5, and 2×10^5 V/cm. (b): Electric field within the interface plane, (i, ii, iii): E =0, 1.1, and 2×10^5 V/cm **[35]**.

Figure 2.22 shows the impact of electric field of bulk and quantum well material. In bulk material, the bands are tilted by the effect of electric field (**Figure 2.22 (a)**), i.e. there is no longer an overall bandgap. Accordingly, the wavefunctions are modified and have exponential tails in the energy gap. In a quantum well structure (**Figure 2.22 (b)**), an electric field along the confinement direction (z direction) causes electrons and holes to shift their mean position to opposite Interfaces. However, excitons are not ionized due to the electric field. With increasing field (for both field directions) the energy position of the absorption edge and the recombination energy is reduced.

Corresponding experimental data are shown in **Figure 2.23 (a) ((i) - (v)) [35]**. The shift depends quadratically on the electric field since the exciton has no permanent dipole moment (mirror symmetry of the quantum well). Thus, only the second-order Stark effect is present in which the field first induces a dipole $p = \alpha\varepsilon$. This dipole interacts with the field with an energy $E = -p.\varepsilon = -\alpha\varepsilon^2$. If the field is within the quantum-well interface plane, the field leads to the ionization of excitons.

The loss of the excitonic peak is visualized in the spectra in **Figure 2.23 (b)**. Note that the effect of an electric field along the transverse direction is of significant interest since in the case of a quantum well, the applied electric field can be either in the plane of the well (longitudinal), where it behaves as a delocalized two dimensional electrons, or in the direction of confinement (transverse) **[59]**.

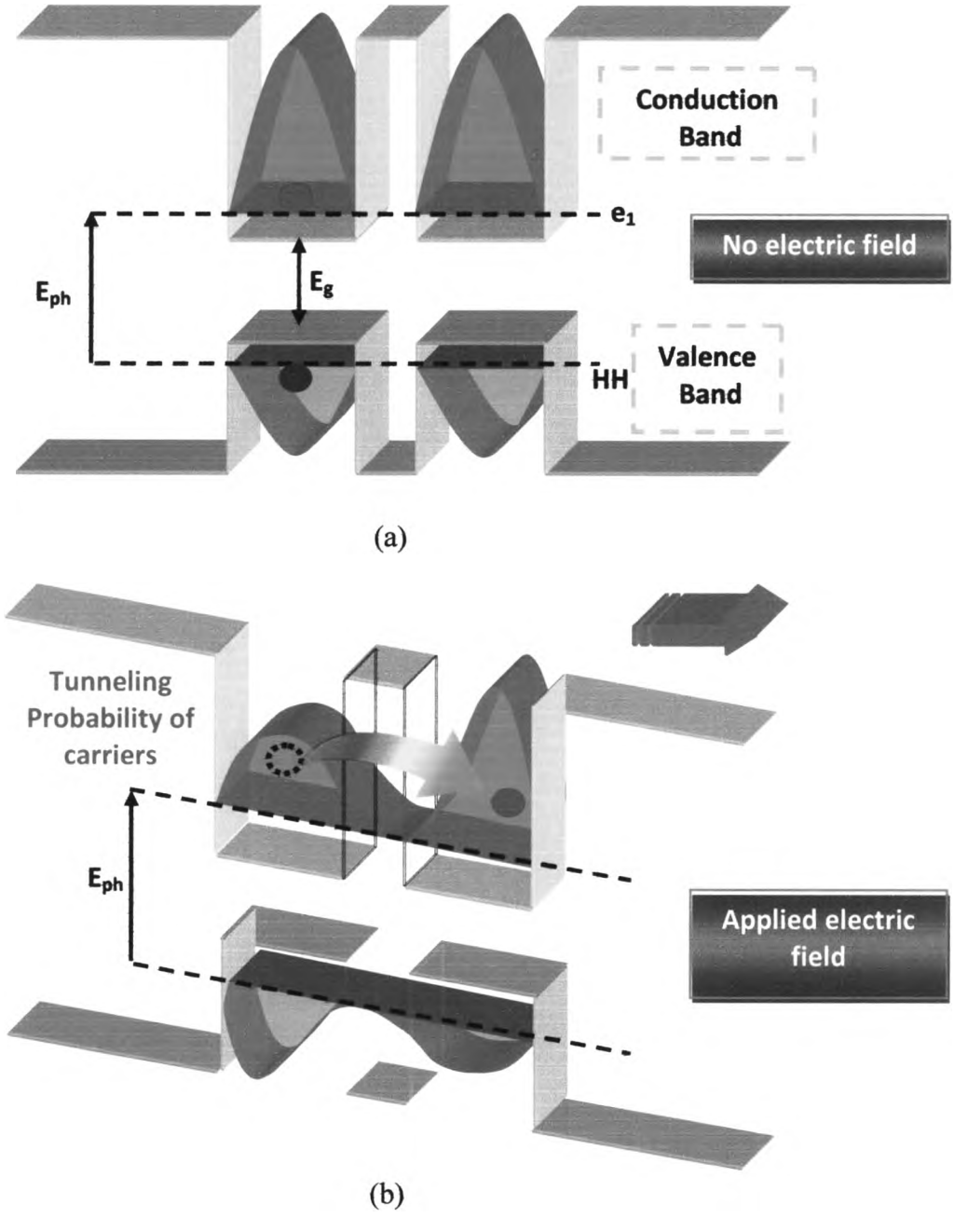

Figure 2.24 Schematic diagram of the QW structure when (a) no applied electric field and (b) the electric field is applied in perpendicular to the layers.

The longitudinal field effect is similar to the bulk problem; the exciton dissociation occurs at a fairly low field (disappearance of excitonic absorption), and the absorption edge shifts to lower energy. Because of the confinement effect, the excitons are not ionized even at applied fields greater than 100 kV/cm.

Again and Again, the major manifestations of the quantum-confined Stark effect produced by the application of an electric field along the confinement direction are summarized as follows.

- The interband separation changes in the electron and the hole wavefunctions as depict in **Figure 2.24**. In the absence of applied field, the ground-state wavefunctions of electron and hole subbands are distributed symmetrically in form of Gaussian function. When the transverse electric field is applied, both wavefunctions are distorted and tilted to opposite sides because of different Coulomb effect between them, consequently, it separates the electron and the hole wavefunctions and pushes them to opposite sides of the quantum-confined region.

- Due to the separation of the electron and hole wavefunctions (reducing overlap between them), the binding energy of the exciton decreases or reduction in absorption and in luminescence peaks. This effect is also shown by the spectral changes at various field strength for a AlGaAs/GaAs quantum well **[128]**. In addition, the probability of carriers tunneling out of the well also increases, resulting in a decrease in carrier lifetimes and a broadening of the excitonic peaks. These behaviors lead to shift of the absorption spectrum to lower energies or **red shift**, and the shift is much larger than the Stark shift in bulk materials. However, the shift of the excitonic peak is larger than the broadening.

- The electric field can also mix different quantized states and lead to redistribution of oscillator strength between optically allowed and optically forbidden excited states. For example, in the absence of an electric field, only $\Delta n = 0$ transitions

between the quantized levels of the conduction and the valence bands (such as $n = 1 \rightarrow n = 1$) are allowed for a symmetric quantum well (potential barrier on both sides are the same). Nevertheless, in the presence of an electric field, $\Delta n = \pm 1$ can also become optically allowed.

- A major consequence of all these manifestations is a large change in the optical absorption corresponding to excitonic transitions, as a function of applied electric field in the confinement direction. This effect, also called **electroabsorption** as mentioned repeatedly, which leads to a change Δn in the real part of the refractive index and can be used to modulate the propagation of light by the application of an electric field.

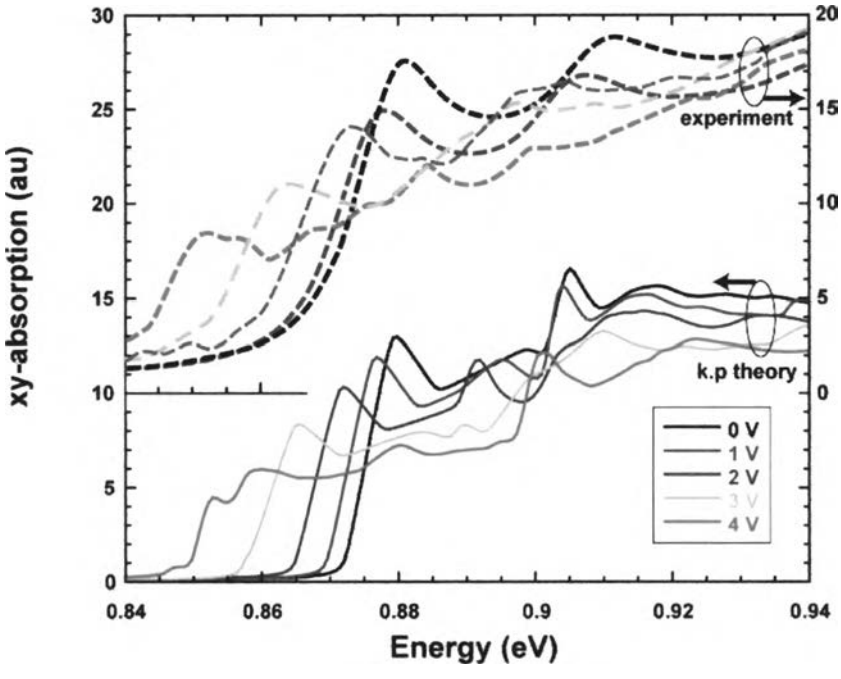

Figure 2.25 Schematic diagram of the absorption spectra versus energy in the presence of applied electric filed on QW structure. The decreasing and broadening of absorption peak is larger when electric field is increased, consistence with the results of both theoretically and experimentally **[130]**.

The quantum-confined Stark effect is used in a major application of the quantum well devices is in electro-optic modulators which can operate at room temperature and allow optical communications signals to be switched on and off rapidly, so this effect can be used for the design and realization of very efficient light modulators. Extensive investigations of electro-absorption in quantum dots have also been carried out **[131-132]**. Another structure used to enhance the manifestation of electric field is an asymmetric quantum well where the potential barriers on both sides of the quantum well are not the same. This feature can be assumed by using compositional variation (x) of the wider bandgap semiconductor regions $Al_xGa_{1-x}As$ such that x has one value on one side of the quantum well GaAs and has another value on the other side. In an asymmetric quantum well, a linear Stark effect on the energy levels can be realized.

2.5.3 Electric Field on Quantum Dot Structure

In previous section, the overall substantial is described the effect of electric field on quantum well material that is a low-dimensional structure. This reveals that confined structures inhibiting the exciton field ionization can produce the strength nonlinear optical properties, therefore, an opportunity to bring a significant progress in optical device applications. To top up a discussion, the quantum confined Stark Effect of extremely confined in all three spatial directions structure or quantum dots is considered as the highlighted topic having been investigated both theoretically **[133-134]** and experimentally **[135-136]**. The zero-dimensional semiconductor structures, such as II-VI compound and III-V compound semiconductors quantum dots are widely used especially InAs/GaAs self-assembled quantum dots **[137]** which have attracted considerable attention because of the new physics **[138]** of a few electron systems and potential applications in optoelectronic devices **[139]**. Both from the pure and applied point of view purpose to clarify the electronic properties of zero-dimensional semiconductor systems **[140-141]** and be able to controlling the

band structure of the systems with high degree of freedom in controlling the band structure and electro-optical properties by both external and built-in internal electric fields. A recent theoretical studies has demonstrated thoroughly by taking some important factors corresponding to the nanostrcutures; strain-induced effect (piezoelectric included), temperature dependent, point defects, interaction of carrier with perturbation, size and shape dependent and the existence of other factors to become precisely as possible **[142-145]**. These effort desire a consistence with experimental which is also modified many equipments of fabrication for producing substrates closely the perfect crystals in order to making an accurately results in measurement, that is, quantum theory and experimental must be concurrently investigated for valuable information that leads to new semiconductor device in the future.

2.5.3.1 Theoretical concept of electric field on semiconductor quantum dot

The theoretical studies of quantum dot in the presence of applied field are introduced in order to create a visualization via mathematical model for perception. Many theoretical approach based on quantum theory have been achieved **[65, 133-134, 142-145]**. One of the interesting information was given by G. W. Wen *et al* **[146]**. G. W. Wen *et al* explained the quantum-confined stark effect on excitons with a uniform electric field in semiconductor quantum dot, having been studied by using a numerical matrix diagonalization scheme. The schematic diagram of confined exciton in a spherical quantum dot (for simplicity) with radius R surrounding by the glass matrix and under the applied electric field $\vec{E}_a$ is shown in **Figure 2.26**. $\in_d$ ($\in_g$) is the dielectric constant for the quantum dot (glass matrix). The z axis is chosen to be antiparallel to the applied field direction. $\vec{r}_e(\vec{r}_h)$ and $\theta_e(\theta_h)$ are the position vector in the spherical coordinate and polar angle of the

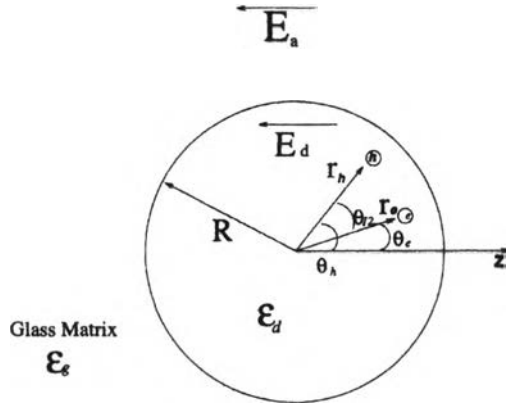

Figure 2.26 Schematic diagram of a confined exciton in a QD of a radius R under the uniform applied electric field $\vec{E}_a$. $\in_d$ and $\in_g$ are the dielectric constants of the QD and the glass matrix, respectively. The z axis is along the direction opposite to the applied electric field $\vec{E}_a$. $\vec{E}_d$ is the electric field inside the QD **[146]**.

electron (hole). The electric field inside the quantum dot, $\vec{E}_d$, is different from $\vec{E}_a$ since the different of dielectric constant ($\in_d$ and $\in_g$). With a uniform $\vec{E}_a$, the electric field inside the quantum dot is reduced to

$$\vec{E}_d = \frac{3 \in_g}{\in_d + 2 \in_g} \vec{E}_a \qquad \textbf{(2.78)}$$

By using the formalism adopted by Hu *et al* **[147]**, the effective-mass approximation was used to assume that the quantum dots size has been assumed to be much larger than the lattice constants of the bulk semiconductor. The Hamiltonian of time-independent Schrödinger equation in exciton states are

$$\hat{\mathrm{H}} = \hat{\mathrm{H}}_e + \hat{\mathrm{H}}_h + \hat{V}_{e-h} + \hat{W}_e + \hat{W}_h \qquad \textbf{(2.79)}$$

where the conduction band minimum of bulk material has been chosen as the energy reference point. The first two terms of **Eq. (2.79)** represent the kinetic energy of electron (hole) with effective mass $m_e(m_h)$, $\hat{H}_i = -\frac{\hbar^2}{2m_i}\nabla_i^2 \ (i = e,h)$. $\hat{V}_{e-h}$ is the Coulomb interaction between the electron and hole, $\hat{V}_{e-h} = -e^2/\in_d \left|\vec{r_e} - \vec{r_h}\right|$. The last two terms are the Stark energy of electron (- sign, $i = e$) and hole (+ sign, $i = h$) under the applied field, $\hat{W}_i = \pm eE_d r_i \cos\theta_i \ (i = e,h)$. The interaction between electron (hole) and its image charge has been neglected since such an interaction does not contribute to the energy of confined excitons inside quantum dot **[147]**. The total angular momentum of an exciton $\hat{L}^2$ (with have not considered the spin variable since photonexcitation and recombination of excitons do not changes of spin so only the spin singlet states of the exciton can be excited by the absorption of photons) that commutes with the Hamiltonian of **Eq. (2.79)** is $\hat{L}^2 = (\hat{L}_e + \hat{L}_h)^2$, where $\hat{L}_i = \vec{r_i} \times (-i\hbar\vec{\nabla}_i)$ is the angular momentum operator for electron ($i = e$) or hole ($i = h$). The eigenfunctions of Hamiltonian of **Eq. (2.79)** can be classified according to their symmetry. Under the electric field, the system has azimuthal symmetry about the z axis. The total angular momentum L is no longer a conservative quantity. However, for a weak electric field, L is still used to label states approximately. The exciton wavefunction $\Phi(\vec{r_e},\vec{r_h})$ is determined by the Schrödinger equation from **Eq. (2.79)**:

$$\left[-\frac{\hbar^2}{2m_e}\nabla_e^2 - \frac{\hbar^2}{2m_h}\nabla_h^2 - \left(e^2/(\in_d \left|\vec{r_e} - \vec{r_h}\right|)\right) - eE_d r_e \cos\theta_e + eE_d r_h \cos\theta_h\right]\Phi(\vec{r_e},\vec{r_h}) = E\Phi(\vec{r_e},\vec{r_h}) \quad \textbf{(2.80)}$$

where E is the energy of the confined exciton related to the minimum of conduction band of bulk materials. Solving **Eq. (2.80)** numerically by the method of diagonalization, expanding the exciton wavefunction $\Phi(\vec{r_e},\vec{r_h})$ on the appropriate basis. Since the Hamiltonian of **Eq. (2.79)** cannot be diagonalized with the basis formed by the single particle wavefunctions because of $\hat{V}_{e-h}$ and $\hat{W}_i$ terms so choosing the couple electron-hole pair states as the basis for expanding the exciton wavefunction $\Psi(\vec{r_e},\vec{r_h})$. Therefore, the eigenfunction of the confined exciton in the absence of electric field, neglecting the coulomb interaction is

$$\Phi_{n_1 l_1 n_2 l_2 LM}(\vec{r_e},\vec{r_h}) = \sum_{m_1 m_2} \langle l_1 m_1 l_2 m_2 \mid LM \rangle \phi_{N_1}(\vec{r_e})\phi_{N_2}(\vec{r_h}) \qquad \textbf{(2.81)}$$

where $\langle l_1 m_1 l_2 m_2 \mid LM \rangle$ is the Clebsch-Gordan coefficient in the Condon-Shortley convention **[148]**, with subscript 1(2) standing for the quantum number of the electron (hole). L and M are the quantum numbers of the total angular momentum and it z component, respectively. $\Phi(\vec{r_i})$ stands for single particle wavefunction of electron $(i=e)$ or hole $(i=h)$ which is the solution of Hamiltonian with the boundary condition $\phi(\vec{r_i}) = 0(r_i \geq R, i=e,h)$ corresponding to the assumption of an infinitiely deep potential between the quantum dot and the glass matrix **[146]**. In order to calculate the quantum-confined stark effect of exciton inside quantum dot by including the Coulomb interaction on the electron and hole with the applied field, the exciton wavefunctions are axpanded as a superposition of wavefunction of **Eq. (2.81)** with different quantum number sets $\{n_1 l_1 n_2 l_2 LM\}$ as

$$\Psi(\vec{r_e},\vec{r_h}) = \sum_{n_1 l_1 n_2 l_2 LM} V(n_1 l_1 n_2 l_2 LM) \times \Phi_{n_1 l_1 n_2 l_2 LM}(\vec{r_e},\vec{r_h}) \qquad \textbf{(2.82)}$$

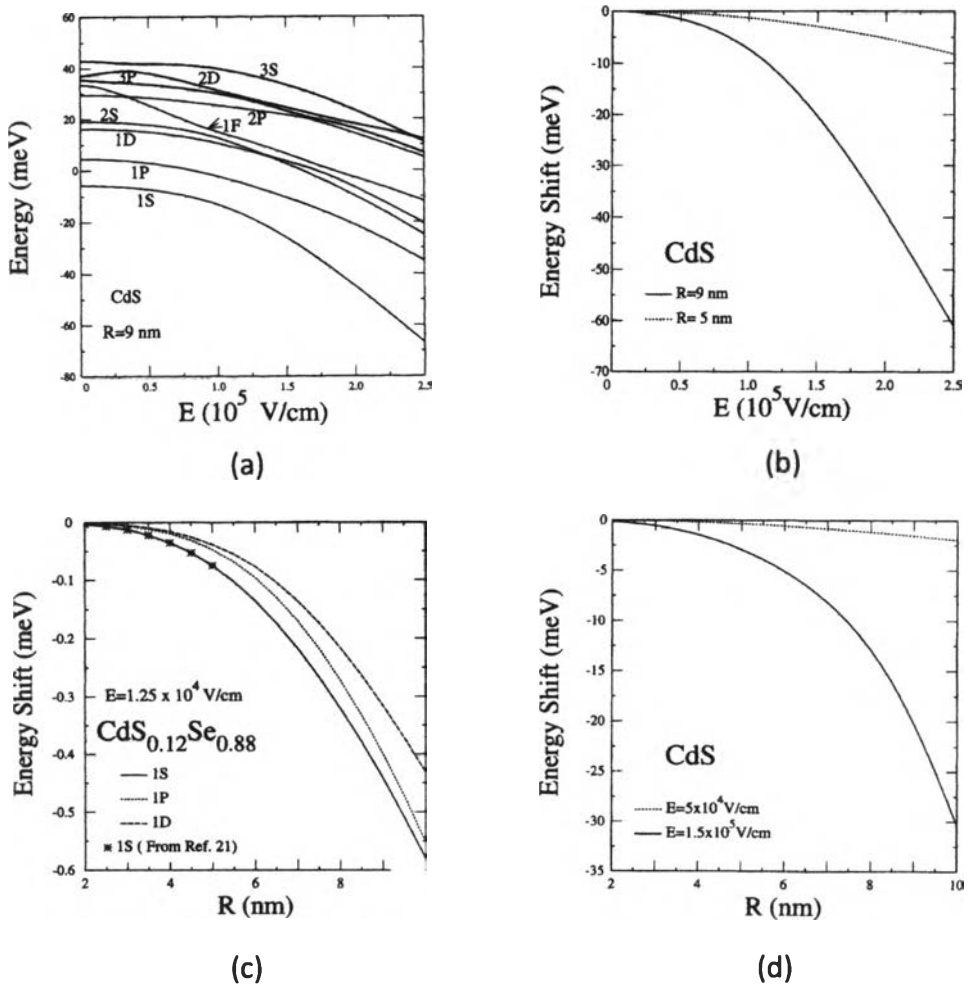

Figure 2.27 Illustration of (a) the energy levels of exciton as a functions of applied electric field in a CdS QD of radius R, (b) energy shifts of the ground state exciton as a functions of applied electric field for QD sizes of $R = 9$ nm (solid line) and $R = 5$ nm (dotted line), (c) energy shifts of the ground state (solid line) and the first (dotted line) and the second (dashed line) of the confined exciton as a functions of QD size with electric field 1.25×10^4 V/cm, and (d) energy shifts of the ground state exciton in QD as a functions of R for two representative electric filed 5×10^4 (dotted line) and 1.5×10^5 (solid line) **[146]**.

where $V(n_1l_1n_2l_2LM)$ are the expansion coefficients determined from the diagonalization the Hamiltonian of **Eq. (2.79)** with the basis of **Eq. (2.81)**. Manipulating

all the equation above with the method mentioned in **[146]** so the Hamiltonian of **Eq. (2.79)** is diagonal respect to M, then, diagonalize the total Hamiltonian which is obtained the eigenvalues and wavefunctions for states with different M. The theoretical interpretation by discussion an energy level, energy shift, electron-hole distribution functions and radiative decay rate of the confined exciton in a quantum dot under an applied electric field are concluded as follows:

A. The Stark shift of the exciton energy level

Figure 2.27 (a) shows many interesting features. First, there are many **"anticrossover"** regions for different states which manifest the anticrossover at dissimilar electric field values. Secondly, the effect of Coulomb interaction between electron and hole in this case ($R = 9$ nm) is stronger than the quantum confinement effect because the energy of the ground state $1S$ is negative or below the bandgap. Third, as energy level shift toward the low energies, the applied electric field increase. The amount of shifting is more for the lower energy level, the same meaning as the quantum confined stark effect in quantum well structure which is already discussed.

Figure 2.27 (b) depicts the Stark shift of the ground state of an CdS quantum dot of size $R = 9$ nm (solid line) and 5 nm (dotted line). The higher order perturbation between the electric field and excitons are important for determing the energy of the exciton which cannot described with a simple E^2. The amount of Stark shift is much larger for large quantum dot. Note that it is very difficult to observe this shift experimentally if the broad quantum dots size distribution exists (in this case, the Stark shift of quantum dot with $R = 5$ nm is only a few meV at applied field about 10^5 V/cm).

Figure 2.27 (c) shows the energy shift of the three lowest states of the exciton functions of the quantum dot for various R under the electric field. The energy shift of the ground state energy is much larger than other two excited states. The results agree very well with those calculation in **[149]**. For a quantum dot with a large radius, the Coulomb interaction between electron and hole become important and the actual eigenstate is a mixture of single particle states with different angular momentum.

Figure 2.27 (d) shows plot of the quantum dot size dependence of the ground state energy of the exciton for two different applied electric field; 5×10^4 (dotted line) and 1.5×10^5 (solid line). The amount of shift is much larger for larger quantum dot corresponding to the results in **Figure 2.27 (c)**. The quantum confined stark effect on excitons in quantum dot depends on the included effective electric dipole moment of the exciton, which is related to the product of E_a and R by the exciton in the larger quantum dot also have larger quantum dot included effective electric dipole moment.

B. Electron and hole distributions inside quantum dot

Figure 2.28 (a) displays the plot of the distribution functions of electron (a) and hole (b) of the CdS quantum dot for different sizes; $R = 2$ nm (solid line), $R = 5$ nm (dotted line) and $R = 8$ nm (dashed line) in the absence of electric field. The widths of the electron and hole distribution functions increase with decreasing radius of quantum dot. This is due to the fact that kinetic energies $\left(\hat{\mathrm{H}}_i = -\frac{\hbar^2}{2m_i}\nabla_i^2\right)$ of electron and hole are larger for smaller quantum dot because of the stronger confinement, which enables them to move farther away from the center.

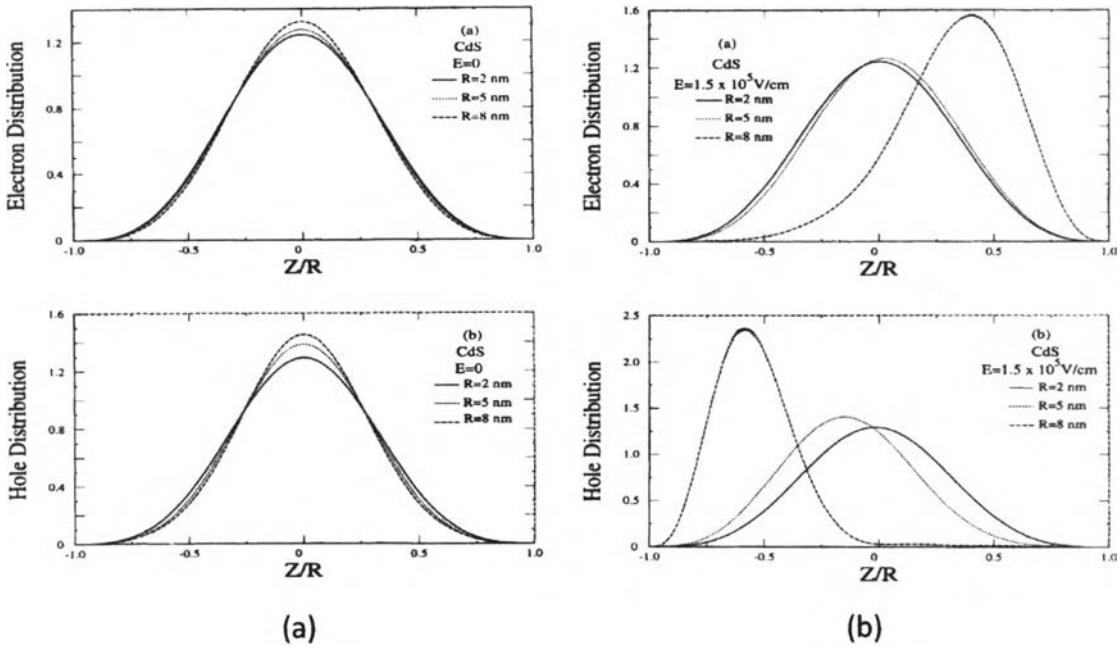

Figure 2.28 Representation of (a) electron and hole distribution functions in the absence of an applied electric field in QD for three different sizes of $R = 2$ nm (solid line), 5 nm (dotted line) and $R = 8$ nm (dashed line) in the absence of electric field, (b) in the presence of an applied electric field 1.5×10^5 V/cm **[146]**.

When electric field is applied in the same condition illustrated in **Figure 2.28 (b)**, the positions of the distribution maxima of electron and hole shift away from the center and the electron (hole) shifts toward the positive (negative) z direction, so excitions in quantum dot are "**polarized**" by the applied electric field. The width of the distribution function for the electron under the electric field is larger than hole since the smaller effective mass (larger kinetic energy) of the electron than that hole, which causes the electron to distribute farther away from the center than the hole. Furthermore, the distribution functions for both the electron and hole become narrower as the quantum dot radius increase. For $R = 2$ nm, the electric field does not significantly change their distributions that consistent with the results as shown in **Figure 2.27 (a) - (d)**.

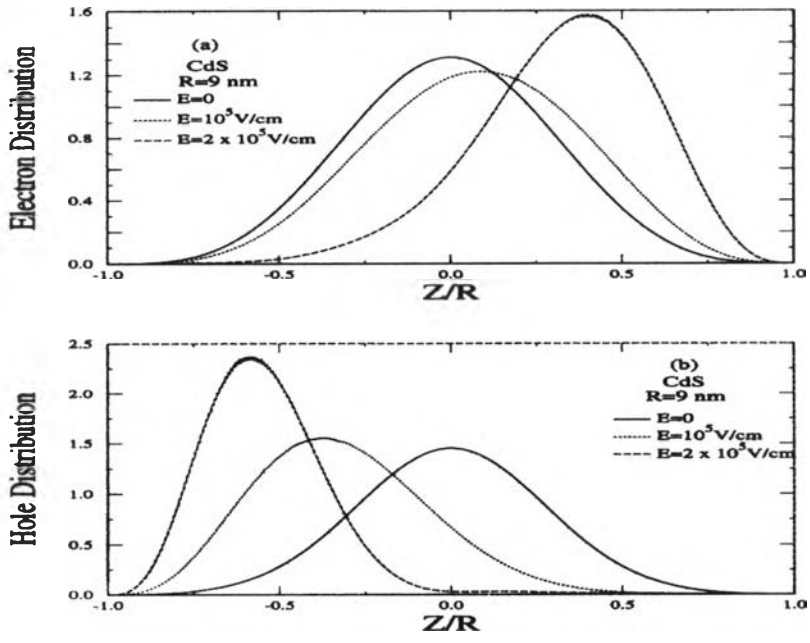

Figure 2.29 The electron (a) and hole (b) distribution functions in QD for three different magnitudes of $E = 0$ (solid line), 10^5 V/cm (dotted line), and 2×10^5 V/cm (dashed line) with $R = 9$ nm **[146]**.

Figure 2.29 plots the electron (a) and hole (b) distribution functions under three representative applied electric fields for fixed quantum dot size at $R = 9$ nm. The distribution maxima move toward the $+z(-z)$ direction for electron (hole) as the electric field increases. Both the electron and hole tend to distribute near the surface under a strong electric field by hole distribution function is narrower than that of the electron as discussed in **Figure 2.28 (a)**.

Figure 2.30 is a plot of effective electric dipole moment for the ground state of an exciton in a CdS quantum dot of radius $R = 9$ nm as a function of applied field. The averaged distance between the electron and hole in the z direction (or induced electric dipole moment of the exciton) increases as the electric field increases. Note that the induced electric dipole moment of the exciton is determined by the competition between the Coulomb interaction of excitons and the Stark effect.

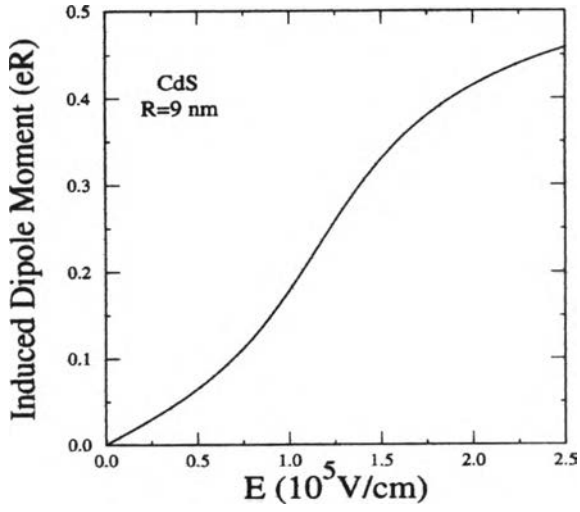

Figure 2.30 The induced electric dipole moment as a function of applied electric field for a QD of size $R = 9$ nm **[146]**.

Three different regions can be observed in **Figure 2.30**. At the lower field region, the Stark effect is weaker and the electron and hole behave more like a pair which induces a small effective electric dipole moment. At the intermediate field region (8×10^4 to 2×10^5 V/cm), the induced electric dipole moment increase more rapidly. At the high field region (above 2×10^5 V/cm), the induced electric dipole moment of exciton tends to be saturated due to the confinement of the quantum dot.

C. Exciton decay rate

Figure 2.31 shows the applied electric field dependence of the radiative recombination rate can be calculated from **[146]** for CdS quantum dot of $R = 9$ nm (solid line) and 5 nm (dotted line). For a larger quantum dot, the recombination rate decreases slowly initially. It decreases very fast when the applied electric field strength is in the range between 0.8 and 1.8×10^5 V/cm and becomes flat again when the field is above 2×10^5 V/cm. The exciton lifetime under the electric field of 2.5×10^5 V/cm is about six times that under zero field for the same quantum dot size ($R = 9$ nm). The recombination rate for the smaller quantum dot is much weaker than that, which is consistent with the fact that a smaller quantum dot is less

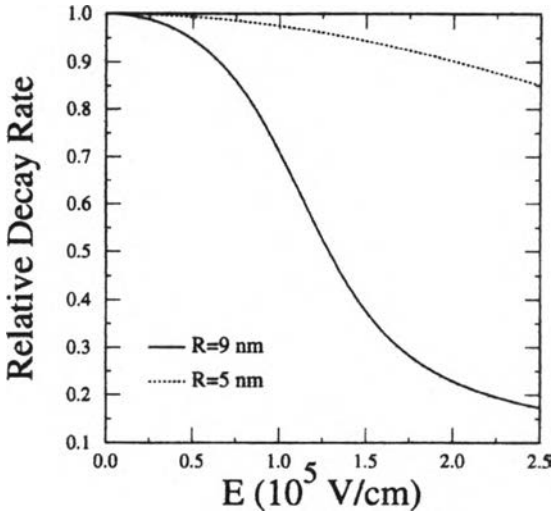

Figure 2.31 The relative decay rate of exciton as a function of the applied electric field for the ground state exciton in QD of size $R = 9$ nm (solid line), 5 nm (dotted line) **[146]**.

influenced by the electric field due to a stronger confinement.

These theoretical results can make a short summary as follows: the electron and hole wavefunction overlap decreases under an applied field, which implies an increased exciton recombination lifetime due to the quantum confined stark effect. The energy level redshift and the enhancement of the exciton recombination lifetime are due to the polarization of the electron-hole pair under the applied electric field. The calculated results are consistent with electroabsorption and photoluminescence experiments on the quantum confined stark effect in quantum dot **[149-150]**.

2.5.3.2 Theoretical studies of vertical and parallel electric field on semiconductor quantum dot

Recently, because of experimental in many groups have been focused on InAs/GaAs self-assembled quantum dot since attractively optical properties **[65, 137-138, 141, 143, 151]**, therefore, theoretical studies related with were also investigated for characterization some behaviors and development to the novel optoelectronic devices based on quantum dot. Grundman *et al* studied the strain distribution, optical phonons, and electronic structures of InAs/GaAs quantum dot **[70]**. Taking into account the effect of valence band mixing and strain, Cusack *et al* studied the electronic structure of InAs/GaAs self-assembled quantum dot **[151]**. In case of electric field effect on the direction dependence were achieved by Shen Li *et al* **[152]**, who theoretically study the electron and hole energy level structures and optical transition energy of InAs self-assembled quantum dot in different direction of electric field; the perpendicular electric field and the parallel electric field. Shen Li *et al* gave a theoretical model for calculating the electronic structures of an InAs self-assembled quantum dot in the presence of an electric field by choosing the growth direction (100) as the z direction of coordinate system, and assuming the InAs self-assembled quantum dot as a cylinder with radius R in the parallel direction and height L in the z direction. The time-independent Schrödinger equation with Hamiltonian of electrons by Burt and Foreman's effective mass envelope function theory **[153-154]** neglecting the second and higher order terms in the presence of electric field F in the z direction is

$$H_e = \mathrm{P}\frac{1}{2m^*(r)}\mathrm{P} + V(r) - eFz \qquad \textbf{(2.83)}$$

where P is the electron momentum operator and

$$m^*(r) = \begin{cases} m_1^* & \text{for } |z| < L/2 \text{ and } x^2 + y^2 < R^2 \\ m_2^* & \text{elsewhere} \end{cases} \qquad \textbf{(2.84)}$$

$$V_e(r) = \begin{cases} 0 & \text{for } |z| < L/2 \text{ and } x^2 + y^2 < R^2 \\ V_{e0} & \text{elsewhere} \end{cases} \quad \textbf{(2.85)}$$

where m_1* and m_2* are the electron effective masses in InAs and GaAs materials, respectively. For the electron envelope function equation $H_e\Psi_e = E_e\Psi_e$, solving the eigenvalues and eigenfunctions of the system by using period boundary conditions, and expanding Ψ_e in terms of normalized plane-wave states, and diagonalizing the resultant matrix **[151]**. Then, the electron wave functions have the following forms

$$\Psi_e(r_e) = \frac{1}{\sqrt{L_x L_y L_z}} \sum_{nml} C_{nml} e^{i\left[(k_x + nK_x)x + (k_y + nK_y)y + (k_z + nK_z)z\right]} \quad \textbf{(2.86)}$$

with $K_i = 2\pi / L_i$ ($i = x, y$ or z), L_i is normalized lengths along the corresponding direction. For a cylindrical quantum dot, $L_x = L_y$ and $n, m, l = 0, \pm 1, \pm 2, \ldots$.

For the hole wave functions, using the normalized plane-wave expansion method **[151]**, the formula is the same as **Eq. (2.86)**, but replaced C_{nml} terms with $\left[a_{nml}\ b_{nml}\ c_{nml}\ d_{nml}\right]^T$. Calculating the matrix element with parameters included with the effect of finite offset, valence band mixing, and strain are all taken into account given in **[152, 155]**, the results was shown in **Figure 2.32** and **Figure 2.33**.

Figure 2.32 (a) and **(b)** give the first two energy levels of electrons as a function of electric fields along the growth direction and along the parallel direction, respectively. **Figure 2.32 (a)**, the electronic ground state energy level is weakly affected by the vertical electric field when the electric field is lower than 3×10^5 V/cm because the quantum dots have a small height (3 nm). Along the parallel direction, the quantum dot have a large diameter (10 nm), and strongly affected by

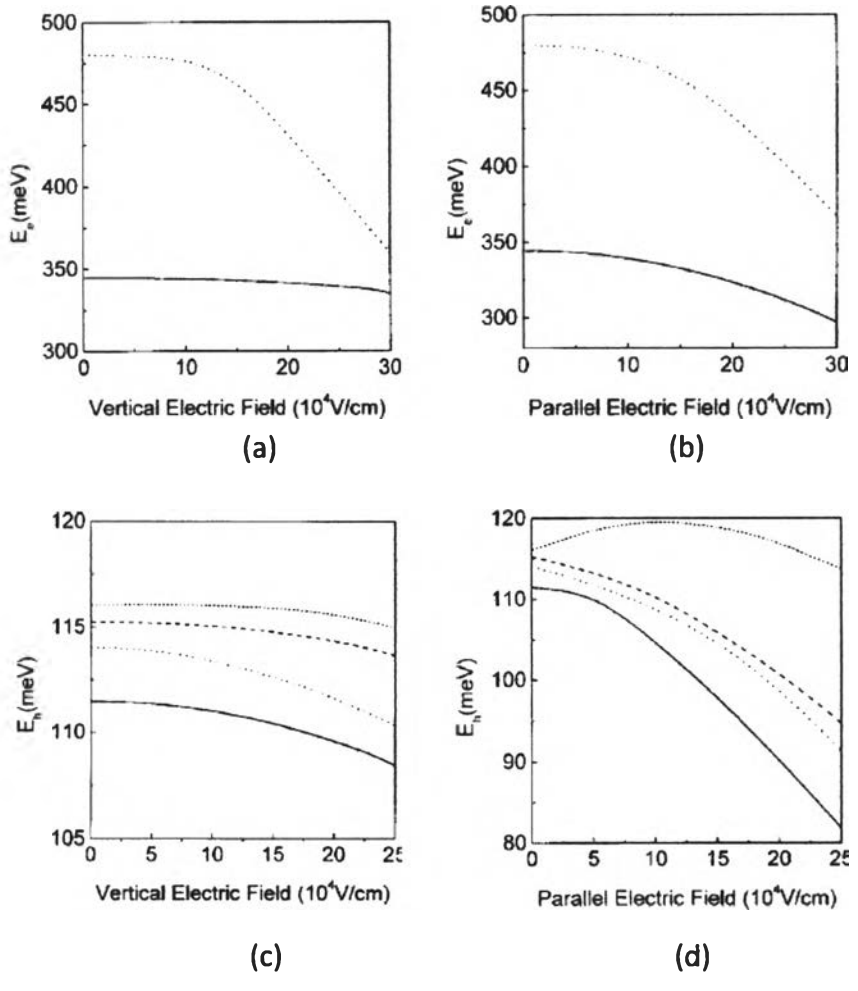

Figure 2.32 The ground state energy level (solid lines) and the first excited state energy level (dotted lines) of electron as a function of electric fields along the growth direction (a) and along the parallel direction (b) with the diameter and height of the QD are 10 and 3 nm, respectively. The first four energy levels of the hole as functions of electric fields along the growth direction (c) and along the parallel direction (d) with the same diameter of the QD. The solid lines, dotted lines, dashed lines, and short-dashed lines in (c) and (d) correspond to the first heavy-hole, the first light-hole, the second heavy-hole, and the third heavyhole energy levels, respectively **[152]**.

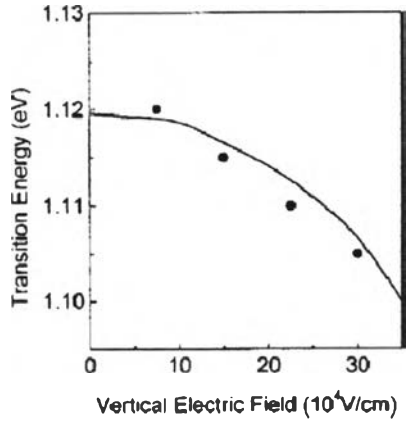

Figure 2.33 The transition energies of the first electron energy level to the first heavy-hole energy level along the growth direction. The diameter and height of the QD are 5 nm **[152]**. The black circles are experimental results **[156-157]**.

the parallel electric field, corresponding to **Figure 2.32 (b)**. From **Figure 2.32 (a)** and **(b)**, the two energy levels decrease when the electric field increase by the first excited state energy levels (dotted line) are affected by an electric field stronger than the ground state energy levels (solid lines). The energy difference between the ground state and the first excited state decreases as the electric field increases. **Figure 2.32 (c)** and **(d)** show the first four energy levels of the hole as a function of electric fields along the growth direction and along the parallel direction, respectively. The hole energy levels have complicated structures due to the **"valence band mixing"** between the heavy hole and light hole. **Figure 2.33** depicts the transition energies of the first electron energy level to the first heavy-hole energy levels along the growth direction under the perpendicular electric filed. The optical transition energies (solid line) have clear redshifts in the vertical electric filed. This theoretical result is very close to the experimental data (black circle) studied by Fry *et al* **[156-157]** in the research of the electronic states as a function of applied vertical electric field in InAs/GaAs self-assembled quantum dot using photocurrent spectroscopy. The quantum dot in the different direction of electric field are very interesting for both theory and application.

Studying the electronic structure properties of quantum dot can provide useful information on the potential application of them. In application, a quantum controlled logic gate may be realized by quantum dot under an external static electric field **[158]**. A single-electron quantum dot embedded in a semiconductor is a candidate for the solid-state qubit, which is used in solid state quantum computing **[159]**. Others are useful for the application of quantum dot to photoelectric devices.

2.5.3.3 Experimental investigation of electric field on quantum dot structure

Some experimental of electric field on quantum dot structure will be discussed in this topic tentatively though it is not relate to a scope in this thesis, but the purpose is to illustrate of the real system for comparison with the theoretical studies, then build up overall point of view later. The interesting experimental mentioned above was published by Peng Jin *et al* **[160]** about quantum-confined stark effect and built-in dipole moment in self-assembled InAs/GaAs quantum dot. Peng Jin *et al* introduced by the fact that the theoretical studies of electronic structure in In(Ga)As quantum dot have shown that spatial separation of the electron and hole wave functions (i.e., interband built-in dipole moment) exists in the dots, which results in asymmetric Stark shift in an applied electric field **[70, 151]**. For pure InAs or InGaAs quantum dot with homogeneous composition profile, the electron wave function should locate above that of the hole, which tends toward localizing closer to the base of the dot **[162-163]**. The electron–hole alignment can be inverted in the dot with graded InGaAs composition [**[161-163]** and this effect has been experimentally observed in many researches **[163-163]** which is related to the temperature. At such temperatures, In-Ga interdiffusion and In segregation of substances are believed to produce the nonuniform composition distribution in quantum dot. The built-in dipole moment induced by intersubband electron–electron transition has been studied in **[164]** which is affected on lasing properties of quantum dot laser diodes **[167]** Peng Jin *et al* investigated the interband transition energy of InAs self-assembled quantum dot embedded in GaAs *p–i–n* structure

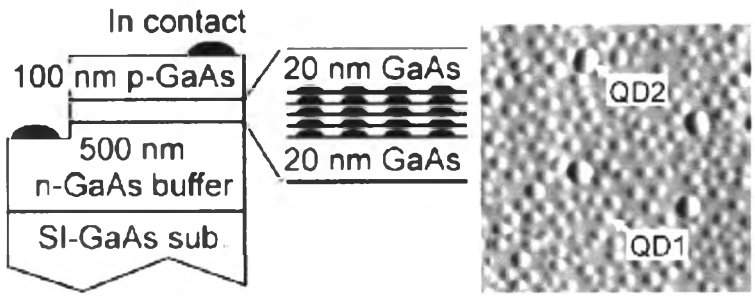

(a) (b)

Figure 2.34 Schematic of sample structure (a) and the AFM image of the Reference sample (b). The quantum dots exhibit bimodal size distributions. QD1 and QD2 are assigned to denote the small and the large quantum dots, respectively **[160]**.

by electroreflectance (ER) **[170]** as a function of the applied electric field.

Figure 2.34 (a) represents the sample structure. The five stacks of quantum dot were grown by molecular beam epitaxy system at relatively low temperature ($460°C$) so that In–Ga interdiffusion and In segregation can be weakened during the growth. The electric field in the undoped GaAs layer as a function of the bias voltage is determined by Franz–Keldysh oscillations (FKOs) **[168]** above the GaAs band gap. Two indium contacts were formed on the *p*-type GaAs contact layer and the *n*-type GaAs buffer. The reference sample for atomic force microscopy (AFM) measurement, which left the top layer of quantum dot stacks uncapped, was grown with the same growth parameters shown in **Figure 2.34 (b)**. It was found that quantum dot with bimodal size distributions were formed: smaller (QD 1) and larger (QD2) quantum dot. ER measurements have been performed under various bias voltages at 77 K in the photon energy range of 1.24–2.5 eV. **Figure 2.35** is an ER spectrum under zero bias voltage. The results are separated in two conditions:

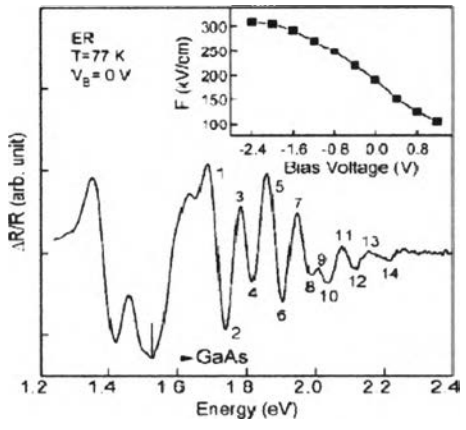

Figure 2.35 The ER spectrum in the photon energy range of 1.24–2.4 eV of the investigated sample under zero bias voltage at 77 K. Integers are FKO extremum indices. The bias voltage dependence of the built-in electric field in the undoped GaAs layer is presented in the inset by closed squares. The solid line is intended as visual guides. **[160]**.

- Above the GaAs band gap, a large number of FKOs from the undoped GaAs layer of the *p–i–n* structure have been observed.

- Below the GaAs band gap, which overlap the ER signal from GaAs below the band gap, come from InAs wetting layer. The electric field F in the undoped GaAs layer of the sample can be determined quantitatively by the relationship between the energy position E_n of FKO extrema and the extremum index n

$$\frac{4}{3}\left[(E_n - E_g)/(\hbar\theta)\right]^{3/2} + \varphi = n\pi \qquad \textbf{(2.87)}$$

The explanation of the equation is the same as that in **[169]**. **Eq. (2.87)** shows that $(E_n - E_g)^{3/2}$ versus n should be a straight line with a slope of $\frac{3\pi}{4}(\hbar\theta)^{3/2}$ from which one can obtain the electric field F. The inset **in Figure 2.35** shows the dependence of the electric field on the bias voltage. The applied voltage

(x coordinate) is taken as positive when the external potential of the *p*-type contact layer is higher than that of the *n*-type buffer layer. The electric field F is positive when the field lines point from the *n*-type buffer to the *p*-type layer. The nonlinear relation between the electric field and the bias voltage is probably caused by the formation of nonohmic contacts between In electrodes and doped GaAs layers.

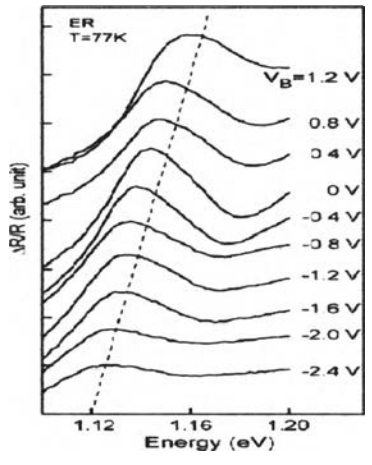

Figure 2.36 The ER spectra for QD1 under various bias voltages at 77 K (shifted vertically for clarity). The dashed line is a guide for the eyes. **[160]**.

Figure 2.36 shows an ER feature in the energy range of 1.1–1.2 eV under various bias voltages. By comparing the ER spectra with the photoluminescence spectrum, in which the ground-state interband transitions for QD1 and QD2 are at 1.143 and 1.079 eV, respectively. It was found that the ER signal moved to the higher energy when the bias voltage increased. The tilting of the ER spectra is probably caused by the superposition of the ER signal from GaAs below the band gap and/or of the signal from InAs wetting layer. In the ER measurement in the energy range of 1.1–1.2 eV, the second-order diffractive light in the range of 2.2–2.4 eV from the monochromator was filtered by a long-wavelength-pass filter with the cutoff wavelength of 700 nm, so that ER signals from GaAs in the energy range of 2.2–2.4 eV could not produce any influence on the ER line shape of quantum dot.

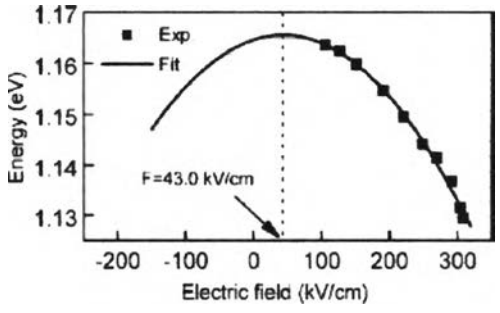

Figure 2.37 The electric field dependence of the ground-state interband transition energy of QD1. The solid parabola is a least-squares fit to **Eq. (2.88)**. When the electric field is 43.0 kV/cm, the parabola reaches its top. **[160]**.

The experimental dependence of the transition energy on the electric field is plotted in **Figure 2.37** by closed squares. When the electric field increases from 105 to 308 kV/cm, **"redshift"** of 34 meV is observed because of the quantum confined stark effect. It is obtained by theoretical studies and confirmed by some experiments that quantum dot should exhibit a quadratical dependence of the interband transition energy E_T on the applied field F **[161-163]**,

$$E_T = E_T(0) + pF + \beta F^2 \qquad \textbf{(2.88)}$$

where $E_T(0)$ is the zero-field transition energy, p is the built–in dipole moment in quantum dot, and β is a measure of the polarizability of the electron and hole wave functions (i.e., the quantum confined stark effect). A least-squares fit to **Eq. (2.88)**. for the experimental field dependence of the transition energy is displayed by the solid curve in **Figure 2.37**. The fitting curve exhibits obvious asymmetry about the zero electric field. When the electric field is equal to 43.0 kV/cm, the parabola reaches its top. This implies that the electron wave function lies above that of the hole at zero electric field, with the dipole pointing from the dot apex to the base and the resulting dipolar direction is the same as that predicted by theoretical calculations **[70, 151]** for ideal pyramidal InAs quantum dot. However, most experiments for In(Ga)As quantum dot **[163-165]** have observed a dipole moment

which is opposite from that in ideal quantum dot. The inverse dipole direction is considered to be due to nonuniform InGaAs composition in those dots. In this work, since the sample were grown at relatively low temperature, at which In–Ga interdiffusion and In segregation can be weakened and nearly pure InAs quantums are expected to be formed. As a result, the sign of the dipole in the dots is consistent with that in ideal InAs quantum dot predicted by theoretical calculations. The existence of built-in dipole moment in quantum dot is **"unfavorable"** for quantum dot laser devices because it would reduce the ground-state electron–hole overlap **[167]**. In the above, the sign of the dipole moment in InAs/GaAs quantum dot s grown at low substrate temperature can be reversed as compared with that in quantum dot grown at relatively high temperature reported in **[163-164]**. It is expected that InAs/GaAs quantum dot with zero dipole moment can be obtained at a moderate substrate temperature.

In conclusion, there are other important theoretical models about electric field on quantum dot, particularly the size and shape dependence **[69, 171]** which is related to the effect of strain distribution for calculation in the refinement results. Nevertheless, in the framework of this thesis overemphasizes the prediction of quantum electronic phenomena so the non-complicated quantum dot structure was used. The structure of quantum dot presented in thesis work is "Rectangular Quantum Dot" for simplicity, and it was reported about the research of this quantum dot shape in electric field as follows: "Dynamical localization of a square quantum dot molecule under magnetic and electric fields" **[172]**, "Dynamical control of correlated states in a square quantum dot" **[173]**. Especially the research topic "DC Electric Field Effects on the Electron Dynamics in Double Rectangular Quantum Dots" **[174]** that our thesis work will be presented in the same idea (in case of shape), but in the different way investigating and extending the model to the "Aligned Rectangular Quantum Dots" with the more precisely than the ones. Furthermore, the calculation will manifest some interesting results that were not appeared in the reference paper **[172-174]** under the scope of thesis work.

2.6 POLARIZATION STUDIES OF THE QUANTUM DOT

More and more interest, the subject matter had progressed to the main point of thesis work, that is, **"theoretical studies of polarization effect on the quantum dots structure"**. Basically, polarization is a property of certain types of waves that describes the orientation of their oscillations. Electromagnetic wave is a transverse wave which has both an electric and a magnetic component. In other words, the transverse nature of an electromagnetic wave is closely related to the light. In terms of light, a light wave is an electromagnetic wave which are produced by vibrating electric charges. In general, the oscillation of electric field in electromagnetic waves is not specify a certain direction. A light wave which is vibrating in more than one plane is referred to as unpolarized light such as light emitted by the sun. Such light waves are created by electric charges which vibrate in a variety of directions, thus creating an electromagnetic wave which vibrates in a variety of directions. To transform unpolarized light into polarized light, the process of removal of undesired component of light is called "polarization of light waves". By convention, the polarization of light is described by specifying the orientation of the wave's electric field at a point in space over one period of the oscillation. Sometime the undesired components from the light wave is necessary to remove in order to reduce its intensity for utilizing in some purposes.

The phenomena of polarization is significant in areas of science and technology dealing with wave propagation, such as science, seismology, telecommunications and optics. The application from polarization effects also deal with everyday life, for example, biology, geology, chemistry, communication, electronics,...etc **[175-176]**. In the application of optical semiconductor devices (especially modulator devices and optical fiber), which refer the knowledge of electronics branch, is a complex issue since some complicated concepts are investigated such as Pockels effect, non-linear effect (Kerr effect), electrooptic

effect, electrorefraction (birefringent), photon polarization, and other effects related with them **[177]**.

2.6.1 Polarization Anisotropy in Quantum Dot Structure

Recently, self-assembled quantum dots have been intensively studied during the past decade from the viewpoint of fundamental physics and optoelectronic device applications because the atomic-like electronic characteristics are expected to bring significant progress in applications **[54]**. Polarization properties of self-assembled quantum dots are of interest from fundamental and device point of view, not only waveguide structures **[54]**, but also for the application of QDs in quantum spintronics (i.e. processing of quantum information with spin states in quantum dots) **[178]**. For optoelectronic devices, the carriers dynamic between the conduction band and valence band is important to investigate obviously for applying their performance, which is linked to the optical transitions. The optical transitions are very sensitive to the symmetry of the confinement structure. This means that shape anisotropy, composition gradients, strain, etc, can induce polarization asymmetry and non-parabolic bands **[179-180]**. The polarization anisotropy in photoluminescence has been investigated theoretically as well as experimentally by many groups. It has been reported that a strong polarization dependence in the photoluminescence spectrum was appeared in asymmetric shaped quantum dots **[179-180]** and has been used to improve optical device performance **[181]**.

To extending the meaning of **"polarization anisotropy"**, one may described in terms of **"linear polarization"** for clearly understanding. The linear polarization or plane polarization of electromagnetic radiation is a confinement of the electric field vector or magnetic field vector to a given plane along the direction of propagation. Consider the quantum dots, assuming that the intensity of light emitted

from the dots has component in x (I_x) and y direction (I_y). Consequently, the "linear polarization degree" (LPD) of two-dimension is introduced by **[182]**

$$LPD = \left| \frac{I_x - I_y}{I_x + I_y} \right| \tag{2.89}$$

LPD is a quantity used to describe the portion of an electromagnetic wave which is polarized. If I_x larger than I_y, so $LPD > 0$. The increasing of LPD value indicated that luminescence from the dots is partially polarized, and therefore can be represented by a superposition of a polarized and unpolarized component. This value is between 0 and 100%. In case of $I_x \approx I_y$, $LPD \approx 0$ or the light is unpolarized. The another case when $I_x >> I_y$, $LPD \approx 1$ or the light is perfectly polarized and emitted mostly in the x direction. The physical interpretation means that the transition probability of carrier in x direction is higher than one, so optical transition in the x axis is dominant. On the other hand, the quantum dots shape is elongated in x direction which increase the transition probability, then I_x is increased. Now, the transition in the x and the y direction are not the same, thus quantum dot with non-isotropic shape show a certain linear polarization degree as was reported in **[180]**.

Figure 2.38 Different polarization states of laser emission, illustrated for a few cycle pulse propagating from left to right **[183]**.

The example of device following this effect, although not all, in case of the output of laser, is polarized. This normally means a linear polarization state, where the electric field oscillates in a certain direction perpendicular to the propagation direction of the laser beam. There are cases (occurring i.e. with fiber lasers) where a different, i.e. elliptical but also more or less stable polarization state is generated, which can be transformed into a linearly polarized beam by using an appropriate combination of waveplates. Polarized laser emission is important for a range of applications such as, nonlinear frequency conversion (where phase matching in a nonlinear crystal is normally obtained only for one polarization direction), polarization-coupled (or polarization beam combining), processing of laser beams in polarization-dependent devices (i.e. interferometers, semiconductor optical amplifiers, and optical modulators). However, some lasers (in many fiber lasers) do not generate a polarized output. This does not necessarily mean that the laser output is truly unpolarized, containing equal optical powers in two polarization components at any time ($I_x \approx I_y$), without any correlation of the corresponding amplitudes. The polarization state may simply be unstable due to temperature drifts, or randomly switch between different directions.

The degree of linear polarization is often quantified with the **polarization extinction ratio** (PER) **[184]**, defined as the ratio of optical powers in the two polarization directions, often specified in decibels, and measured by recording the orientation-dependent power transmission of a polarizer. Note that the polarization state of the laser output can be disturbed e.g. by random (and temperature-dependent) birefringence, such as occurs e.g. in optical fibers (if they are not polarization-maintaining or single-polarization fibers) and also in laser crystals or glasses as a result of thermal effects (or depolarization loss). If the laser gain is isotropic, small drifts of the birefringence may lead to large changes of the polarization state, and also a significant variation in the polarization state across the beam profile.

The optical anisotropy in case of quantum dots structure is discussed in terms of asymmetric strain in the surrounding matrix of quantum dots. The polarization of the photoluminescence is related to the strain in a material by way of the given material's photoelasticity tensor. Generally, the fabrication of quantum dots does not give an exactly uniform size (with the length in all direction are equivalent or isotropic shape). The light emitted from this ideal quantum dots are nearly unpolarized or randomly distributed in all direction (same as LED) **[185]**. In fact, the effect of strain field is mainly significant to push the real quantum dots shape away from the isotropic case, that is, optical anisotropy in real quantum dots are probably occurred.

Investigation the effect of optical anisotropy in the realistic quantum dots has been achieved exterimentally. Nakaoka *et al* **[186]** studied the optical anisotropy of self-assembled InGaAs quantum dots embedded in wall-shaped and air-bridge structure. The observation from photoluminescence spectra in quantum dots structure found that that large optical anisotropy in the quantum dots is induced by lateral patterning of the matrix of the dots, although the anisotropy is absent in the as-grown dots the quantum dots (in which originally isotropic). This is due to the fact that the strain effect on optical anisotropy of quantum dots having been investigated by changing the surrounding matrix of the dots. A reduction of the optical anisotropy is observed by changing the laterally patterned structure into a free-standing structure or an air bridge as depicted in **Figure 2.39 (b)**. The anisotropy in the wall-shaped structure can be reduced in the air bridges which is mainly attributed to the strain relaxation in the air bridge (strain asymmetry in the fabricated structures). The presence of the strain asymmetry is confirmed by the observation of spectrally resolved photoluminescence in single quantum dot structure. This is consistent with the combined effect of strong electron–hole exchange interaction in the presence of the asymmetric strain. and its relaxation.

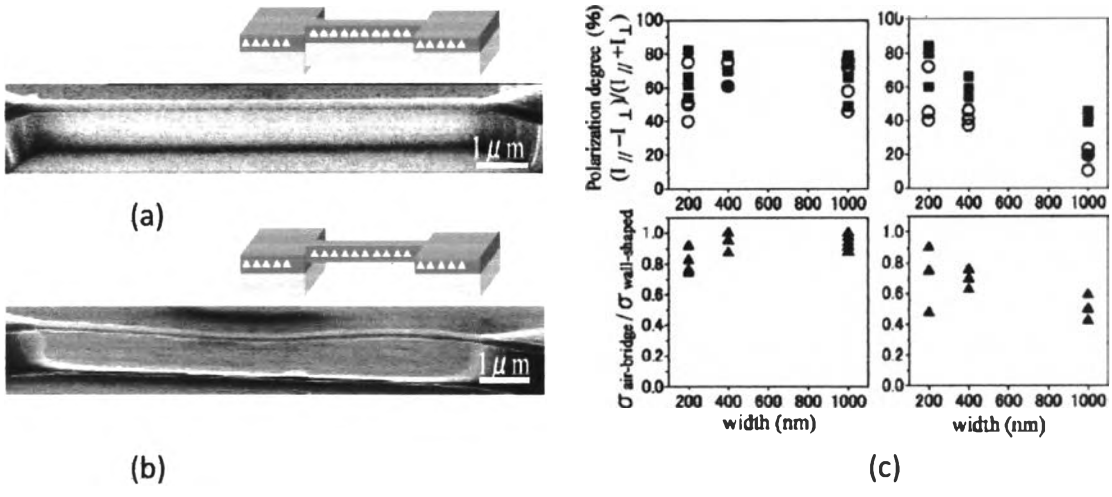

Figure 2.39 Schematic illustrations and SEM images of (a) a wall-shaped structure and (b) an air bridge, both with a length of 10 mm and a width of 400 nm. The thickness of the air bridge is 50 nm. (c) Polarization degrees in wall-shaped structure (solid squares) and air bridges (open circles). The ratios of the polarization degree in the wall-shaped structure to that in the air bridge, measured at the same positions, are shown by triangles **[186]**.

The experimental mentioned above manifests briefly in the appearance of the optical anisotropy for quantum dot structure. Now, the theoretical studies will be discussed because the scope of thesis work focuses to this point. Again and again, the quantum mechanics are used to describe the theoretical interpretation. To analysis the polarization properties, utilizing the electron and the hole wavefunctions, the polarization property for each transition can be theoretically calculated. The polarization property is determined with the localization of the wavefunctions of carriers. In bulk materials, the electrons and holes can move around in every direction without any restriction (their wavefunctions distribute uniformly), and thus the dipole moment which is determined by the overlap integral of the wavefunctions of electrons and holes has no directional dependence. Therefore, the emission PL spectrum has no polarization property. The situation is different by the introduction of the quantum-confined structures which restrict the

movement of electrons and holes, the wavefunctions tend to localize. Especially, the quantum dot structure produces the complete localization of wavefunctions, which leads to the polarization of the luminescence for each transition **[187]**.

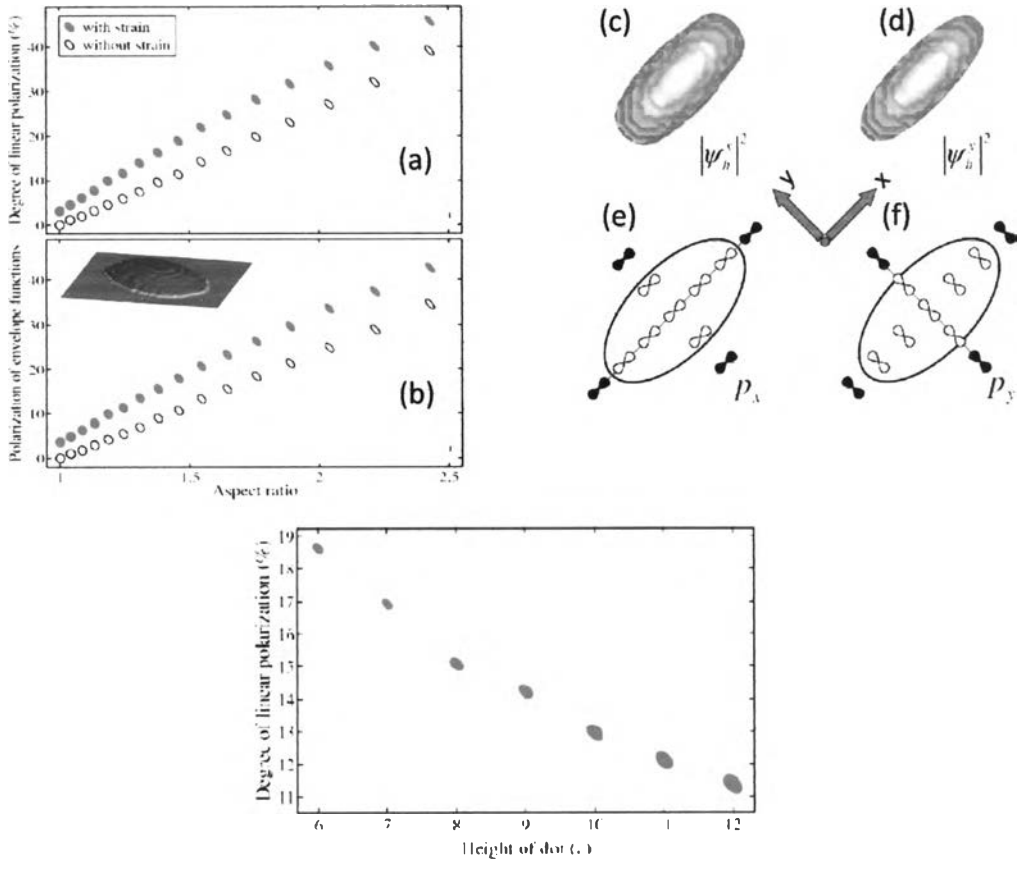

Figure 2.40 Illustration of degree of linear polarization of interband transitions (a), and (b) polarization of envelope functions of p_x and p_y orbitals calculated as a function of aspect ratio. The probability density of a valence-band electron occupying the p_x orbital (a) and p_y orbital (b) and schematic distribution of p_x (c) and p_y (d). (g) Plot an optical anisotropy calculated as a function the height of the QDs **[188]**.

Some of the interesting theoretical studies will be discussed as follows: Sheng *et al* **[188]** represented the optical anisotropy in quantum dots. Sheng *et al* modeled the **"elongated"** InAs/GaAs self-assembled quantum dot, as shown in the inset of **Figure 2.40 (b)**. This lens shaped quantum dot can be varied the degree of elongation via aspect ratio $\beta = d_x / d_y$ where d_x and d_y are the dimension along the long ($x = [1\bar{1}0]$) and short ($y = [110]$) axes of the elongated structure, respectively. The degree of linear polarization of interband transitions is defined by

$$P_{eh} = \frac{\left|\langle \Psi_e | \hat{p}_x | \Psi_h \rangle\right|^2 - \left|\langle \Psi_e | \hat{p}_y | \Psi_h \rangle\right|^2}{\left|\langle \Psi_e | \hat{p}_x | \Psi_h \rangle\right|^2 + \left|\langle \Psi_e | \hat{p}_y | \Psi_h \rangle\right|^2} \qquad \textbf{(2.90)}$$

where Ψ_e and Ψ_h are the ground states of electrons and holes, respectively. The electron and hole states are calculated by an empirical sp^3 tight-binding method **[189-190]**. The p_x and p_y orbitals are chosen to align along the long and short axes of the dots, respectively. **Figure 2.40 (a)** plots the degree of linear polarization of interband transitions P_{eh} calculated as a function of the aspect ratio β. When the aspect ratio is small ($\beta < 1.2$), the strain field is found to play a more important role. While for the dots of larger aspect ratio, the elongated geometry becomes dominant. In both cases, P_{eh} increases with almost linearly. In order to achieve nonzero optical anisotropy P_{eh}, it is clear that the occupation probabilities of electrons in the p_x and p_y orbitals must be different, i.e., the envelope functions must be polarized. **Figure 2.40 (b)** plots the polarization of envelope functions **[188]** calculated in terms of $P_{ef}(\beta)$. It is seen that the envelope functions become more polarized as β increases, i.e., the more the dot elongates along the *x* direction, the greater the possibility to find valence-band electrons in the p_x orbitals. Comparison between the results shown in **Figure 2.40** reveals a close correlation between P_{eh} and P_{ef}. For the dots of small β, P_{eh} and P_{ef} are almost identical. For the large

aspect ratio, P_{eh} becomes a little larger than P_{ef}. Hence, it is evident that it is this selective occupancy that directly leads to the optical anisotropy.

The effect of elongated geometry of the dots on the occupancy of electrons in the individual orbitals is shown in **Figure 2.40 (c) – (f)**. **Figure 2.40 (c)** and **Figure 2.40 (d)** plot the probability density of a valence-band electron in the p_x and p_y orbitals, respectively. The result confirms that the total probability of the electron (corresponds to the area that the isosurface plot occupies) in the p_x is larger than that in the p_y. Especially, the probability of finding the electron in the p_x in the center of the dot is larger than in the p_y. **Figure 2.40 (e)** and **Figure 2.40 (f)**, respectively, plot the distribution of the p_x and p_y orbitals. It is seen that the orbitals inside the dot interact sequentially to those outside ones with higher on-site energies (filled with dark color). The p_x and p_y orbitals in the center of the dot are in a very different confinement: the p_x is mainly confined along the *x* direction while the p_y is confined along the *y* direction. As y being the short axis of the elongated structure, the p_y orbital is seen to be confined more strongly than the p_x. The different confinement for the p_x and p_y orbitals induced by the anisotropic structure explains why the valence-band electrons prefer to occupy the the p_x orbitals. The effect of structural confinement on the internal orbitals sometimes is referred as the quantum confinement effect. It is known that the quantum confinement effect has sensitive dependence on the dimensions of the structure (its influence becomes dramatically weaker as the dimensions increase). **Figure 2.40 (g)** plots the calculated optical anisotropy as a function of the dimensions of the dots. The result shows that P_{eh} decreases rapidly as the dimensions of the dots increase, which verifies that the optical anisotropy originates from the quantum confinement effect.

Sheng *et al* 's studies show that the mechanisms how shape anisotropy lead to optical anisotropy are identified by an empirical tight-binding approach. The anisotropic structure of quantum dots is shown to impose stronger confinement for

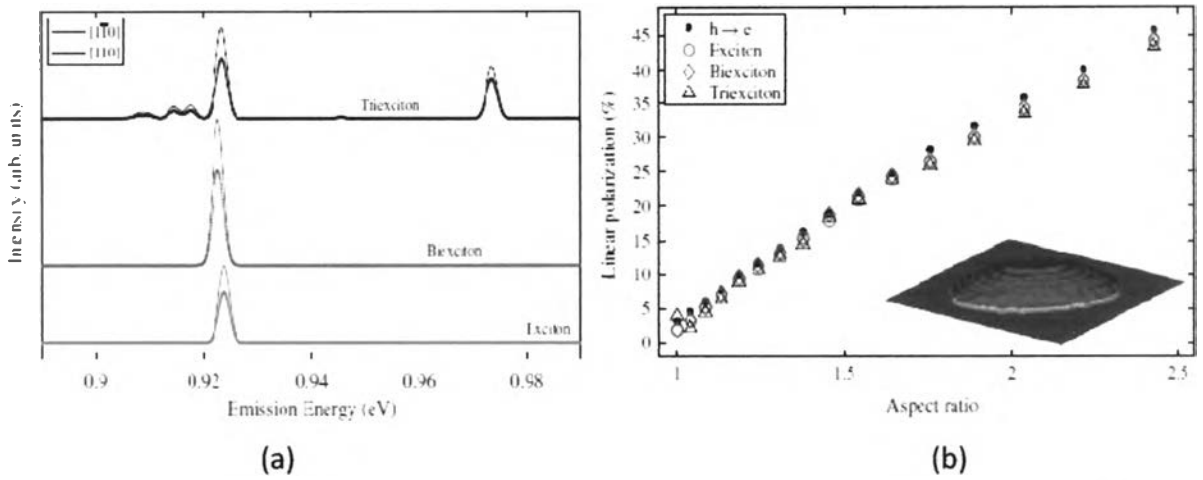

Figure 2.41 (a) For an InAs/GaAs self-assembled QD elongated along the $[1\bar{1}0]$ direction, the intensity of the emission, respectively, polarized along the $[1\bar{1}0]$ (thin lines) and $[110]$ (thick lines) directions calculated for single exciton, biexciton, and triexciton. (b) For a non-interacting of electron–hole pair, single exciton, biexciton and triexciton, calculated linear polarization as a function of the aspect ratio of the QD. Inset: a schematic view of an elongated QD **[191]**.

the localized p orbitals aligning along the short axis due to their directional coupling. In self-assembled quantum dots, these orbitals are also seen in a higher potential produced by the strain field. As a result, the valence-band electrons prefer to occupy the orbitals aligning along the long axis, which leads to stronger optical emission polarized along that direction, then the optical anisotropy is occurred.

These studies had extended the results to the linear polarization in the emission spectra of multiexciton states in InAs/GaAs self-assembled quantum dots **[191]**. To identify the origins of optical anisotropy in the emission spectrum requires the understanding of not only the composition of electron and hole states, but also the role of the excitonic effect in the optical transitions. Sheng *et al* adopted a theoretical study of the optical anisotropy in the emission spectra by adding the multiexciton complexes effect in InAs/GaAs self-assembled quantum dots via empirical tight-binding and configuration-interaction approach to investigate the

role of Coulomb interaction in the optical anisotropy in quantum dots. Then, applying the configuration interaction approach of electron and hole states to obtain the multiexciton states **[192]**. The linear polarization in the multiexciton emission is also calculated as a function of the aspect ratio of the structures, same as the previous studies **[188]**. The results were shown that the Coulomb interaction does not play an important role in the optical anisotropy in elongated self-assembled quantum dots. The linear polarization defined for non-interacting electron–hole pairs (P_{eh}) well reflects the optical properties of multiexciton states. Furthermore, the optical anisotropy in the emission spectra of multiexciton states is found to rely only on the geometry of the quantum dots structures, which is almost independent of carrier–carrier interactions as mentioned above.

2.6.2 Effect of Electric Field on the Polarization in Quantum Dots

The previous discussions about the optical anisotropy for quantum dots were shown the important of this subject having been extensive studied for utilizing in the optoelectronics applications. The other interesting studies of anisotropy in quantum dots has remained investigating both theoretically (i.e., optical anisotropy in nonspherical quantum dots **[193]**, dephasing processes and carrier dynamics in (In,Ga)As quantum dots **[194]**) and experimentally (i.e., polarization anisotropy of photoluminescence from multilayer InAs/GaAs quantum dots **[195]**, polarization anisotropy in self-assembled quantum dots within transient absorption bleaching **[196]**). In order to adopt these to produce the semiconductor optoelectronics devices. One considerable question is "how about polarization in quantum dots when the electric field is applied ?". This reflects that in the operation of some semiconductor devices (particularly in the polarization modulator), the external electric field is essential for driving these devices to be usable (corresponding electro-phenomena related with) and controlling them appropriately.

The outstanding research about polarization in quantum dots with applied electric field (which is also an important motivation in this thesis work) was appeared in Gotoh *et al* **[197]**. The author reported on the anisotropic excitonic optical properties (polarization dependent photoemission and photoabsorption) induced by applying a lateral electric field in a single semiconductor quantum dot. The excitonic optical polarization characteristics are examined using theoretical calculation which was numerically analyzed taking into account the quantum dot potential, electric field, and electron–hole Coulomb interaction. The properties of these quantum dot based light sources depend strongly on their optical polarization properties, which are determined by the spatial shape of the dots **[198-199]**.

In general, the main characteristics of both conventional and quantum optical devices reflect the near "band edge" optical transitions properties. The optical polarization properties of the optical transitions near the band edge of direct band-gap semiconductors are determined from the spatial symmetry of the hole wave function, following the **k.p** theory **[63, 187]**. It is necessary to change the shape of the hole wave function in order to control the optical polarization properties. Gotoh *et al* proposed a thin quantum dot structure with a lateral electric field, as shown in **Figure 2.42**, for controlling polarization properties with an electric field. In this configuration, an electron and a hole are strongly confined in the z direction and weakly confined in x and y directions. When an electric field is applied in the x direction, the electron and the hole move in opposite directions along the x direction and the spatial shape of the wave functions becomes asymmetric in the x and y directions, corresponding to the quantum confined stark effect. Moreover, optical responses such as photoemission and photoabsorption remain strong even in an electric field due to large Coulomb interaction caused by strong confinement along z direction. This large optical anisotropy while maintaining a strong optical response has not yet been observed in other structures such as bulk and quantum wells.

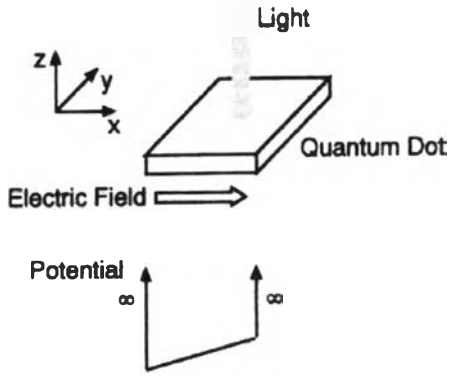

Figure 2.42 Thin quantum dot considered in theoretical calculation. The electric field is applied along the x direction. Both electron and a hole are confined in the quantum dot by an infinitely high confinement potential. **[197]**.

Consider an electron and a hole confined in a GaAs thin quantum dot with an infinitely high potential barrier where the electric field is applied in the *x* direction (as shown in **Figure 2.42**). The calculation method was reported the theory in **[200-201]** and will be mentioned briefly as follows. For the Schrödinger equation $H\Psi = E\Psi$, Hamiltonian *H* for this system is $H = H_{kin} + V_{e-h} + eE_w x_c - eE_w x_h$, where H_{kin} denotes kinetic energy, V_{e-h} is the electron–hole Coulomb potential and E_w is the electric field. Therefore, the exciton wave function Ψ (the electron and hole combine to form an exciton) and energy *E* are determined by the Schrödinger equation. In thin quantum dots, Ψ can be expressed as a product of the envelope part and Bloch part. Expanding the envelope part of the wave function using orthogonal functions for the electron and hole. Since the electron and hole to be confined by the infinite potential, orthogonal sinusoidal functions were used, which are eigenfunctions of the quantum dot when there is no Coulomb interaction. Then, manipulate them and utilize the optical matrix elements as described in **[63, 200-201]**, the optical matrix elements for the free electron–hole transition can be analytically expressed using k_x, k_y and k_z, which are elements of the wave vector

for the hole wave function and the probability of a transition between Bloch functions. Consequently, the optical matrix element $|M|_i^2$ is

$$|M|_x^2 = \frac{k_z^{eff^2} + k_y^{eff^2}}{k_x^{eff^2} + k_y^{eff^2} + k_z^{eff^2}} \frac{3}{2}|M_b|^2 \ , \ |M|_y^2 = \frac{k_z^{eff^2} + k_x^{eff^2}}{k_x^{eff^2} + k_y^{eff^2} + k_z^{eff^2}} \frac{3}{2}|M_b|^2 \qquad \textbf{(2.91)}$$

where $k_i^{eff} = (\pi L_i / L_i^{eff^2})^{1/2}$ are wave numbers with effective dot size L_i^{eff} and $|M_b|^2$ is a bulk matrix element. Finally, degree of optical polarization was defined as

$$D = \frac{|M|_y^2 - |M|_x^2}{|M|_y^2 + |M|_x^2} = \frac{k_x^{eff^2} - k_y^{eff^2}}{2k_z^{eff^2} + k_x^{eff^2} + k_y^{eff^2}} \qquad \textbf{(2.92)}$$

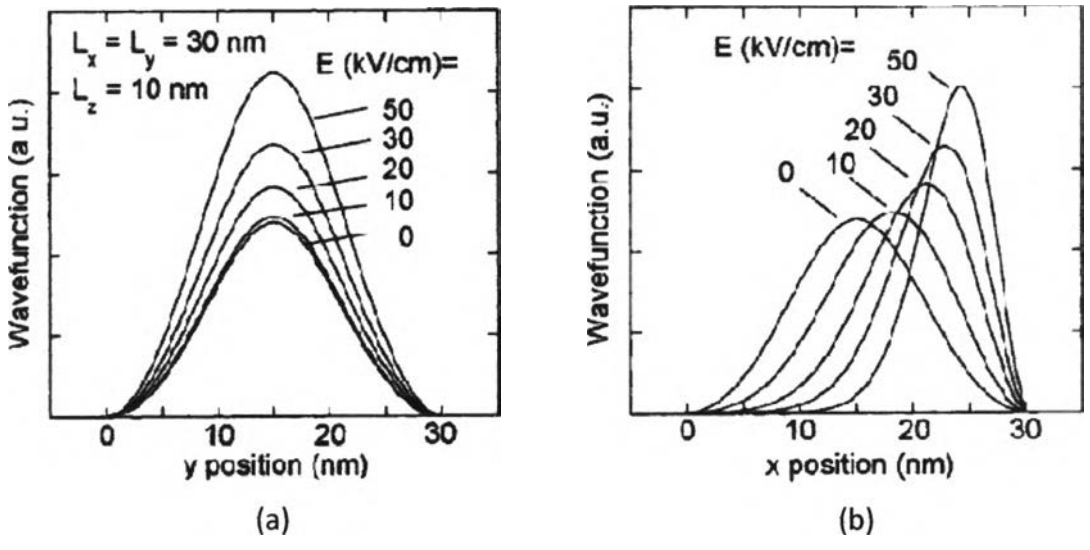

Figure 2.43 Calculated hole wave functions for a $L_x = L_y = 30$ nm QD. Wave functions as a function of the (a) y position, and (b) x position. In (a), the wavefunctons are plotted for the y position with the x position set at the maximum wave function. In (b), the y position is fixed at 15 nm, which is the center of the QD. **[197]**.

For spatially isotropic quantum dots where L_x is equal to L_y, the optical polarization is also isotropic ($D = 0$) because $k_x^{eff^2} = k_y^{eff^2}$. When an electric field is applied to quantum dots, k_x^{eff} becomes larger than k_y^{eff}, leading to a polarized

optical matrix element in the *y* direction ($D > 0$). The polarization properties of the excitonic optical transition were analyzed using **Eq. (2.92)**.

Figure 2.43 shows the calculated envelope part of the hole wave functions in a quantum dot of $L_x = L_y = 30$ nm and L_z was fixed at 10 nm. The hole wave functions was plotted because it is easier to observed about the change at the presence of applied electric field than the electron wave functions. Since the exciton wave functions are linear combinations of free electrons and hole wave functions, the electron (hole) part of an exciton can be shown by integrating the hole (electron) part **[200-201]**. The wave functions are plotted as a function of the y position (**Figure 2.43 (a)**) and x position (**Figure 2.43(b)**) for different electric fields obtained by integration in the z direction. With an increase in electric field, the wave functions simply increase along the y direction but maintain their spatial symmetry, as shown in **Figure 2.43 (a)**, and the wave functions concentrate along the x direction and move to the maximum position seen in **Figure 2.43 (b)**. Although the hole wave functions are changed by the electric field in the x direction, these wave functions are oppositely attracted by electrons via electron–hole Coulomb interaction.

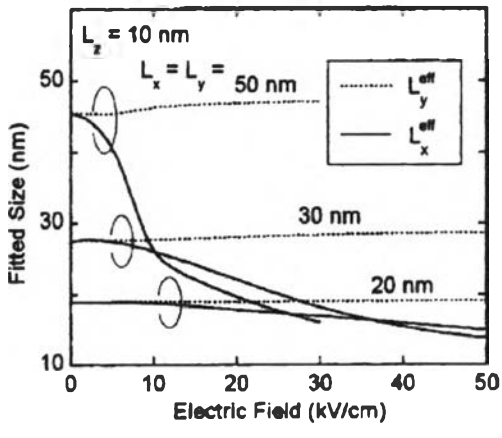

Figure 2.44 Effective dot sizes plotted as functions of the electric field. They are obtained from calculated wave functions by fitting them to sinusoidal functions. **[197]**.

Due to this Coulomb interaction, the shapes of the wave functions in the x direction remain nearly spatially symmetric with respect to the maximum points of the wave functions even in a strong electric field. If there is no Coulomb interaction, the shapes of the wave functions become highly asymmetric in the x direction.

Figure 2.44 shown the effective dot sizes L_i^{eff} (obtained from **Figure 2.43** by fitting the wave functions to sinusoidal functions) as a function of the electric field for quantum dots with different lateral sizes. Note that in a zero electric field, the L_i^{eff} values are not the same as the actual lateral sizes of the quantum dots because the Coulomb interaction leads to a concentration of electrons and holes at the center of the quantum dot, resulting in a L_i^{eff} that is smaller than the lateral size. In **Figure 2.44**, because the spatially isotropic quantum dots were consider, so $L_x^{eff} = L_y^{eff}$ in a zero electric field. When an electric field is applied, L_x^{eff} becomes smaller than L_y^{eff}. The electric field pushes electrons and holes in opposite directions along the x axis and the spatial expansion of the electron wave function and hole wave function is spatially localized. This effect is prominent in "larger quantum dots" because electron and hole wave functions can greatly change inside the quantum dot and because the Coulomb interaction is small. The differences between L_x^{eff} and L_y^{eff} leading to differences in effective wave vectors and induces optical anisotropy.

The degree of optical polarization calculated using **Eq. (2.92)** was shown in **Figure 2.45 (a)**. In a zero electric field, $L_x^{eff} = L_y^{eff}$ and $k_x^{eff} = k_y^{eff}$, leading to a zero degree of optical polarization, meaning that the optical polarization is completely spatially isotropic. When an electric field is applied, L_x^{eff} becomes smaller and k_x^{eff} becomes larger than k_y^{eff}, which results in a finite value for the degree of polarization, and spatially polarized optical absorption and photoemission.

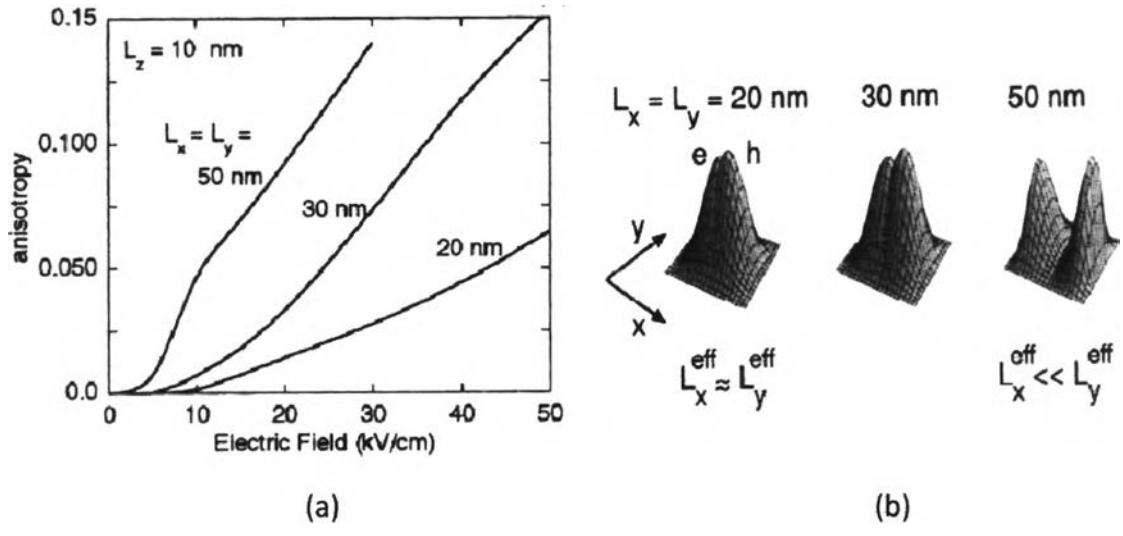

Figure 2.45 (a) Electric-field dependence of the calculated degree of polarization. The degree of polarization has a positive value for polarized optical emission and absorption in y direction. (b) Calculated wave functions of electrons and holes for quantum dots with different lateral sizes. The electric field is 30 kV/cm **[197]**.

This electric-field-induced optical anisotropy increases with increases in the electric field and in the lateral size of the quantum dot. To understand these dependences, **Figure 2.45 (b)** shown the electron and hole wave functions in an electric field of 30 kV/cm for quantum dots with different lateral sizes. In all QDs, the electrons and holes are separated along the *x* direction and spatial expansion of the hole wave function is smaller than that of the electron wave function. In smaller quantum dots, there are electrons and holes nearly all over the quantum dot and the spatial shapes of the wave functions are almost isotropic ($L_x^{eff} \approx L_y^{eff}$), leading to a small degree of polarization. Whereas in larger quantum dots, the electrons and holes are spatially localized and the wave functions become spatially asymmetric ($L_x^{eff} << L_y^{eff}$). This large asymmetry leads to the large positive degree of polarization seen in **Figure 2.45 (a)**.

As described above, optical properties such as optical absorption and photoemission depends on optical matrix elements. Thus, their polarization properties directly reflect the spatial symmetry of the hole wave function. With the larger quantum dots in a strong electric field, the hole wave function is largely localized and large optical anisotropy appears. As seen in **Figure 2.45 (a)**, optical anisotropy is clearly prominent in larger quantum dots. In thin quantum dots, large optical responses are achieved due to the large Coulomb interaction. However, the optical responses become weaker in the larger quantum dots when a strong electric field is applied. In larger quantum dots, the spatial symmetry of hole wave functions greatly changes, and this causes large optical anisotropy. Simultaneously, the electrons and holes are widely separated from one another inside the quantum dot, leading to a small spatial overlap between the electron wave functions and the hole wave functions. This results in lower oscillator strength and weaker optical response. Specifically, when the electric-field potential is larger than the exciton binding energy, the field overcomes Coulomb interaction and the optical responses decrease greatly. When designing optical devices using thin quantum dots, the dot size and electric field should be determined by taking both the polarization characteristics and optical response properties into consideration.

To verify the calculated results, Gotoh *et al* also manifested experimentally examined the effect of an electric field on the optical properties in a quantum dot. For the measurement, two quantum dots located in the center of an electrode connected to a voltage source were chosen which have different lateral size. The structure of their energy was evaluated by the photoluminescence excitation technique **[202]**, which was measured the polarization resolved low excitation PL at different bias voltages for the two quantum dots. **Figure 2.46** shown the photo-luminescence spectra of the larger dot and the smaller dot taken at 10 K and 0° and 90° indicate that the polarizations are parallel and perpendicular to the electric field, respectively. *R* is the ratio of the 0 V PL intensity to the 4 V PL intensity. For both polarizations, the photoluminescence intensity decreases with the application of bias

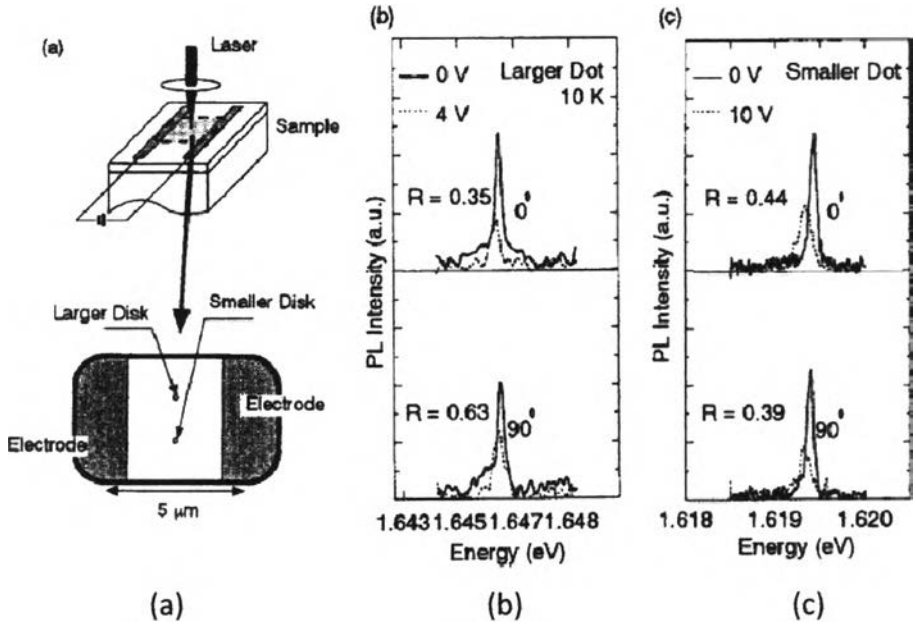

Figure 2.46 (a) Schematic diagram of the sample used in the measurement. Two QDs positioned centrally between the electrodes were detected in The measurement. (b) Polarization resolved PL with application of the electric field for the larger dot. 0° means that the PL polarization is parallel to the electric field. R represents the PL ratios between 0 and 4 V. The excitation intensity is 2 mW, which is under a low excitation condition. (c) Polarization resolved PL with application of the electric field for the smaller dot **[197]**.

voltage. In **Figure 2.46**, 0° PL, which is the same polarization as the electric field, decreases more (R = 0.35) than 90° PL (R = 0.63). But in a small dot, the ratio of 0 V PL to 10 V PL for 0° (0.44) is almost the same as that for 90° (0.39) as shown in **Figure 2.46 (c)**, corresponding to the quantum confined stark effect. The measured result shows that the PL polarization changes when an electric field is applied, and this change become prominent for larger quantum dots. In the calculated results, the electric-field-induced optical anisotropy becomes larger with increases in the lateral size of the quantum dot. Therefore, the measured results agree qualitatively with the theoretical results.

Briefing the main point again, the polarization properties strongly depended on the electric field and the lateral size of the dots as follows:

- Large anisotropy appeared in the large quantum dots, but when a strong electric field is applied so that an electric-field potential energy is created larger than the exciton binding energy, the Coulomb interaction is defeated causing a lower oscillator strength, which results in decreasing of the optical responses.

- In thin quantum dots with large lateral size (non-isotropic shape), the electrons and holes are widely separated and both wave functions have spatially asymmetric shapes. A large spatially asymmetric shape in a hole wave function causes large optical anisotropy. Moreover, due to strong confinement in the z direction, the electrons and holes attract each other, leading to a large overlap of the electron and hole wave functions. This results in a quantum dot with a large optical response as well as large optical anisotropy.

These effects have not yet been observed in other structures such as bulk and quantum well structures. Optical anisotropy is induced simply by the application of an electric field in spatially isotropic quantum dots. The anisotropy can be controlled by controlling the electric field. This tunable anisotropy will provide optical devices with novel functions such as polarization light switching and polarization fixed surface emitting laser operation. Moreover, optical polarization tunability can be used to compensate for the undesirable optical anisotropy in quantum dots.

In the discussion above, phenomena of electric field on the polarization in single quantum dot is attractive and interested in extending these results to complicated models, following the fabrication of the new quantum dot structure. Despite the development of this study has seldom appeared in the publication at the present, some interesting research related with have found which were mostly

focused on the coupling effect of two quantum dots **[203-206]**. These exhibit an important information like the small jigsaws combining as the key that manifests an interesting phenomenon, leading to completely overall image.

However, many investigation about this topic has been remained enigmatic, so the main objective of thesis work is to examine the optical properties by improving quantum dots model to become different from the previous models. This thesis work is expansion the InAs binary quantum dots model to the InAs aligned quantum dots which pay attention to the coupling effect in adjacent dots. The effect of applied electric field on this aligned quantum dots were also investigated, then extending to the polarization dependence literally. Following this thesis, the analysis will take place with integration of many useful data to increase an intensive estimation. Researching of polarization with electric field dependence on the self-assembled aligned quantum dot is a novel idea since polarization anisotropy was appeared on the single dot with applied electric field. Therefore, the assumption about a strong polarization anisotropy on the ordered dots with applied electric field may be probable by aiming to the coupling influence, so it is essential to verify this prediction straightforwardly and correctly. The procedure of theoretical investigation for examine probability in the assumption will be thoroughly explained in chapter 3.